

University of Warwick institutional repository: <http://go.warwick.ac.uk/wrap>

A Thesis Submitted for the Degree of PhD at the University of Warwick

<http://go.warwick.ac.uk/wrap/4400>

This thesis is made available online and is protected by original copyright.

Please scroll down to view the document itself.

Please refer to the repository record for this item for information to help you to cite it. Our policy information is available from the repository home page.

CRYSTALLINE PHASE DEVELOPMENT IN
CORDIERITE GLASS-CERAMICS

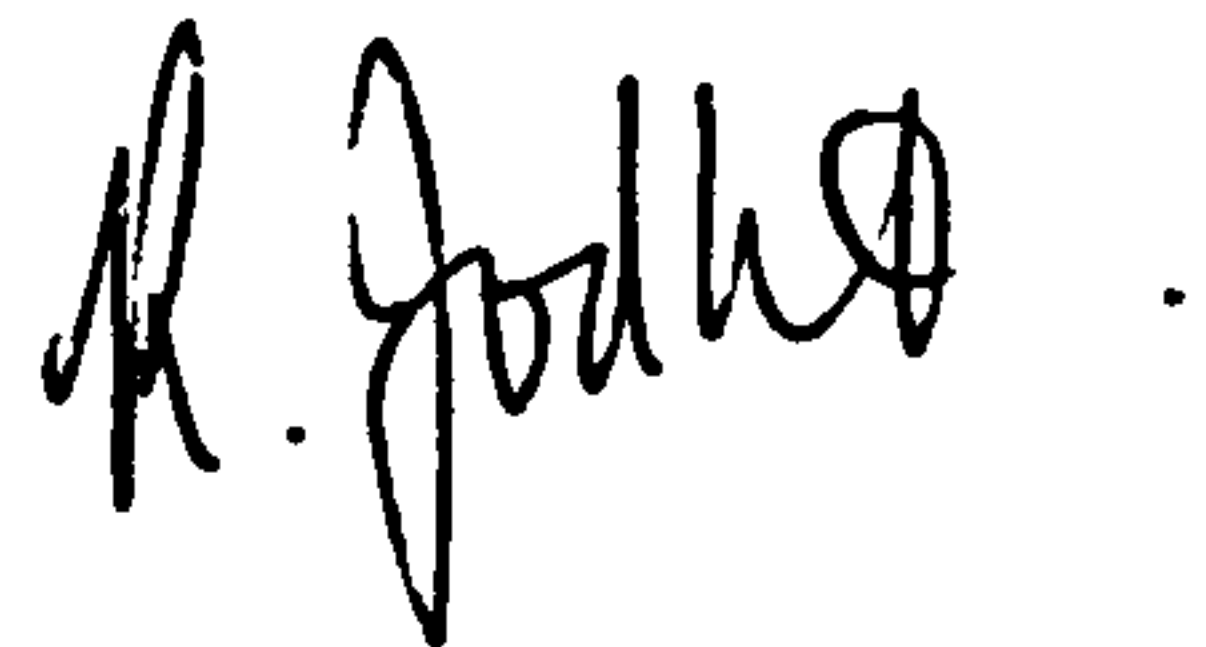
by

R. Todhunter B.Sc.

Thesis for the Degree of Doctor of Philosophy of
the University of Warwick, Physics Department,
University of Warwick, January 1984.

DECLARATION

This dissertation is submitted to the University of Warwick in support of my application for admission to the degree of Doctor of Philosophy. It is an account of my work carried out in the Department of Physics, University of Warwick during the period January 1979 to December 1981 and, except where specifically acknowledged in the text, is a result of my own independent research. No part of this thesis has been submitted in respect of a degree to this or any other university.

A handwritten signature in black ink, appearing to read 'R. Todhunter', with a stylized flourish at the end.

JANUARY 1984

R. TODHUNTER

ABSTRACT

Cordierite glass-ceramics are characterised by their excellent physical properties viz. high mechanical strength and hardness, good thermal shock resistance and chemical durability, and therefore are widely used in materials technology. The microstructure and phase development of these materials during the initial stages of crystallisation has been investigated using X-ray diffraction, Differential Thermal Analysis and Transmission Electron Microscopy. Annealing temperatures were chosen both above and below the glass transition temperature, T_g , which was determined as 720°C by Differential Scanning Calorimetry. Infra-red, u.v-visible and electron paramagnetic resonance spectroscopy were employed as additional techniques to investigate structural changes in the glass during phase transformations. It has been shown that annealing above T_g promotes glass-in-glass phase separation on a scale of $\sim 100 \text{ \AA}$ by spinodal decomposition which may well be enhanced by an incipient ordering during the annealing process. The presence of phase separation is seen to have a profound influence on the subsequent nucleation of a magnesium dititanate phase and the growth of the metastable β -quartz solid solutions, magnesian-petalite and μ -cordierite which are capable of co-existing over the temperature range $800\text{-}100^{\circ}\text{C}$. The effects of annealing and phase separation are manifested as variations in both phase composition and growth morphology for a given crystallisation temperature and holding time.

Contents

| <u>Chapter 1</u> | <u>Introduction</u> | <u>Page</u> |
|------------------|---|-------------|
| 1.1 | Inorganic Oxide Glass Formation | 1 |
| 1.2 | Glass-ceramics | 3 |
| 1.2.1 | Phase separation | 6 |
| 1.2.2 | Solid solutions | 6 |
| 1.3 | The Role of TiO_2 as a nucleating agent | |
| 1.4 | Phase development in Cordierite Glasses containing TiO_2 as a nucleating agent | 11 |
| 1.5 | Plan of Thesis | 18 |
| | | |
| <u>Chapter 2</u> | <u>Experimental Techniques</u> | |
| 2.1 | Glass Preparation | 19 |
| 2.2 | Heat-treatments | 19 |
| 2.2.1 | Nomenclature | 20 |
| 2.3 | Differential Thermal Analysis (DTA) | 21 |
| 2.3.1 | Particle size | 21 |
| 2.3.2 | Heating rate | 22 |
| 2.3.3 | Application of DTA to the determination of reaction kinetics | 22 |
| 2.3.4 | Applications of DTA to the glass-ceramic process | 23 |
| 2.3.5 | DTA apparatus | 24 |
| 2.3.6 | Experimental procedure | 24 |
| 2.4 | Differential Scanning Calorimetry (DSC) | 25 |
| 2.5 | X-ray diffraction | 25 |
| 2.5.1 | Calculation of crystallite-size from line broadening | 26 |
| 2.5.2 | Experimental procedure | 27 |

| | | <u>Page</u> |
|-----------|--|-------------|
| Chapter 2 | | |
| 2.6 | Scanning Electron Microscopy (SEM) | 27 |
| 2.6.1 | Energy Dispersive Analysis of X-rays (EDAX) in SEM | 28 |
| 2.7 | Transmission Electron Microscopy (TEM) | 29 |
| 2.7.1 | Modes of contrast | 29 |
| 2.7.2 | Selected area diffraction | 30 |
| 2.7.3 | Experimental procedure | 30 |
| 2.8 | Infra-red absorption spectroscopy | 32 |
| 2.8.1 | Infra-red spectroscopy of silicate glass and glass-ceramic systems | 32 |
| 2.8.2 | Experimental procedure | 33 |
| 2.9 | UV-Visible - spectrometry | 33 |
| 2.9.1 | Experimental procedure | 34 |
| 2.10 | Density measurements | 35 |
| 2.11 | Electron paramagnetic resonance (EPR) | 35 |
| 2.12 | Chemical analysis for TiO_2 and Fe_2O_3 | 36 |
| Chapter 3 | <u>The observed influence of annealing temperature on subsequent crystalline phase development</u> | |
| 3.1 | Determination of T_g by DSC | 37 |
| 3.2 | DTA studies of base glasses | 37 |
| 3.3 | Calculation of activation energies of crystallisation | 38 |
| 3.3.1 | Heat-treatment schedule and resulting XRD | 39 |
| 3.3.2 | Determination of crystallite size by line-broadening | 42 |
| 3.4 | Summary | |

| | | |
|------------|---|-------------|
| Chapter 4 | <u>Identification of possible physical and chemical differences between the base glasses</u> | <u>Page</u> |
| 4.1 | EDAX analysis in SEM | 44 |
| 4.2 | Chemical analysis by absorptiometric methods | 45 |
| 4.3 | Additional heat-treatments | 46 |
| 4.4 | Density measurements | 46 |
| 4.5 | U.V - Visible spectroscopy of glassy specimens | 48 |
| 4.6 | Infra-red spectroscopy of glassy specimens | 49 |
| 4.7 | Electron paramagnetic resonance (EPR) | 50 |
| 4.8 | Discussion | 51 |
| Chapter 5 | <u>The stability of magnesian petalite and microstructural development in 675- and 750- glasses</u> | |
| 5.1 | Transformation of 675- glass to 750- glass | 55 |
| 5.2 | The stability of the magnesian petalite solid solution | 55 |
| 5.3 | Microstructural development of magnesian-petalite and μ -cordierite | 58 |
| 5.4 | Summary | 64 |
| Chapter 6 | <u>Concluding discussion</u> | |
| 6.1 | Discussion | 66 |
| 6.2 | Conclusions | 72 |
| 6.3 | Future work | 73 |
| References | | 75 |
| Appendices | | 81 |

List of figures

- 1.1 Time-temperature-transformation curve.
- 1.2 Nucleation rate versus supercooling.
- 1.3 $\text{MgO-Al}_2\text{O}_3\text{-SiO}_2$ phase diagram.
- 1.4 Variation of unit cell parameters as a function of SiO_2 content for β -quartz solid solutions.

- 2.1 Heat-treatment furnace.
- 2.2 Temperature profiles for heat-treatment furnace.
- 2.3 DTA apparatus.
- 2.4 Line-broadening of silicon standard.

- 3.1 Determination of T_g by DSC.
- 3.2 DTA of base glasses at $10^\circ/\text{min}$.
- 3.3 DTA of base glasses at $5^\circ/\text{min}$.
- 3.4 DTA of base glasses at $2^\circ/\text{min}$.
- 3.5 Kissinger plots for crystallisation of MgTi_2O_5 in base glasses.
- 3.6 Visual appearance of heat-treated base glasses.
- 3.7 Phase development at $800^\circ\text{C} - 16$ hrs.
- 3.8 Phase development at $875^\circ\text{C} - 4$ hrs.
- 3.9 Phase development at $925^\circ\text{C} - 4$ hrs.

- 4.1 Optical transmission curves for base glasses.
- 4.2 Optical transmission curves for heat-treated glasses.
- 4.3 IR spectra of glassy specimens.
- 4.4 EPR spectra of selected specimens at $g \approx 2$.
- 4.5 EPR spectra of Fe^{3+} in selected specimens.

- 5.1 Approximate volume fraction of magnesian-petalite and μ -cordierite in 675- and 750- glasses as a function of temperature.
- 5.2 Examples of peak-splitting in principal magnesian petalite reflection.
- 5.3 (a) glass-in-glass phase separation in 750/20.
(b) base-glass microstructure.
- 5.4 Growth of MgTi_2O_5 in (a) 675/775/50 and (b) 750/775/50.
- 5.5 TEM of 675/825/4.
- 5.6 TEM of 750/825/8.
- 5.7 Schematic phase diagram.
- 5.8 TEM of 675/925/4.
- 5.9 High magnification of MgTi_2O_5 spherulites and EDAX spectra.
- 5.10 TEM of 750/925/4.
- 5.11 TEM of 750/1000/4.
- 5.12 XRD spectra of (a) 675/775/50/1000/5 and (b) 750/775/1000/5.
- 5.13 TEM of 675/775/50/1000/5.
- 5.14 TEM of 750/775/50/1000/5.
- 6.1 Constitutional supercooling.
- 6.2 Hypothetical phase diagram.
- 6.3 Diffusion controlled ionic mobility
 - A.1 Free energy versus composition for a binary system at various temperatures.
 - A.2 Immiscibility dome.
 - A.3 Concentration profiles as a function of time during spinodal decomposition.

List of Tables

- I. Initial heat-treatment schedule for base glasses.
- II. Crystalline phases encountered during initial crystallisation.
- III. Principal reflections in MgTi_2O_5 .
- IV. MgTi_2O_5 crystallite dimensions in selected heat-treated samples.
- V. Chemical composition of base glasses determined by EDAX.
- VI. TiO_2 and Fe_2O_3 content of base glasses.
- VII. Densities of base glasses.
- VIII. Additional density measurements.
- IX. Heat-treatments of 825/8 samples.
- X. Specimens studied by TEM and their phase composition.
- XI. Electron scattering factors for magnesium, aluminium and silicon.
- XII. X-ray diffraction data for magnesian petalite phases.

Acknowledgements

I should firstly like to thank Professor Peter McMillan for his supervision and encouragement throughout the course of this work and together with Professor P.N. Butcher, for making available the departmental facilities necessary for this research.

I am indebted to Dr. Graham Partridge and his staff of the G.E.C. Stafford Research Laboratories for their assistance in the preparation of materials and general help. Thanks are also extended to Dr. Mike Lewis and Dr. Mike Smith of Warwick University for their kind assistance and advice concerning electron microscopy and EPR measurements respectively. I would also like to thank the technical staff of the Physics Department, especially Gerry Smith, Steve York and Harold Mathers for their invaluable assistance and the secretarial staff, of whom Pat Lewis and June Beaumont deserve special mention, for their help in the preparation of this text and kind support.

Thanks are very much in order to the many members of the glass-ceramics group, both past and present, for much helpful discussion; especially John Taylor, Diane Holland and Nigel Pratten for their many constructive (and otherwise) comments and proof reading of the text.

A special thankyou to Carmel Parrott for her patience and skill in the typing of this manuscript.

I would especially like to thank my immediate family, Grace Bradshaw and Simon and Alfreda Britton without whose constant and unfailing love, support and friendship, this thesis may never have been completed.

Finally, the financial support of the Science and Engineering Research Council and G.E.C. is gratefully acknowledged.

"I dedicate this thesis to my parents
and all others from whose teachings I
have benefited"

1. INTRODUCTION

A glass can be generally described as a rigid material in which the arrangement of atoms and molecules is irregular; in contrast to the highly ordered arrangement found in most crystalline solids. Glasses can be subdivided into groups depending on their chemical composition and the mechanism by which they are formed. By far the most important, in terms of technological application, are the inorganic oxide glasses. These are described by the American Society for Materials Testing (A.S.T.M.) as "the inorganic products of fusion which have cooled to a rigid condition without crystallising". In addition to this group there are organic glasses e.g. perspex and polystyrene, which can be formed either by supercooling of a melt or via a controlled chemical reaction such as polymerisation, non-crystalline solids formed from semi-metallic elements and compounds, e.g. amorphous silicon, chalcogenides etc. and metallic glasses which rely on extremely rapid cooling from the melt in order to remain amorphous. The extensive range of physical properties exhibited by all of these glasses results in them being used for a wide variety of applications in material science and technology.

1.1 Inorganic Oxide Glass Formation

The ability of an oxide system to successfully form a glass can be discussed on the basis of the Random Network Theory, first put forward by Zachariasen (1) in 1932. This theory proposes that both the coordination number of the cation and the cation-anion (oxygen) bond length in a glass will be very similar to those in the corresponding crystalline species and that only slight variations in the cation-oxygen-cation bond angle ($\sim 10\%$) will be sufficient to give a random network. These so called, network forming oxides are ones in which the cation readily forms a highly covalent bond with oxygen. A measure of the ability of a cation to bond covalently

is indicated by the ionic field strength of the cation, F , given by:

$$F = Z/r^2 \quad \dots (1) \quad (115)$$

where Z is the valency and r the ionic radius. Cations with high field strengths are able to attract electrons and form a covalent bond and hence are generally network formers. In addition to a high field strength these oxides have a cation to anion radius ratio which is such that the oxygens readily form tetrahedra around a central cation. It is the linking at all four corners of these tetrahedra, through shared oxygen atoms, which creates the continuous network structure.

Oxides having low field strengths and which are therefore unable to form a network, are called network modifiers; sodium oxide being a good example. The presence of sodium oxide in a glass forming system necessitates the presence of non-bridging oxygens, i.e. the tetrahedra do not link at all four corners and the result is a more open structure with sodium atoms occupying interstices in the network. The presence of network modifiers can have a profound effect on the physical properties of a glass.

Oxides for which the field strength values lie between those of a former and a modifier are known as intermediate oxides and can either join the network or occupy holes in the structure, e.g. Al_2O_3 , TiO_2 , ZrO_2 .

Having fused a suitable glass-forming oxide-system, it is necessary to establish a sufficiently rapid cooling rate from the melt so as to prevent devitrification of the glass. Considering the thermodynamics of the system, increased undercooling of the melt will increase the free energy difference between solidus and liquidus states and hence crystallisation will be encouraged. Balanced against this will be a concurrent increase in viscosity which will inhibit the atomic structural rearrangements necessary to promote crystallisation. These considerations can be represented by a time-temperature

transformation (T-T-T) curve (Fig. 1.1) in which the time taken (t) for a given volume fraction of glass to crystallise is plotted against under-cooling (ΔT).

Clearly, to avoid devitrification, a cooling rate in excess of that represented by the tangent to the curve must be attained.

1.2 Annealing

The cooling rates required for glass formation generally lead to residual density fluctuations throughout the glass which are a result of the departures from equilibrium encountered as the glass passes from the super-cooled to the glassy state. The temperature region over which this occurs is known as the glass transformation temperature, T_g . Density fluctuations are manifested as generally undesirable inhomogeneities within the glass e.g. residual mechanical stress and distortion of the refractive index, but may be removed by heating the glass at temperatures just below T_g . This is known as annealing and is usually applied as the last stage of the manufacturing process.

1.2 Glass-ceramics

Glass-ceramics are produced by the controlled crystallisation of a suitable glass system via an appropriate series of heat-treatments. The process consists essentially of two stages: firstly, a nucleation stage wherein small crystallites are produced within the glassy matrix and secondly, a crystallisation or growth stage, where the final crystalline microstructure is grown upon the "seed" crystals formed during nucleation. The result is a fine-grained crystalline ceramic having improved physical

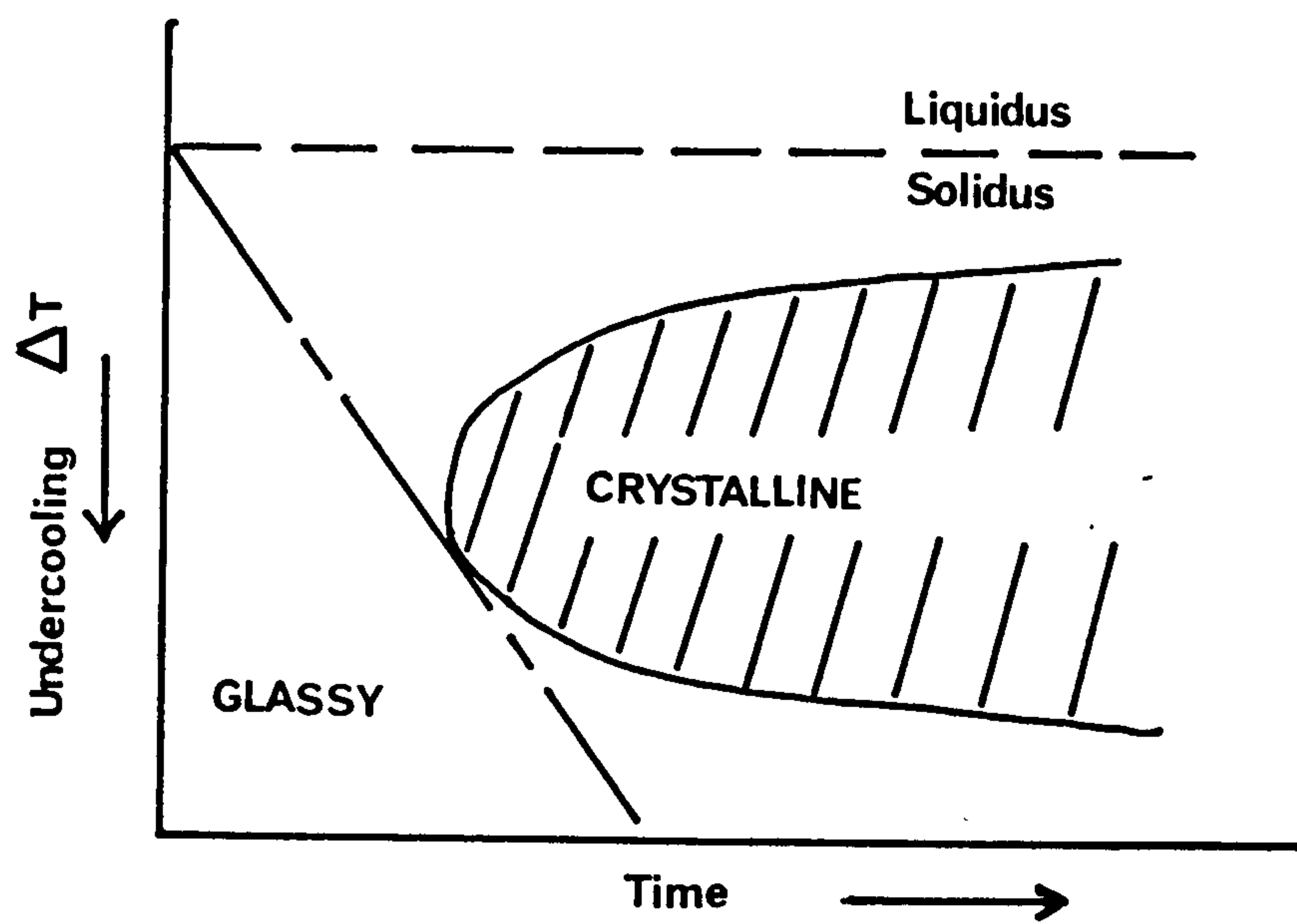


Fig 1.1 - T-T-T curve

properties compared with those of the parent glass. These properties may be considerably influenced by the nature of the heat-treatments adopted.

Nucleation can be achieved by either of two distinguishable mechanisms; homogeneous nucleation or heterogeneous nucleation. In homogeneous nucleation, the crystallites formed are of the same chemical composition as those that will subsequently grow whereas in heterogeneous nucleation they may be of a very different constitution. Completely homogeneous nucleation is very difficult to observe and the large majority of glass ceramics are formed via the heterogeneous mechanism.

Models for nucleation have been proposed by many authors (2-12) and a general expression for the rate of heterogeneous nucleation, I , can be given by;

$$I = A \exp \left[- (\Delta G^* \cdot f(\theta) + Q) / kT \right] \quad (2)$$

where A is a constant expressing the collision frequency or rate at which molecules are attached to a nucleus of a critical size, beyond which the nucleus grows rather than redissolves. ΔG^* is the free energy of formation of such a nucleus and is a combination of volume free energy and surface free energy terms. $f(\theta)$ arises as a consequence of heterogeneities being present and effectively reduces ΔG^* by lowering the barrier to nucleus formation presented by the surface free energy term. Q is an activation energy for molecular transport across the nucleus-matrix interface and being diffusion dependent is considered to be inversely proportional to viscosity. Hence, for a melt subjected to increased supercooling, the increase in volume free energy will reduce ΔG^* until I reaches a maximum, beyond which, further supercooling increases the viscosity and the term in Q will begin to dominate causing a rapid decrease in I . This is represented by the familiar curve of nucleation rate versus supercooling (Fig. 1.2)

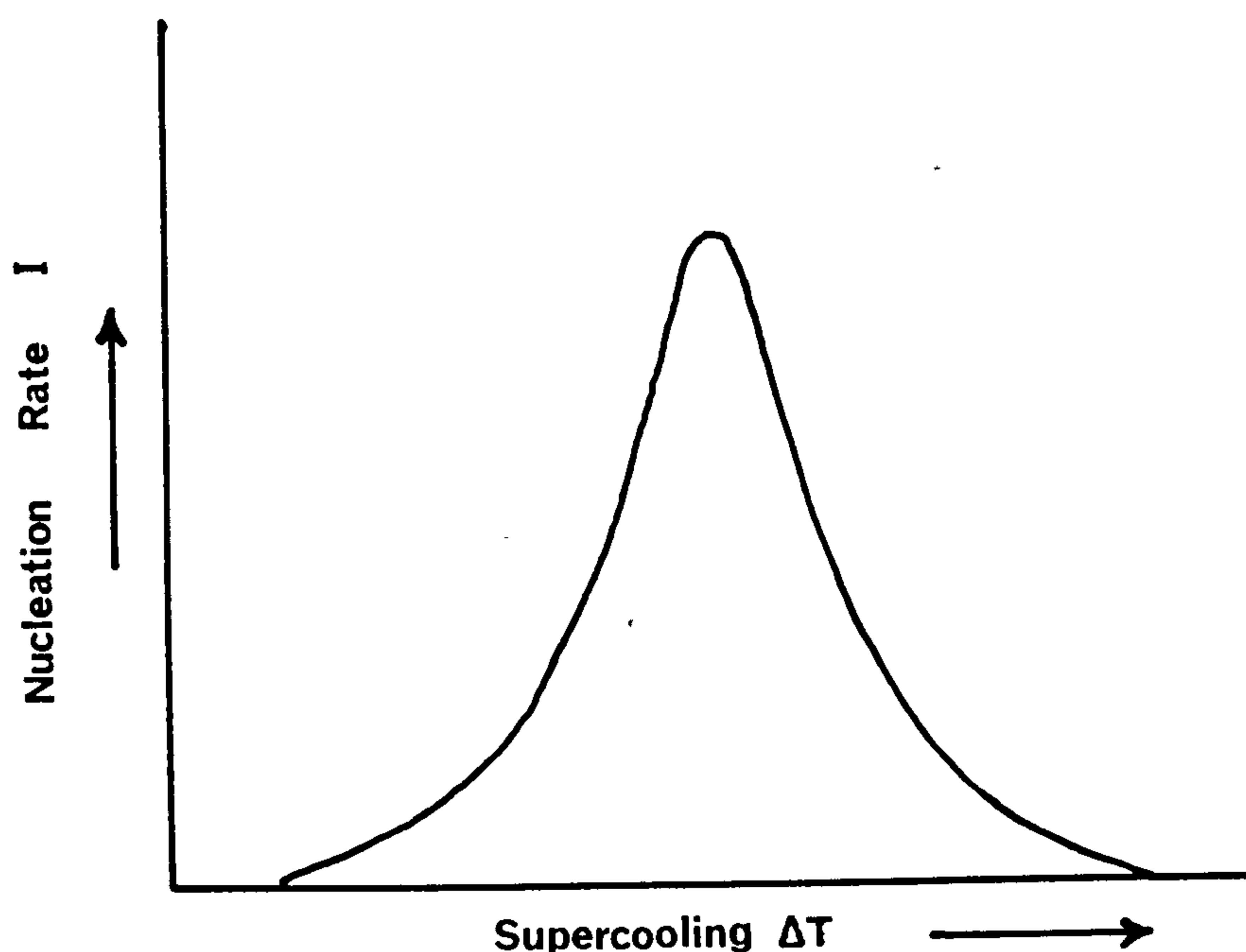


Fig 1.2

To enhance nucleation, nucleating agents are frequently added to the glass in the form of soluble oxides which will precipitate out in the form of either colloidal metallic particles or crystalline compounds, based on the nucleating agent itself, (section 1.3). The nuclei should, ideally, be finely dispersed through the glass so as to facilitate the growth of crystals with the smallest possible grain size to give a glass-ceramic with the highest possible strength.

The mechanism of crystal growth onto stable nuclei has again been extensively modelled (6, 10, 11, 13) and the kinetics of crystal growth rates can be considered as essentially the same as those of nucleation (equation (2)) but with the inclusion of a term which expresses the rate at which molecules reach the phase boundary and the mechanism by which they are placed onto the existing crystalline surface. The subsequent crystalline morphology is strongly influenced by this stage.

1.2.1 Phase Separation

Liquid immiscibility or glass-in-glass phase separation may occur in many glass systems prior to nucleation and its presence can strongly influence subsequent nucleation and growth kinetics. Phase separation arises in glass systems which show two minima in a plot of free energy versus composition, i.e. which are capable of forming two separate phases of different composition. Two mechanisms exist by which separation can occur: nucleation and growth or spinodal decomposition, both of which are discussed fully by Cahn et al (14, 15).

1.2.2 Solid Solutions

A solid solution is formed by the inclusion of foreign atoms, often impurities, in the host lattice of a crystalline material. These atoms may substitute for atoms already present in the lattice or occupy interstitial sites. If enough atoms are incorporated in a sufficiently ordered fashion then a new crystalline species can evolve. A solid solution will only be stable if there is an overall reduction in free energy from that of the parent phase or phases. Oxide systems are capable of forming both continuous series of solid solutions as a function of composition, e.g. $\text{MgO-N}_2\text{O}$, or several discrete, intermediate, crystalline phases which may have varying degrees of long range order, e.g. $\text{MgO-Al}_2\text{O}_3$. A full discussion of solid solutions is given by Kingery (16).

1.3 The Role of TiO_2 as a Nucleating Agent

The exact mechanism by which small additions of titanium dioxide (TiO_2) enhance nucleation is not fully understood but the phenomenon was first discovered by Stookey (17). He found that for several glass compositions the addition of 2-20 wt% of TiO_2 was effective in promoting nucleation.

Buzhinskii et al (18) working on glasses in the spodumene field

containing TiO_2 used optical and electrical techniques to monitor changes in the physical properties of these glasses when heat-treated in the range $550\text{--}900^\circ\text{C}$. They suggested that very fine particles of rutile titania or titanate compounds precipitate on cooling of the melt which are difficult to detect and which do not appreciably alter the properties of the glass. Subsequent heat-treatment of the glass in the region of the annealing temperature results in the formation, on these nuclei, of small droplets of a glassy phase which differ in composition from that of the parent glass. A conclusion was reached that structural changes within the droplet phase led to the formation of a crystalline lattice only after considerable amounts of this phase had separated out. Further support for this idea of "precipitated crystallites" is given by Blinov (19) who included TiO_2 as a nucleating agent in $\text{Li}_2\text{O--Al}_2\text{O}_3\text{--SiO}_2$ and cordierite glasses. He suggests that the precipitation of a crystalline compound isomorphous with the major crystalline phase occurs at temperatures which are $70\text{--}90^\circ\text{C}$ below those at which the major phase first appears. It was also suggested, for example, that the formation of $2\text{MgO} \cdot 2\text{TiO}_2 \cdot 5\text{SiO}_2$ would precede the growth of cordierite ($2\text{MgO} \cdot 2\text{Al}_2\text{O}_3 \cdot 5\text{SiO}_2$) although no X-ray diffraction data were presented as evidence. In conclusion it was proposed that nucleated crystallisation of these glasses was due to the initially spontaneous precipitation of these isomorphous phases and although some microphase separation occurs it is not the dominant mechanism.

A somewhat different view is presented by Ohlberg et al (20) who investigated magnesium alumino-silicate glasses with 7% additions, by weight, of TiO_2 . They noticed that rutile TiO_2 was the last phase to crystallise out which suggested that crystallisation was not catalysed by TiO_2 crystallites. They proposed that the presence of TiO_2 enhances glass-in-glass phase separation and that the subsequent crystallisation of the droplet phases forms finely dispersed nuclei of a titanate compound.

Support for this model is given by the work of Vogel (21,22) who, using electron microscopy, showed the presence of microphase separation as a precrystalline state in many glasses and concluded that this was a fundamental process in the formation of any glass-ceramic. Further support was provided by Vogel and Gerth (23, 24) who developed this work. They suggested that the high cationic charge of titanium enhanced phase separation.

Maurer (25, 26) used light-scattering techniques to study such phase separation in glasses from the $\text{MgO-Al}_2\text{O}_3\text{-SiO}_2$ system with additions of 9 wt% of TiO_2 . Special consideration was given to the intensity and depolarisation of the scattered light. Data from the glass before heat-treatment indicated the possible presence of isotropic scattering centres, i.e. the formation of a droplet phase in the glass. The subsequent large increases in depolarisation of the light from samples heat-treated in the temperature range $725\text{-}770^\circ\text{C}$ coupled with the relatively unchanged scattered intensity was interpreted as the crystallisation of this droplet phase. Evidence of this was given by X-ray diffraction data which showed the development of a magnesium dititanate phase (MgTi_2O_5) and, a comparison of particle size calculated from both line-broadening techniques and light-scattering theory showed good agreement; the sizes being $70\text{-}200\text{\AA}$ over the temperature range investigated.

TiO_2 is considered to be an intermediate oxide (section 1.1) and a limited number of Ti^{4+} ions will be capable of occupying tetrahedral sites in the silicate glass network, i.e. four-fold coordinated. In the crystalline state, however Ti^{6+} ions occupy octahedral sites, i.e. a coordination number of six. Weyl (27) suggested that on cooling a glass melt containing TiO_2 , titanium will assume this six-fold coordination and be expelled from the silicate glass structure. In the presence of a divalent metal oxide, e.g. MgO , which would provide the necessary charge balance to accommodate this change in coordination number, titanium would

be capable of forming another glass phase. Subsequent crystallisation of this phase would result in small crystallites of a titanate phase, e.g. MgTi_2O_5 . Similar ideas have been expressed by Bobovich (28) who studied the mechanism of TiO_2 action in spodumene glasses using Raman spectroscopy and offered a tentative interpretation of the data collected. He suggested that during heat-treatments in the annealing temperature range titanium gradually passes from tetrahedral to octahedral coordination. This was characterised by growth of a band at $\sim 600 \text{ cm}^{-1}$ - ascribed to linked TiO_6 octahedra vibrations - at the expense of the band at 900 cm^{-1} - TiO_4 vibrations. The form of all other bands in the spectra, along with these two, remained unchanged which is characteristic of the glassy state. It was therefore asserted that crystallites, defined as "geometrically ordered regions of definite composition", are not present at this stage. The source of oxygens necessary for this change in coordination could be conceivably supplied by the transfer of lithium ions into the titania containing phase or equally by the conversion of an initially octahedrally coordinated aluminium to tetrahedral or indeed a combination of both. Further heat-treatment would lead to the formation of crystallite nuclei of rutile TiO_2 or a crystalline compound of the form $m \text{Al}_2\text{O}_3 \cdot n \text{TiO}_2$.

Zdaniewski (29), working on glasses in the $\text{MgO-Al}_2\text{O}_3\text{-SiO}_2$ system with additions of 7-9 wt% TiO_2 , observed changes in the physical properties of the glasses over a temperature range immediately below that at which crystallinity was first detected. A colour shift from brown to blue in transparent glass was attributed to partial reduction of Ti^{4+} to Ti^{3+} (30, 31) which resulted in microphase separation and it was suggested that one of the phases may have been rich in titania. This phase subsequently crystallised. Evidence of phase separation prior to observable crystallisation has been noted by several other workers (32-34).

Recent work by Hanada and Soga (35) on glasses prepared from melts in the $\text{Na}_2\text{O}-\text{SiO}_2-\text{TiO}_2$ system would indicate that titanium occupies six-fold coordination in glasses of low TiO_2 content, i.e. $\text{TiO}_2 : \text{SiO}_2 < 1$. Using chemical shifts in X-ray emission spectra they showed that titanium assumed lower coordination, i.e. four-fold, as the ratio $\text{TiO}_2 : \text{SiO}_2$ approached 1 but then reverted to six-fold coordination on further additions of TiO_2 . For glasses containing four-fold coordination, subsequent crystallisation resulted, not surprisingly, in a change to six-fold coordination. Throughout this work the Na_2O content was standardised at 20-25 wt%. Unfortunately, few data were presented from samples which had undergone heat-treatments in the region immediately prior to crystallisation; the results being confined to totally vitreous or predominantly crystalline materials.

It is interesting to consider the results of Hanada and Soga alongside those of Sandstrom et al (36) who concluded that for a binary system of $\text{TiO}_2-\text{SiO}_2$ the ratio of six-fold to four-fold coordinated titanium ions in the glass increased with increasing TiO_2 content. Employing Extended X-ray Absorption Fine Structure (EXAFS) and near-edge analysis techniques, they proposed the existence of two distinct Ti sites within the glass network. The primary site was one occupying substitutional positions in the silicate structure, i.e. tetrahedrally coordinated with a Ti-O bond length of 1.82\AA . A second site with a longer Ti-O bond length of 2.1\AA was shown to be indicative of six-fold coordination. Any comparison of these data must be made with regard to the inclusion of Na_2O as this would almost certainly have some effect on the silicate structure and may have strongly influenced the oxidation state of titanium.

In attempting to summarise the role of TiO_2 in glass systems it would appear that in glasses quenched from the melt titanium is capable of occupying both octahedral and tetrahedral sites in the silicate network or

indeed, a combination of both. The relative proportions of different sites occupied would seem to depend on two main factors:

1. The amount of TiO_2 in the glass composition.
2. The amount and chemical nature of other oxides present in the glass.

There is considerable evidence, as presented, of phase separation acting as a necessary precursor to the formation of crystalline nuclei although the nature of the changes in coordination number of the titanium ion throughout this process is not fully understood. The nuclei formed by the crystallisation of the precipitated phase facilitate the growth of the major crystalline phase constituting the glass-ceramic end product (see section 1.4).

1.4 Phase Development in Cordierite Glasses Containing TiO_2 as a Nucleating Agent

Cordierite glasses can be defined as those with compositions on the $\text{MgO-Al}_2\text{O}_3\text{-SiO}_2$ phase diagram (Fig. 1.3) which will crystallise to yield cordierite ($\text{Mg}_2\text{Al}_4\text{Si}_5\text{O}_{18}$) as the major ceramic phase. Additions of TiO_2 , typically of the order of 5-15% by weight, are sufficient to enhance efficient nucleation (section 1.3). Heat-treatment of these glasses at temperatures just above the annealing temperature, i.e. 800-900°C, will initiate growth of the first crystalline phase which need not necessarily be cordierite. The composition of this phase will be influenced by the nucleation achieved in the glass, but will almost certainly be based on a metastable solid-solution of β -quartz incorporating Mg and Al atoms (section 1.2). On further heat-treatment at elevated temperatures Mg and Al are exsolved or absorbed and can be accompanied by abrupt phase transformations. Hence, phase development in cordierite glasses is a complex process which is strongly dependent on initial glass composition, nucleation and heat-treatments employed. A review of work in this field and an attempt to explain some of the mechanisms involved is now offered.

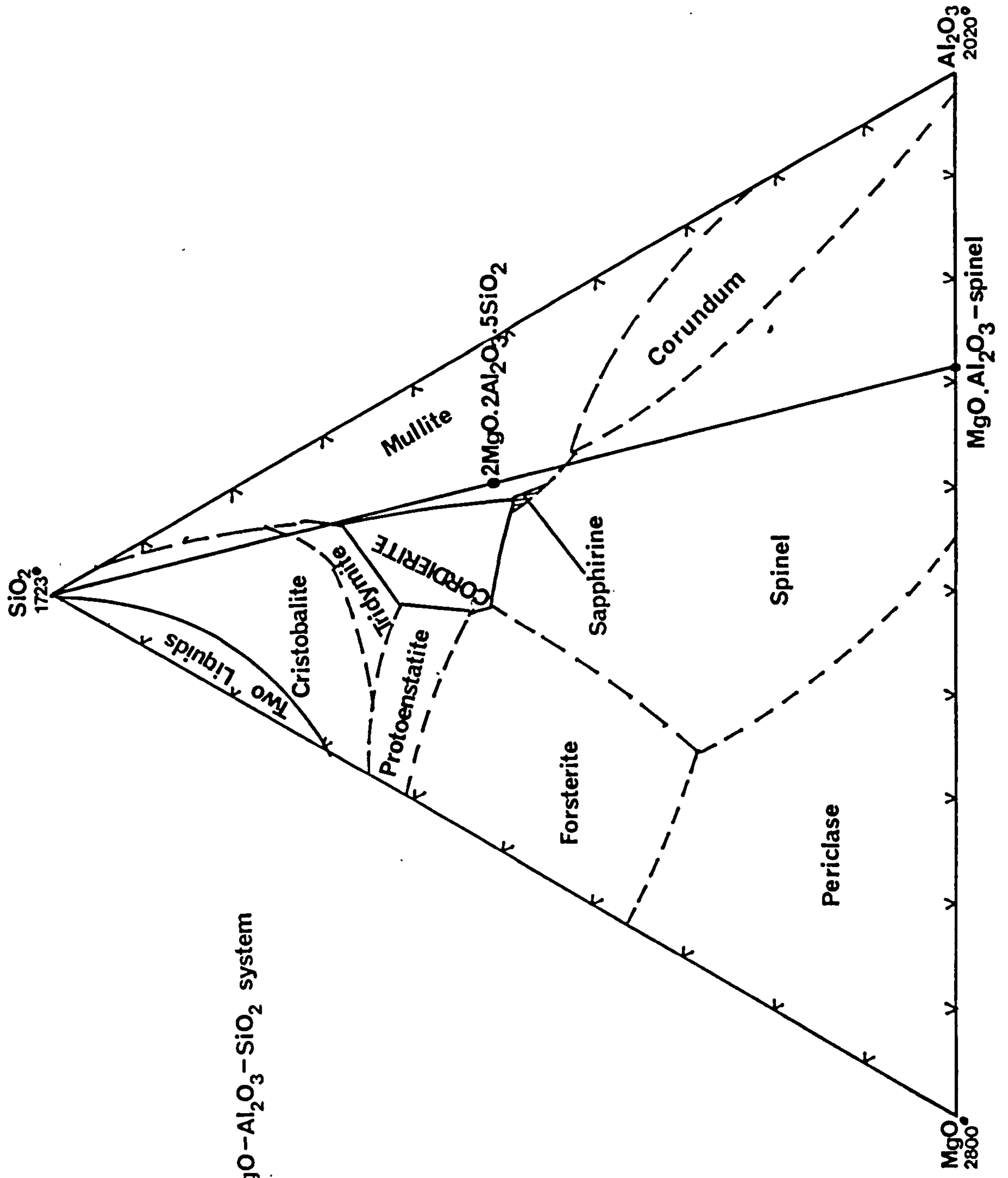


Fig 1.3 - MgO-Al₂O₃-SiO₂ system

The first evidence for the existence of β -quartz solid solutions or "stuffed-quartz" derivatives, as they are frequently called, was presented by Winkler (37) who successfully synthesised a high temperature form of the mineral eucryptite (LiAlSiO_4). Principal reflections on X-ray diffraction photographs showed this compound to have a β -quartz cell with Al substituting for one half of the Si and with Li filling hollow spirals in the lattice in order to maintain charge balance. This phenomenon was confirmed through subsequent work on the $\text{Li}_2\text{O}-\text{Al}_2\text{O}_3-\text{SiO}_2$ system (38-41). According to Winkler, Li^+ ions have a favourable size to enter the quartz structure in interstitial sites whereas Na^+ and K^+ ions are too large. It was thus expected that Mg^{2+} , being almost the same size as Li^+ , could also enter the quartz structure and therefore high-quartz derivatives should exist in the $\text{MgO}-\text{Al}_2\text{O}_3-\text{SiO}_2$ system.

Rankin and Merwin (42), working on this system, discovered what they believed to be an unstable form of cordierite which exhibited a considerable range of solid solution. This compound was also synthesised by Karkhanarala and Hummel (43) who named it μ -cordierite. A comparison of the optical and thermal properties studied and presented by these authors indicated that μ -cordierite had a close structural relation to β -quartz. This was later confirmed by Schreyer and Schairer (44) and by Roy (45). Since the crystalline structures of the various polymorphs of cordierite are drastically different to those of β -quartz and its stuffed derivatives, the term " μ -cordierite" used to describe a quartz solid solution can be misleading. However, for the purpose of this thesis, the term μ -cordierite will be used throughout but it must be noted that the structure of μ -cordierite in no way resembles that of cordierite.

Much early work was carried out on magnesium alumino-silicate glasses which contained no heterogeneous nucleant (e.g. TiO_2). Schreyer and Schairer (46) investigated 46 compositions in the $\text{MgO}-\text{Al}_2\text{O}_3-\text{SiO}_2$ system

and discovered a wide range of quartz solid solutions which could be crystallised in the temperature range 800-1050°C. Of the 10 compositions studied in detail, they concluded that of those lying on the $\text{SiO}_2\text{-Mg-Al}_2\text{O}_4$ (spinel) line (Fig. 1.3) a quartz solid solution (q.s.s.) was the only crystalline phase to appear. However, for a SiO_2 content in excess of 70% residual glass was present at low temperatures and other crystalline species were found to co-exist with the q.s.s. at elevated temperatures. From X-ray diffraction studies on a series of glass compositions based on cordierite ($2\text{MgO} \cdot 2\text{Al}_2\text{O}_3 \cdot 5\text{SiO}_2$) and heat-treated at 900°C for 20 hours they determined a q.s.s. displaying hexagonal symmetry and with lattice parameters $a = 5.20\text{\AA}$ and $c = 5.345\text{\AA}$. The possible existence of reflections corresponding to a doubling of these cell edges - indicative of a multiple cell or long range order - was acknowledged. Variation of the SiO_2 content of these glasses produced a correlation of both a and c with composition (Fig. 1.4) which was rendered only semi-quantitative due to the observed presence of residual glass or other crystalline species. Nevertheless, a general trend towards a high quartz cell with increasing SiO_2 content was noted.

Schulz et al (47) heat-treated a series of pre-powdered glass compositions and, using powder X-ray diffraction, observed shifts in the principal reflections as a function of composition and heat-treatment. In addition they presented evidence for the existence of a superstructure, i.e. long range ordering of the q.s.s. unit cell. This was subsequently confirmed using a precession X-ray photograph technique on single crystals grown from fibres. The main and superlattices were both shown to exhibit hexagonal symmetry with the superstructure being more defined after longer heat-treatments and displaying a periodicity which was dependent on composition but generally of the order of 30 unit cells. In conclusion, it was proposed that in a Mg-Al q.s.s. the Al-Si distribution can be highly

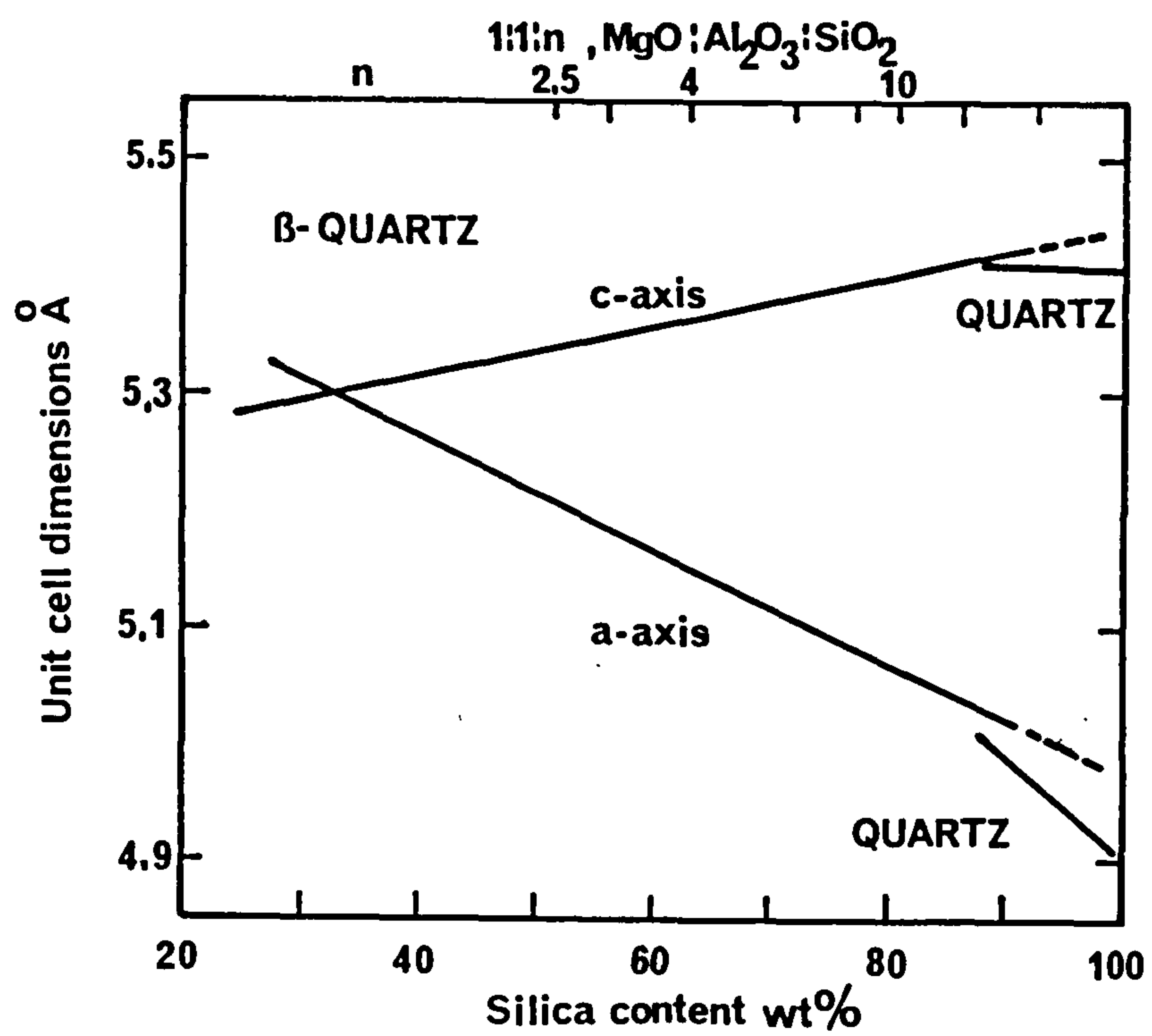


Fig.1.4

ordered and that the lattice parameters and periodicity of the super-lattice are determined by the arrangement of the Mg atoms; the ordering of which increases with both temperature and time over the range 800-950°C but which is destroyed on subsequent heating above 1000°C.

Further work by Schreyer and Schairer (48) led to the discovery of two new metastable compounds in the $\text{MgO-Al}_2\text{O}_3\text{-SiO}_2$ system, both of which are capable of co-existing with the β -quartz solid solution previously mentioned. The first of these was found to be structurally akin to the naturally occurring mineral osumilite ($\text{Na}_2\text{O}.5\text{MgO}.12\text{SiO}_2$) and with a composition close to $\text{MgO}. \text{Al}_2\text{O}_3.4\text{SiO}_2$. This was crystallised from a glass of approximate composition 10% MgO, 26% Al_2O_3 , 64% SiO_2 at temperatures of 1050-1250°C with both cordierite and cristobalite also present. It was deduced that this "osumilite" phase would therefore have a composition lying between cordierite and cristobalite on the SiO_2 - spinel line (Fig. 1.3). X-ray diffraction data for this phase are presented in Appendix I. The second phase discovered had a strong structural relationship to the mineral petalite ($\text{LiAlSi}_4\text{O}_{10}$) and was crystallised from a glass of 20% MgO, 17% Al_2O_3 , 63% SiO_2 between 900 and 1000°C. Co-existence of this phase with q.s.s. and cordierite was again noted. No firm conclusions were reached regarding the chemical composition of this so-called "magnesian-petalite" or Mg-petalite phase but from consideration of substitutions in the petalite lattice of:

- a) Mg^{2+} for Li^+ giving $\text{MgAl}_2\text{Si}_8\text{O}_{20}$ (1:1:8)
- b) $\text{Mg}^{2+} + \text{Al}^{3+}$ for $\text{Li}^+ + \text{Si}^{4+}$ giving $\text{MgAl}_2\text{Si}_3\text{O}_{10}$ (1:1:3) and
- c) 2Mg^{2+} for Li^+ and Al^{3+} giving MgSi_2O_5 ,

it was assumed that the actual composition lay in the ternary phase field bound by these theoretical formulae. X-ray diffraction lines for this

magnesian petalite phase along with those observed by Holmquist (49) are presented in Appendix II.

It should be noted that the glass compositions hitherto mentioned have been based purely on the $\text{MgO-Al}_2\text{O}_3\text{-SiO}_2$ oxide system and have not included TiO_2 as an additional oxide and nucleating agent. The inclusion of titania in cordierite glasses has been shown to modify the mechanism of crystalline phase development in two ways; (i) by lowering the temperature of onset of crystallisations and (ii) where the glasses have been heat-treated at temperatures just above T_g , by strongly influencing the chemical nature of subsequent metastable phases through which cordierite finally grows and hence altering the temperature at which cordierite appears. Some of the more outstanding work concerned with these aspects is now outlined and discussed.

De Vekey et al (50) concerned themselves with a glass composition of 45.7% SiO_2 , 31.1% Al_2O_3 , 12.2% MgO and 11% TiO_2 and through dilatometry and D.T.A. showed that the addition of TiO_2 lowered the temperature of onset of crystallisation. They noted a first exotherm at 950°C which they associated with the formation of a crystalline phase with principal reflections at 3.42\AA , 3.2\AA and 2.075\AA . This phase was tentatively identified as a q.s.s. although the possibility of it being some form of magnesium titanate was not ruled out. A second q.s.s. phase was also found to appear at 950°C with lines at 4.79, 3.33, 2.58, 1.92 and 1.71\AA which persisted to 1140°C . A third phase appeared again at around 950°C with lines at 2.58, 1.92 and 1.71\AA but was not identified. Clearly, the apparently simultaneous existence of three phases two of which may be a q.s.s., presents problems in accurately identifying these phases especially from visual estimates of powder diffraction lines which was the technique employed. Hexagonal cordierite first appeared at 1090°C and increased progressively until 1180°C ; coexisting at this temperature with synthetic

sappharine and a q.s.s. which was different from those encountered at lower temperatures. At 1230°C it was postulated that sappharine and this q.s.s. would react to give further cordierite. At 1260°C TiO_2 in the glass was found to crystallise out as rutile. In addition to this mechanism of phase development it was shown that, if the same glass composition was subjected to a prolonged heat-treatment at temperatures just above T_g then new isotherms appeared at different temperatures to those for the untreated glass. In addition, the intensities and d-spacings of diffraction data were altered and new phases identified, e.g. for an exotherm now appearing at 900°C the crystalline phase or phases existing at this temperature had lines at 4.77, 3.35, 2.69, 2.08, 1.92 and 1.79\AA . This may be due to changes in the packing arrangements and hence lattice parameters of the various solid solutions formed which could be a result of phase separation in the glass prior to nucleation.

Zdaniewski (29) presents a more simplistic sequence of phase developments but for a composition of 64.8% SiO_2 , 18.5% Al_2O_3 , 9.3% MgO and 7.4% TiO_2 . In this work only one DTA exotherm was observed at 930°C and this was confirmed by X-ray diffraction to result from the crystallisation of μ -cordierite. This was the only q.s.s. identified and although limited to 1100°C by the apparatus it was postulated that a further exotherm would appear above this temperature representing the μ to α cordierite transition. On the basis of isothermal heat-treatments in the range 740 - 1200°C both the morphological growth of μ -cordierite and the variation in its lattice parameters as a function of temperature were studied using electron microscopy and X-ray diffraction respectively. The change in unit cell dimensions of μ -cordierite was assumed to be due to substitution of Al^{3+} ions by smaller Si^{4+} ions in the solid solution lattice.

Barry et al (51) based their studies on a glass composition near to the stoichiometric composition of cordierite, i.e. $\text{MgO}:\text{Al}_2\text{O}_3:\text{SiO}_2 = 2:2:5$.

To this base composition they added amounts of TiO_2 ranging from 0 - 11.5 wt%, and observed the crystallisation characteristics using DTA and X-ray diffraction. Only one exotherm other than that for the formation of cordierite was observed at around 950°C , the position and intensity of which was seen to vary with TiO_2 content: no exotherm was observed at this temperature for the composition lacking in TiO_2 . Although unidentified, this peak was assumed to indicate the formation of a q.s.s. whose lattice parameters were seen to vary with both temperature and composition due to exsolution of MgO and Al_2O_3 and in good agreement with the work of Schreyer and Schairer (44). By a dubious manipulation of the proportion of constituent phases to fit a rough visual estimate of X-ray data, a plot of fractional composition against temperature was presented. Although inconclusive, this proved a good indication of the wide variety of phase compositions attainable as a function of the proportion of nucleating agent present. It was proposed that crystallisation to cordierite would occur by exsolution of spinel and sappharine from the q.s.s. and subsequent reaction of sapparine with pseudo-brookite above 1150°C and with the presence of cristobalite.

In conclusion, it would appear that the phase development in a cordierite glass is clearly dependent on initial composition in the $\text{MgO}-\text{Al}_2\text{O}_3-\text{SiO}_2$ phase field but that the crystallisation process within any given composition is indeed very complicated and further influenced by the proportion of TiO_2 present and thermal history of the glass, especially in the pre-nucleation temperature zone.

1.5 Plan of Thesis

This thesis is divided into six chapters and two appendices.

- Chapter 2 - describes the experimental techniques employed with theory where relevant. In some sections a brief review of the application of the techniques to glass and glass-ceramics is included.
- Chapter 3 - gives an account of thermal analysis of the glasses used and presents X-ray diffraction data from an initial heat-treatment schedule.
- Chapter 4 - investigates possible physical and chemical variations between the base glasses as annealed and discusses the findings with reference to glass structure.
- Chapter 5 - presents additional data on further heat treatments and the development of microstructure in partially crystallised glass-ceramic materials.
- Chapter 6 - is a conclusion in which the salient features of this work are summarised and discussed in the general context of phase development and transformations.
- Appendix 1 - deals in brief with the theoretical origins of spinodal decomposition.
- Appendix II - presents X-ray diffraction data of magnesian-petalite phases.

Chapter 2 - Experimental Techniques

2.1 Glass Preparation

Glass was prepared, both at Warwick University and G.E.C. Laboratories, Stafford, adopting the same procedures and having a nominal composition, by weight, of:

SiO_2 - 56%

Al_2O_3 - 20%

MgO - 15%

TiO_2 - 9%

Powder batches of 100-500g were prepared from 'laboratory reagent' grade chemicals and rolled for 16 hrs to produce a homogeneous mixture. Melts were made in platinum crucibles at 1500°C in an electric furnace and refined for 16 hrs before casting into graphite coated steel moulds to give slabs of approximate dimensions 125 x 100 x 25 mm or cylinders of length 100mm x 25mm diameter. On casting, glasses were immediately transferred to a muffle-furnace, annealed for 3 hours at various temperatures and allowed to cool slowly. Subsequent inspection of the glasses in polarised light was performed to determine the degree of residual strain and assess the suitability of the annealing temperature and time in this respect. In order to eliminate any surface effects the cast surfaces were removed to a depth of $\sim 2\text{mm}$ by grinding and test samples were cut from the resulting blocks and cylinders.

2.2 Heat-treatments

The majority of results presented in this work were obtained from glass samples provided by G.E.C. Stafford Laboratories in approximately 500g batches. Initially an annealing schedule of 675°C for 3 hours was used on their advice. Subsequent analysis of this glass by differential

scanning calorimetry (DSC - section 2.4.) showed T_g to be in the region of 720°C and in order to investigate the effects of annealing above T_g a further annealing temperature of 750°C was employed for 3 hours. The resulting effect on subsequent phase development prompted the use of a third and intermediate annealing temperature, i.e. 710°C (also for 3 hours).

In addition to these glasses, two 100g batches of the same composition were prepared at Warwick under similar conditions and separately annealed at 675°C and 750°C for 3 hours. This was felt to be necessary as a check on production variables, especially composition. Simultaneous heat-treatment of equivalent G.E.C. and Warwick glasses showed identical results and therefore the preferably larger batches of G.E.C. glasses were used exclusively throughout.

Further heat-treatments were carried out in the front-loading muffle-furnace represented schematically in fig. 2.1 and whose temperature profile along the axis X-X was determined for various set temperatures. Plots of observed temperature as a function of distance into the furnace are shown in fig. 2.2. Test samples were placed in the pre-heated furnace in close proximity to the monitoring thermocouple and in a region of the furnace displaying the least temperature gradient. The output of the monitoring thermocouple was recorded throughout heat-treatments. On completion, samples were left to cool slowly in the furnace.

2.2.1 Nomenclature

As only one composition was used throughout, base glasses will be referred to by the temperature at which they were annealed, i.e. 675, 710 and 750 glass respectively. Additional heat-treatments will be identified by the temperature at which they occurred and their duration, e.g. 710/825/4, represents 710 glass subsequently heat-treated at 825°C for 4 hours.

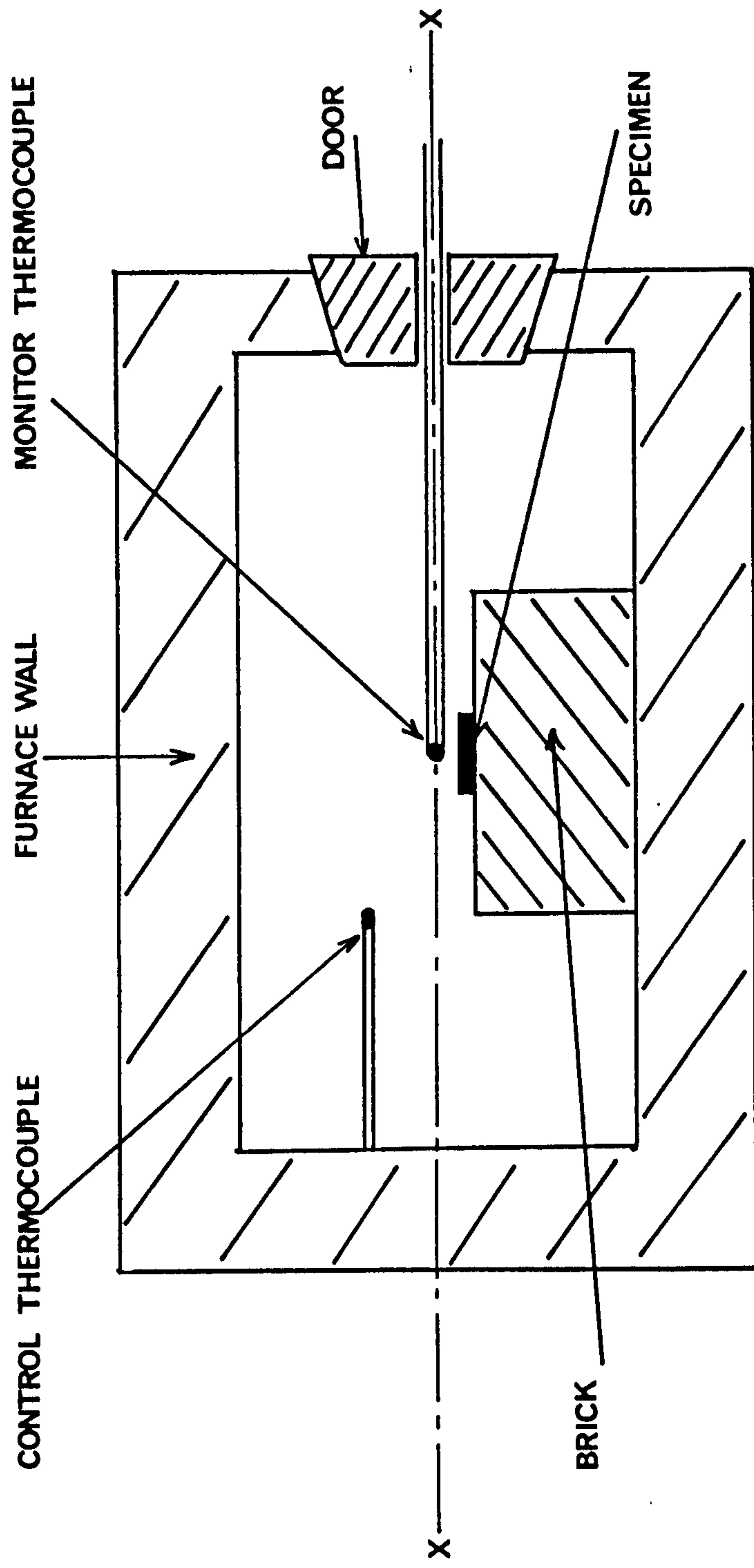
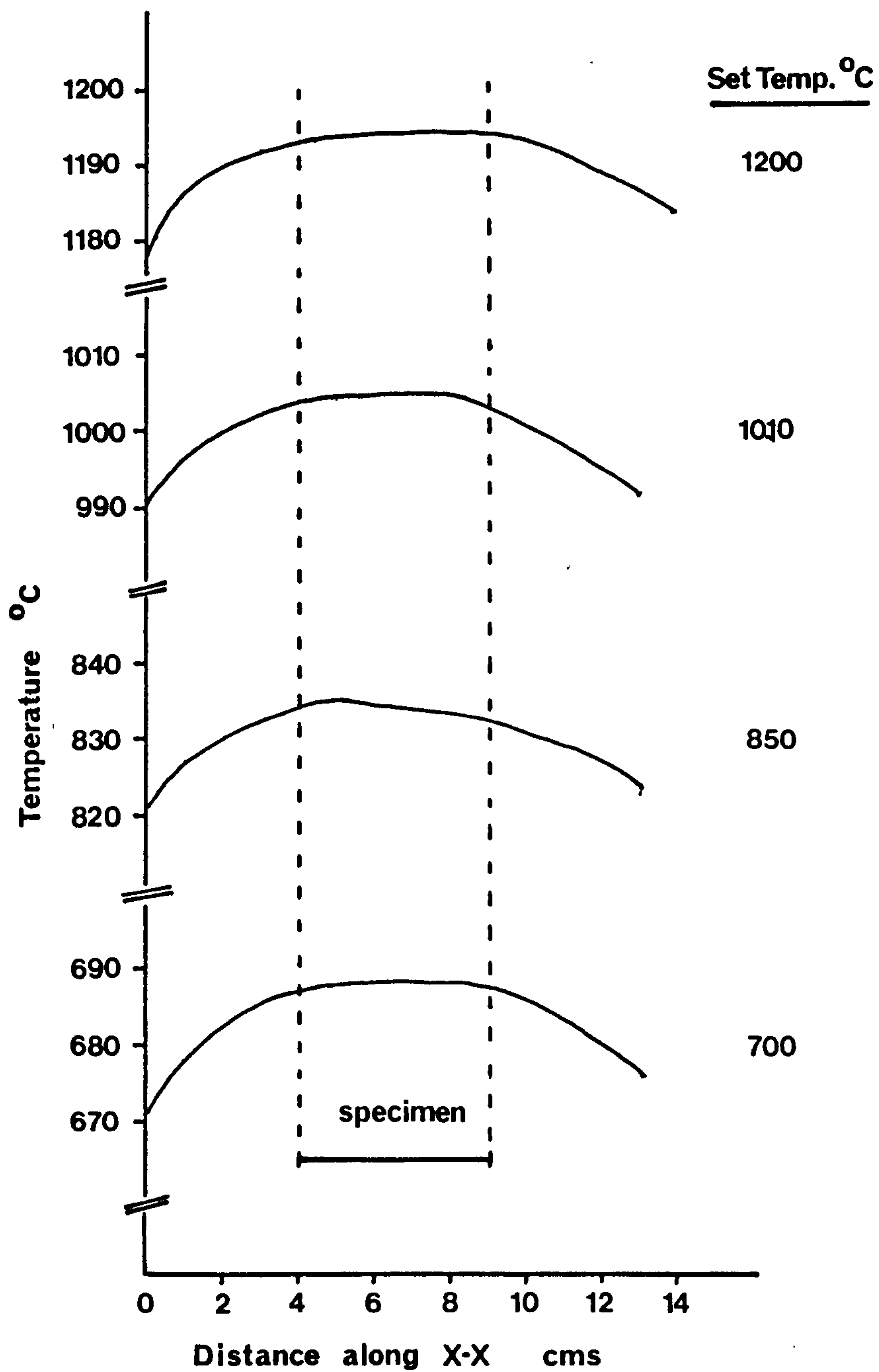


Fig.2.1 – Heat-treatment furnace



Temperature variation over specimen region $\sim 1^{\circ}\text{C}$

Fig.2.2

2.3 Differential Thermal Analyses (DTA)

DTA involves the detection of heat flows which accompany physical or chemical transformations within a material when it is subjected to heating (or cooling). The experimental technique is generally based on the heating of both specimen and reference with the opposing halves of a differential thermocouple embedded in each. The reference is chosen so as to be inert over the temperature range under investigation so that any observed effects are due only to the specimen.

For a typically exothermic transformation e.g. crystallisation, the onset of the reaction causes the temperature of the specimen to rise steadily. The resulting temperature difference between specimen and reference is registered as an e.m.f. in the differential thermocouple and can be recorded. The highest value of this e.m.f. is represented by a peak on the DTA curve and corresponds to a maximum in the rate of reaction. The positions of peaks with respect to the reference temperature and their shape are influenced by two main factors viz. particle size and heating rate and can now be considered separately.

2.3.1 Particle size

Specimens for DTA generally take the form of fine powders which allow good thermal contact with the thermocouples in the DTA cells. The effect of particle size on the nature of thermograms has been the subject of some investigation (52-55). However, most of these studies were conducted using clays whose complex structures can be assumed to change significantly as a function of particle size. For the purpose of this thesis, particle size was only considered significant if surface crystallisation was occurring when the increased surface areas of finer powders would have a marked effect. The inclusion of TiO_2 as a nucleating agent would be expected to promote bulk crystallisation of the glass and hence the effects of particle size would be minimised.

2.3.2 Heating rate

The effect of heating rate on peak shape can be explained by considering the difference in temperature, ΔT , between specimen and reference, and the resulting magnitude of the differential e.m.f. For a low heating rate there will be sufficient time for any temperature differences to equalise as a result of heat flow across the DTA head-block and therefore ΔT will be small. This results in a flat peak which is spread over a considerable temperature range. Increasing the heating rate will increase ΔT giving rise to sharper peaks. However, if an excessively high heating rate is used then loss of thermogram detail can occur e.g. the resolution of two peaks lying close to each other on the temperature axis. In this case there may be insufficient time for the specimen and reference temperatures to equalise between reactions and the peaks may appear partially overlapped or as one broad peak. The necessity for a finite heating rate in DTA means that observed peaks for a given reaction will generally occur at higher temperatures than those reported for the same reaction under isothermal conditions. This is due to heat transfer from the head-block to the specimen and temperature differences of 3-12°C have been observed (56). Shifts in observed peak temperatures will be more marked as the heating rate increases.

2.3.3 Application of DTA to the determination of reaction kinetics

For a glass system which crystallises via a nucleation and growth process the fraction transformed at a time t , $n(t)$ can be expressed by the Johnson-Mehl-Avrami (57, 58) equation i.e.,

$$n(t) = 1 - \exp(1 - Kt^n)$$

where n is an exponent which reflects the nucleation rate and growth morphology and K is a rate constant which would be expected to exhibit

an Arrhenius temperature dependence:

$$K = K_0 \exp \left[-Q/kT \right]$$

where Q is an activation energy, T the absolute temperature and k Boltzmann's constant.

For constant heating rate modes, activation energies can be determined by the Kissinger (59) method. The temperature, T , at which a given fraction is transformed, is related to the heating rate, H , by the following expression;

$$\ln \left[\frac{H}{T^2} \right] = \frac{-Q}{kT} + C$$

Hence the activation energy can be calculated from the dependence of the crystallisation onset or peak temperature on heating rate. Henderson (60) has shown the fraction transformed to be a constant at the peak maxima for a given glass.

2.3.4 Applications of DTA to the glass-ceramic process

Investigations of crystallisation in glass-ceramics are widespread. Briggs and Carruthers (61) have used DTA in conjunction with hot-stage microscopy to determine crystal growth kinetics for a $\text{CaO-MgO-Al}_2\text{O}_3\text{-SiO}_2$ system. Matusita et al. (62) have studied the effect of added oxides on the precipitation of lithium disilicate crystals from the $\text{Li}_2\text{O} - \text{SiO}_2$ system. The crystallisation of cordierite glasses containing additions of WO_3 and V_2O_5 was investigated by Gregory and Veasey (63) using predominantly DTA techniques. The oxide additions were found to have a marked effect on the thermogram for the base glass. Barry et. al (64) looked at the role of TiO_2 as a nucleating agent in $\text{Li}_2\text{O} - \text{Al}_2\text{O}_3 - \text{SiO}_2$ glasses and more recently (65) the growth of cordierite from the $\text{MgO} - \text{Al}_2\text{O}_3\text{-SiO}_2$ system with additions of both TiO_2 and ZrO_2 . The onset of crystallisation was in both cases shown to be lowered as a function of the weight percentage of nucleating agent.

2.3.5 DTA apparatus

DTA measurements were made using the apparatus represented schematically in fig. 2.3. Powders were contained in platinum crucibles which were matched in weight to 0.05g. Temperatures were measured using Pt/Pt.13% Rh thermocouples with the head temperature recorded by a digital thermometer accurate to $\pm 5^{\circ}\text{C}$ over the range 500–1300°C. The linearised output of this was fed to one channel of the chart recorder with the differential e.m.f. fed via the fixed-gain amplifier to the other.

2.3.6 Experimental procedure

Glass cullet was prepared by crushing in a percussion mortar after which a strong magnet was used to extract any steel particles which may have been introduced at this stage. The cullet was finely ground and different particle size categories obtained by sieving i.e. 85–200 mesh (150 – 75 μm) and less than 200-mesh. Powdered 'Analar' Al_2O_3 was adopted as a standard.

A fixed mass (0.4g) of powder was packed gently into the crucibles using a rounded glass rod. Samples of 675-glass of the two particle sizes were subjected to a heating rate of $5^{\circ}/\text{min.}$ and in the absence of any significant difference in thermograms a particle size of 85–200 mesh was adopted as standard. All glasses were subjected to heating rates of 2° , 5° and $10^{\circ}/\text{min.}$, the results of which are presented in section 3.2. Where possible peak identification was attempted by rapidly quenching samples from temperatures at which the corresponding reactions were taking place and analysing these by X-ray diffraction (section 2.5).

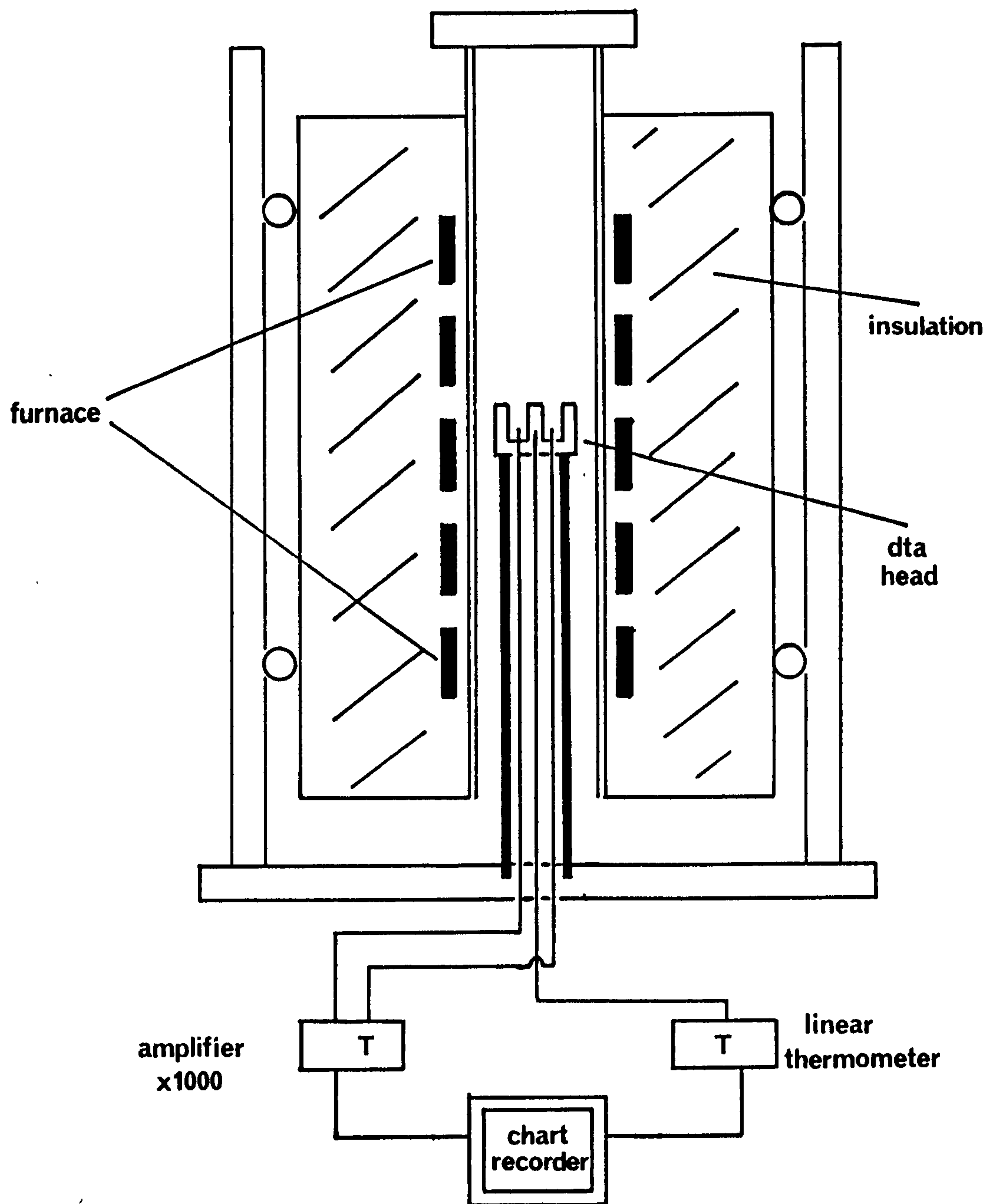


Fig.2.3 - DTA apparatus

2.4 Differential Scanning Calorimetry (DSC)

DSC, like DTA, is a comparative technique but differs in the way in which heat flows are detected. In DSC, the rate of heat evolved or absorbed by a sample, compared with an inert standard, can be measured directly as a function of temperature or time. The result is a more reproducible and sensitive technique, as many of the problems involving temperature measurement are removed. Measurement of heat flow and hence heat content of a sample allows many important thermodynamic parameters to be calculated whilst measurement as a function of time may give information about the kinetics of phase transformations.

Experiments were carried out using a SETARAM DSC with an upper temperature limit of around 800°C. This severely limited studies on the glass samples but information about T_g was obtained. Both powdered (85-200 mesh) and solid samples were used and contained in matched platinum crucibles. Samples were analysed against an alumina powder standard.

Isothermal studies were attempted over the temperature range 750-800°C but met with little success due to the lack of a significantly large phase transformations in these glasses at these temperatures.

2.5 X-ray diffraction

This is a very well established technique and will therefore not be discussed in detail. A full treatment of both X-ray scattering theory and experimental applications is given by Klug and Alexander (66). The essential conditions for diffraction from a crystalline solid are those which satisfy the Bragg equation:

$$n\lambda = 2d \sin \theta$$

where λ is the wavelength of incident X-rays, $2d \sin \theta$ is the path difference on diffraction and n the order of the reflection. Analysis of

diffraction data yields values for the inter-planar spacings, d , within a crystal which can be compared with the standard ASTM powder file to identify crystalline species present.

2.5.1 Calculation of crystallite-size from line broadening

An extensive treatment of the theory of line-broadening calculations is again given by Klug and Alexander (66) but the essential points for determination of crystallite size are summarised below. Scherrer (67) first related the mean dimension, D , of crystallites to the pure X-ray diffraction broadening, β , by the equation,

$$D = \frac{K\lambda}{\beta \cos \theta},$$

where K , the crystallite shape factor is of the order unity; its exact value being dependent on the way in which β and D are defined. The accuracy with which the Scherrer equation can be applied is limited by uncertainties in both K and β .

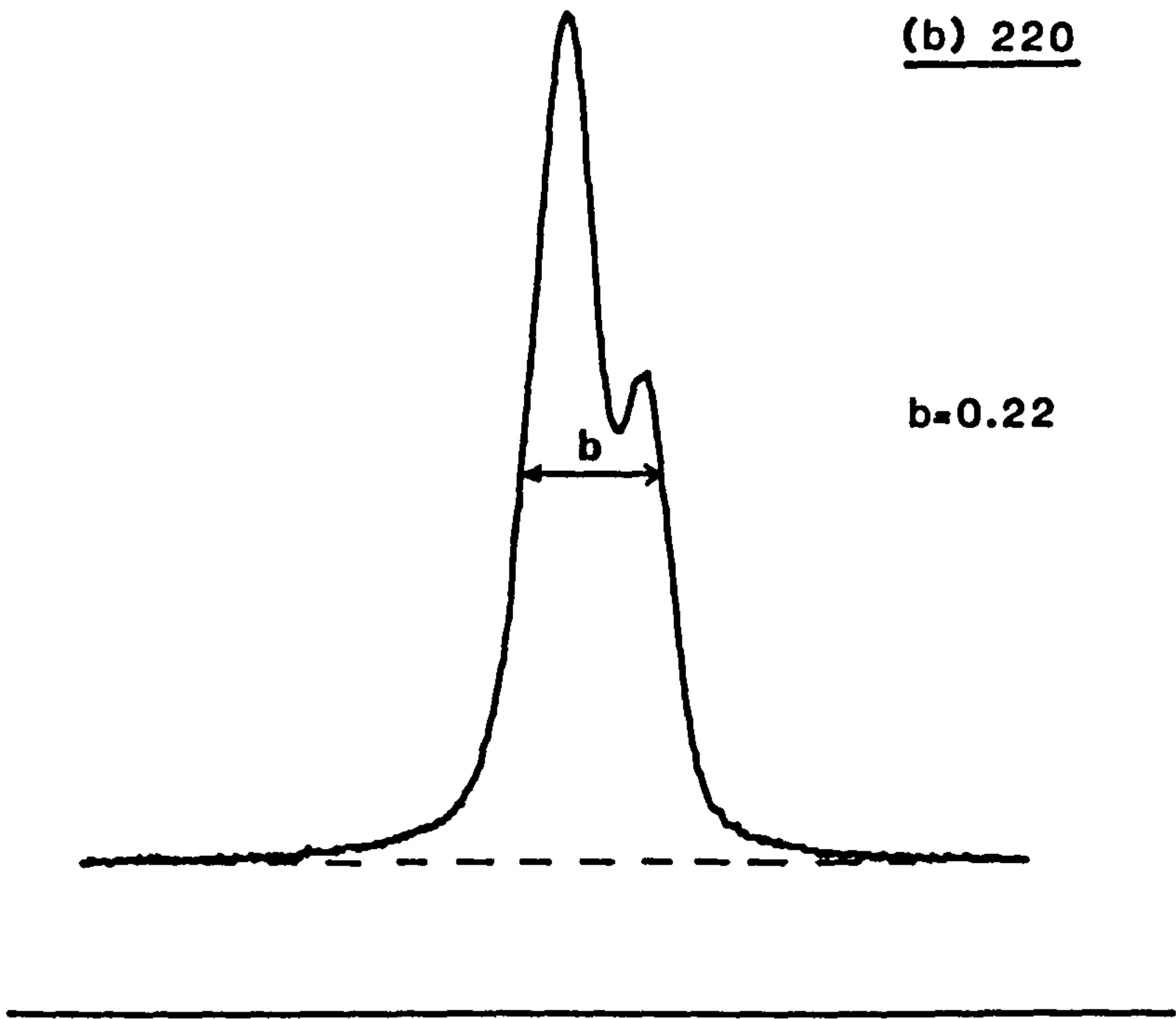
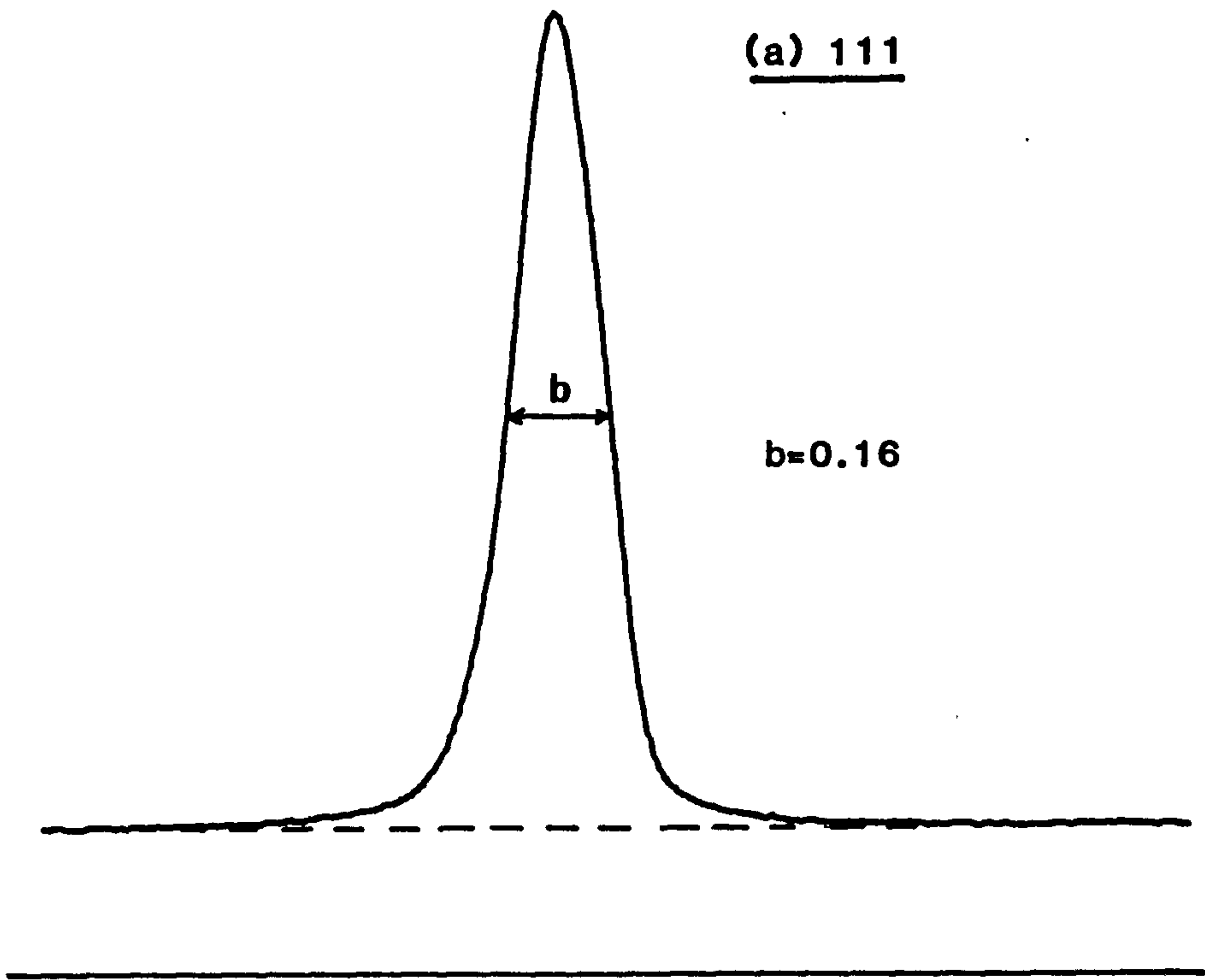
β can be expressed as the difference between observed line breadth, B , and the breadth, b , of a line produced under similar geometrical conditions by a material with a crystallite size in excess of 1000\AA

$$\text{i.e. } \beta = B - b$$

For the purpose of this work b was taken to be the width at half peak height of the (111) and 220) reflections from a polycrystalline silicon standard at 28.4° and 47.3° 2θ , fig. 2.4. The observed values were 0.16° and 0.22° 2θ respectively and were used to correct for instrument broadening at these angles. Although $K\alpha_1$ and $K\alpha_2$ lines were partially resolved in the Si standard (fig. 2.4(b)), this was not the case for any of the crystalline materials analysed in this work and hence no further correction was made in respect of this.

In the absence of any knowledge of their morphology, crystallites were assumed to be approximately spherical and a value of 0.9 assigned to K . Previous work (66-70) has shown this to be adequate providing β is

Fig.2.4 - Line broadening of Si standard



defined as a half-maximum line breadth ($\beta_{\frac{1}{2}}$). Hence the crystallite size equation may be written as:

$$D = \frac{0.9\lambda}{\beta_{\frac{1}{2}} \cos \theta}$$

This equation was used for subsequent calculations.

2.5.2 Experimental procedure

X-ray analyses of samples were carried out on a standard Philips diffractometer. In this instrument the specimen holder (θ drive) and detector (2θ drive) rotate about the same axis in the same direction and at a speed ratio of 1:2 in order to maintain conditions for Bragg reflections. Scanning speeds of $\frac{1}{8}^{\circ}$ to 2° 2θ /min were available of which 1° 2θ /min was found to be adequate for most predominantly crystalline materials. For glassy specimens or where improved peak resolution was required the slowest speed ($\frac{1}{8}^{\circ}$ /min) was employed. Specimens were prepared as either rectangular blocks (20 x 15 x 5 mm) or discs (25mm diameter x 5 mm) and mounted in aluminium holders; the flat surface of the specimen being flush with the machined faces of the holder. For the powdered samples used in the identification of DTA peaks, the powders were packed into the window of the holder with a small amount of binder. Specimen and beam alignment was performed as specified in the manufacturer's manual (71). Cu $K\alpha$ radiation from an X-ray tube operating at 40kV and 30mA was used throughout. Data were collected on a single-pen chart recorder or suitably interfaced PET computer. Identification of crystalline samples was made with reference to the ASTM powder file.

2.6 Scanning Electron Microscopy (SEM)

SEM is a well established technique and will therefore not be discussed in detail. A complete account of SEM in terms of instrument performance

is given by Bowen and Hall (72). The present studies were conducted on both Cambridge IIA and S250 instruments at accelerating voltages of typically 20keV. Specimens were prepared from bulk samples by the following two methods:

1. a fracture surface of the material was lightly etched in 5% HF solution for durations of typically 10-60 seconds.

2. a flat ground and polished surface was prepared to a $1\mu\text{m}$ finish and lightly etched as above. Both types of specimen were coated to a thickness of $\sim 20\text{nm}$ with gold or carbon to prevent surface charging. The fine scale of the microstructure generally encountered during this work ($\sim < 0.1\mu\text{m}$) resulted in poor topographical contrast and this, coupled with the generally small amount of atomic number contrast, imposed severe limitations on the use of SEM in both secondary and back-scattered modes and the use of TEM (see section 2.7) was preferred.

2.6.1 Energy Dispersive Analysis of X-rays (EDAX) in SEM

Although SEM was limited in its application to this work in terms of imaging, rapid bulk chemical analyses of glasses could be made as a first check on possible compositional discrepancies. An EDAX detector coupled to an EDAX 9100 microcomputer allowed rapid collection of spectra over the energy range 0-20keV.

For a thin section of material containing two elements, the relationship between their relative concentrations, C_1/C_2 , and the ratio of their observed X-ray intensities, I_1/I_2 , can be expressed as

$$\frac{C_1}{C_2} = K_{12} \frac{I_1}{I_2}$$

where K_{12} is a correction factor for ionisation cross-section, fluorescence yield and detector efficiency for X-rays from the two elements. For a multi-component system there will be a set of K-values. These are known as the atomic number corrections and are often written as Z. Subsequent

analyses of spectra for bulk specimens require additional lengthy corrections for absorption (A) and secondary fluorescence (F). Application of the full ZAF correction allows the composition as weight percentages of elements or oxides to be determined.

Flat, polished, carbon-coated specimens were used at an accelerating voltage of 20keV and an X-ray take-off angle of 39° . Under these conditions an accuracy of $\sim \pm 5\%$ can be expected. Ten different areas of each specimen were analysed, the size of which were typically $\sim 300\mu\text{m}$ square.

2.7 Transmission Electron Microscopy (TEM)

A full description of the transmission electron microscope and the physical principles behind many of the observed phenomena are beyond the scope of this thesis; instead the relevant chapters of Bowen and Hall (72) are referred to. However some of the more relevant aspects of TEM to this particular work are discussed briefly below.

2.7.1 Modes of contrast

The modes of contrast most commonly encountered in TEM are those of absorption and diffraction. Absorption contrast relies upon the fact that the elastic and inelastic scattering of fast electrons is dependent on atomic number and thus regions of a specimen with a high atomic number will scatter more of the incident electron beam through angles which are excluded from the image by the objective aperture and therefore appear dark. In glassy specimens this is the predominant mechanism contributing to contrast and the degree of contrast exhibited by, for example, a phase separated structure will depend on the difference in average atomic number between the two phases which may be slightly enhanced by a reduction in the objective lens aperture.

In specimens containing crystalline material there exists an additional mechanism of contrast i.e. that resulting from the coherent scattering or diffraction of electrons by the crystalline lattice, viz.

diffraction contrast. If the lattice planes are in such an orientation with respect to the incident beam so as to satisfy conditions for a Bragg reflection then strong scattering will result in all the electrons in the incident beam being scattered into a diffracted beam. If only the transmitted beam is allowed to pass through the objective aperture then the image from this particular region of the specimen will appear dark. As the specimen is tilted away from the Bragg reflection then the intensity of transmitted beam will increase with a concurrent reduction in contrast magnitude. In a polycrystalline specimen where individual grains have different orientations only a small proportion may be observed for a given angle of specimen tilt and in the absence of sufficient absorption contrast may be indistinguishable from any glassy matrix present.

2.7.2 Selected area diffraction

By parallel illumination of a crystalline specimen the resulting diffracted beams will be travelling parallel to each other and can be suitably focussed to give a diffraction pattern on the viewing screen. By inserting a selected area aperture the source of diffracted beams can be confined to this area and hence the diffraction pattern formed will be characteristic of the feature isolated by this aperture. This can be checked and confirmed by imaging one of the diffracted beams using the objective lens aperture. In the resulting dark-field image only the diffracting feature will have any appreciable contrast. Hence the orientation and symmetry of crystals within a material may be identified using this technique.

2.7.3 Experimental procedure

All observations were made using a JEM100C instrument with an accelerating voltage of 100kV on thin sections of materials. The methods of preparing thin sections are numerous but only those most suitable for

specimen preparation from glass and glass-ceramic materials were utilised and are as follows:

(a) Ion beam thinning

Parallel slices, $\sim 300\mu\text{m}$ in thickness, were cut from bulk specimens using a diamond saw, and mounted on a brass block with a suitable resin. The slice was then reduced in thickness from both sides to $\sim 50\mu\text{m}$ or less by mechanical polishing using progressively finer grades of abrasive. Several brass specimen rings (3mm diam.) were then adhered to the slice and the slice removed from the block. The slice was then trimmed around the outer edges of the rings to release single specimens. These were further thinned to electron transparency ($\sim 1000\text{\AA}$ for these materials) using ion beam thinning. This technique is fully discussed by Glauert (73) and is essentially the removal of material from specimen surfaces by bombardment with Argon ions accelerated by voltages typically 4-6kV in magnitude.

(b) Crushing and grinding

Materials were crushed and ground with an agate pestle and mortar and a fine suspension of these particles was prepared in amyl acetate with a small addition of adhesive. The suspension was allowed to settle partially before samples from the upper portion were pipetted onto carbon-coated copper grids. Although this method provides TEM specimens relatively quickly, the quality of these is generally poor in terms of the total useful area available and for the scale of microstructure generally encountered in this work, much fine detail was unobservable. It was therefore decided to restrict specimen preparation to the preceding method (2.7.3(a)).

2.8 Infra-red absorption spectroscopy

The application of this technique depends upon the interaction of electromagnetic radiation in the infra-red (ir) region of the spectrum with the vibrational and rotational states of molecules or molecular groups within a material. The radiation is required to be coupled to these states via a change in magnitude and/or direction of the dipole moment. In liquids and solids the intermolecular interactions result in a general smearing out of rotational modes and modification of the vibrational spectra, analysis of which may yield useful information about the structure of the material. Many comprehensive theoretical treatments of the application of infra-red spectroscopy are available (77-78) along with reviews on the ir region of oxide glasses (75,76). In view of this only the ir absorption of silicates will be discussed here.

2.8.1 Infra-red spectroscopy of silicate glass and glass-ceramic systems

The vibrations of the tetrahedral SiO_4 group may be described in terms of either bending or stretching vibrations. Bending modes involve much smaller force constants and are therefore characterised by much lower frequencies than for stretching modes which are associated with silicon-oxygen bond-stretching vibrations, typically 1100cm^{-1} for Si-O-Si (80). A full review of the interpretation of ir spectra for fused SiO_2 and various crystalline polymorphs is given by Sigel (81) who also discusses the effect of alkali additions. The main feature of ir spectra of alkali-silicates is the appearance of a strong absorption band in the region $940\text{-}950\text{ cm}^{-1}$ at the expense of the 1100 cm^{-1} band. This has been attributed (79,82) to bond stretching of Si-O^- or O=Si-O^- non-bridging oxygen groups which would be expected in a weakened structure.

The infra-red spectra of both glassy and crystalline silicate structures have been widely studied and a comprehensive review is offered by Farmer (83). With particular reference to cordierite glass-ceramic

systems a review by Gregory and Veasey is referenced (84), however, little information on the infra-red spectra of cordierite systems containing TiO_2 is available although many structural changes may be interpreted with reference to the stoichiometric system.

2.8.2 Experimental procedure

Finely ground powdered samples were prepared of which about 0.05g added to approximately 1g of KBr gave a satisfactory dispersion. The resulting mixture was further ground to produce a homogeneous mixture. Discs were pressed in a hardened steel mould at 50 tons/sq.in for 3-5 minutes. Specimens were scanned over the range 4000 cm^{-1} to 200 cm^{-1} with a scan time of 6 mins. using a Perkin-Elmer 983 spectrometer. Spectra were stored on magnetic disc for subsequent analysis. Care was taken to eliminate water bands in the KBr by using previously dried KBr stored in an oven at $\sim 120^\circ\text{C}$.

2.9 UV-Visible - spectrometry

Useful reviews on the optical properties of glasses in the visible and u.v. spectrum already exist (78,81) and a theoretical treatment will not be attempted here. Discussion will be confined to silicate glasses and the influence of titania upon visible absorption and the u.v. edge.

Ti^{4+} is an example of an empty shell d^0 system and in theory would not be expected to exhibit optically absorbing ligand field bands. Several workers (85-88) have observed no visible colouration in sodium silicate and silica glasses containing $< 5\text{wt}\%$ TiO_2 . However, when TiO_2 is present at about $10\text{wt}\%$ a characteristic amber colour is produced (89). Weyl (27) has suggested that this is due to iron impurities in the glass. The presence of TiO_2 is known to reduce the viscosity of a silicate system and he suggests that this allows the Fe^{3+} ion to shift from a relatively colourless modifying site (FeO_6) to a strongly absorbing network position

(FeO_4). This has more recently been disputed by Kurkjian and Sigety (90) who showed Fe^{3+} to be predominantly in tetrahedral coordination even when TiO_2 was not present in the glass. Other workers (91-93) have observed yellowish colouring of TiO_2 - SiO_2 glasses, with $< 10\%$ TiO_2 , which has disappeared on subsequent annealing. This has been attributed to the presence of Ti^{3+} which is oxidised to Ti^{4+} . Ti^{3+} possesses a d^1 electronic configuration and exhibits ligand field transitions; generally producing a strong blue-violet colouration. It is not readily formed in most silicate systems and requires melting in a reducing atmosphere.

Sigel (81) has suggested three factors contributing to the u.v. absorption edge of silicate glasses;

1. Electronic excitations of the Si-O network.
2. Introduction of network modifiers and formers.
3. The presence of transition metal ions.

These are fully discussed and essentially the u.v. cut-off in SiO_2 glass is attributed to an observed band gap at 160nm (8.0eV) and any weakening of the network will result in an average reduction of the chemical bond strengths with a resulting shift in the u.v. edge to longer wavelengths.

2.9.1 Experimental procedure

Parallel slices of glass specimens were ground to a thickness of $900\mu\text{m}$ with a $1\mu\text{m}$ surface finish. Spectra were obtained over the range 900nm to 190nm using a Varian DMS90 spectrometer at a scanning rate of 50nm/min and with a monochromator slit width of 1nm.

As only trends through a series of samples were sought rather than absolute determinations of absorption coefficients, corrections were not made for surface reflectivity, i.e. by comparison of two samples of the same material with differing thickness.

2.10 Density measurements

Elementary density determinations for selected glasses were obtained using Archimedes' Principle which in essence states that the density of a body ρ , can be expressed as

$$\rho = \frac{W_A}{(W_A - W_W)} \rho_i$$

where W_A and W_W are respectively the weights of the body in air and an immersion fluid of known density ρ_i .

A number of bubble-free polished samples of each glass were selected with a mass not less than 3g, ultrasonically cleaned in acetone and allowed to dry at room temperature. All samples were then weighed in air. Distilled water was chosen as the immersion fluid and a density of 1000g/cm³ was assumed. All samples were then weighed and immersed in water using a supporting cradle of 'nichrome wire'. In both cases an Oeterling R20 balance was used and weights recorded to within 0.1mg. Care was taken to check the zero before each measurement. Samples were always immersed to a fixed depth and possible adherence to the surface of air bubbles or contact with the sides of the vessel was monitored. Finally the temperature of the immersion fluid was recorded on both commencement and completion of measurements. Results, along with an appreciation and calculation of errors, are presented in section 4.4.

2.11 Electron paramagnetic resonance (EPR)

Electron paramagnetic resonance occurs in electronic systems which possess a non-zero total angular momentum. If the ground state of the system is split by an imposed magnetic field then transitions between the resulting states can be coupled to microwave electromagnetic radiation to produce resonant absorption. The nature of this absorption is characteristic of the ground state and is affected by the nearest neighbour

coordination. The theoretical aspects of EPR are couched in quantum mechanical terms and such a treatment will not be offered; instead the relevant sections of Wong and Angell (78) are referred.

The three main types of paramagnetic sites in glasses which give rise to an EPR response are (1) radiation induced defects (2) paramagnetic impurities and (3) optically induced paramagnetic states. Of most relevance to the present work is (2) in which paramagnetic transition ions i.e. Ti^{3+} and Fe^{3+} are capable of EPR interaction. Studies of glasses containing both Ti^{3+} and Fe^{3+} by EPR are extensive and the technique has been used not only to confirm the presence of these paramagnetic centres but to gain structural information. Changes in the coordination geometry of these ions on crystallisation is reflected by corresponding changes in the EPR signal.

Room temperature measurements were made on clean, solid samples and g-values calculated by comparison with known standards. The apparatus used was a standard Decca X-band EPR spectrometer and comparative measurements were performed under standardised operating conditions.

2.12 Chemical analysis for TiO_2 and Fe_2O_3

The TiO_2 and Fe_2O_3 contents of glasses were determined by the absorptiometric methods set out in British Standard 2649:Part 2:1957. These essentially involve the dissolution of powder glass samples ($\sim 60\text{mg}$) in acid followed by colouration with specified reagents. The absorptions were measured at $430\mu\text{m}$ (TiO_2) and $540\mu\text{m}$ (Fe_2O_3) and compared with standard calibrations. Several assays were performed to improve accuracy.

Chapter 3 - The observed influence of annealing temperature on subsequent crystalline phase development

3.1 Determination of T_g by DSC

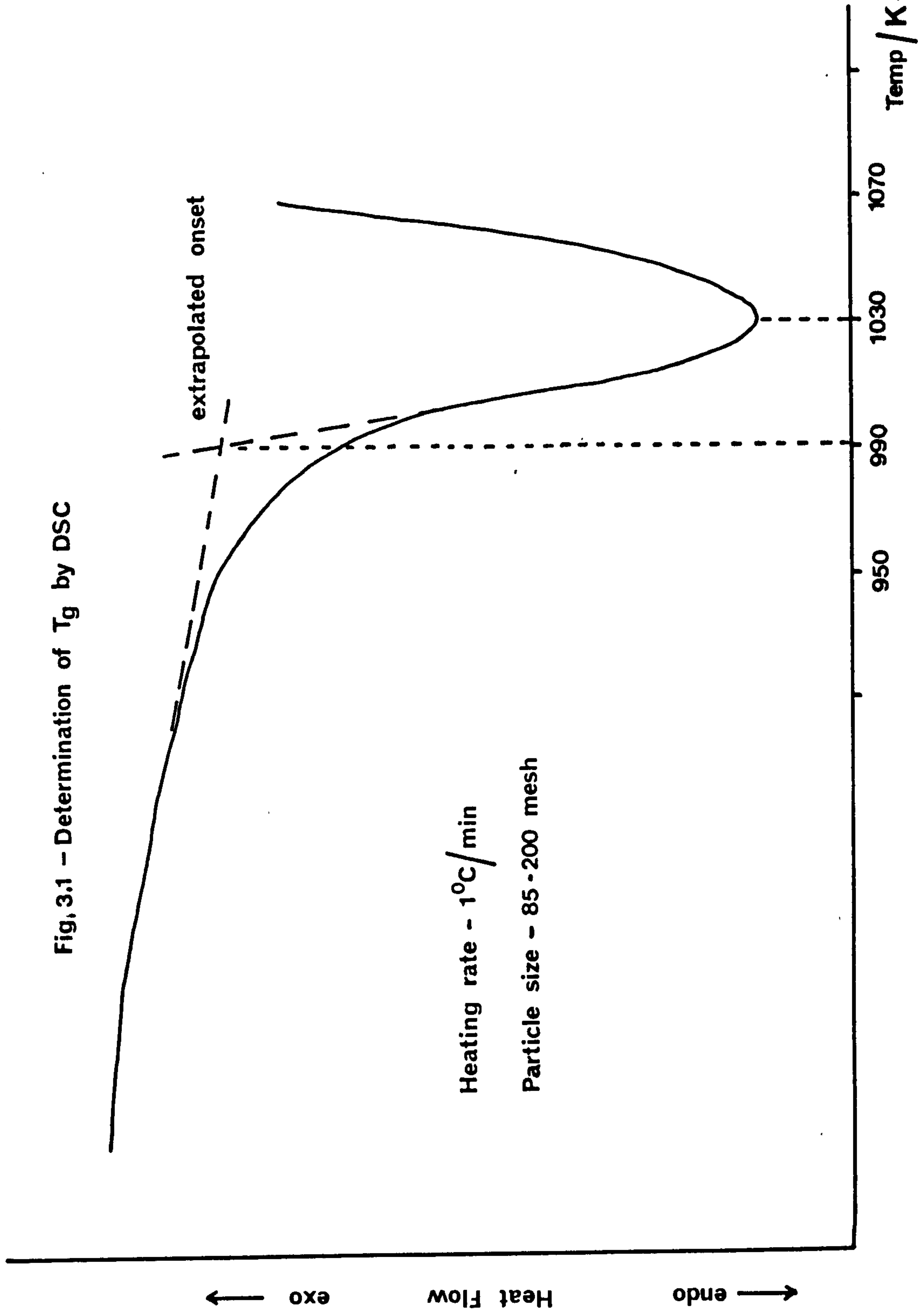
The DSC thermogram of 675-glass for a heating rate of 1K/min over the range 950-1070K is shown in fig. 3.1. T_g was taken to be the extrapolated onset of transformation rather than the peak temperature and determined as 991K, i.e. 718°C.

3.2 DTA studies of base glasses

Figs. 3.2 to 3.4 present DTA thermograms of the base glasses at heating rates of 1° , 5° and 10° per minute respectively. The first observable exotherm in 750-glass was identified by X-ray diffraction as the formation of $MgTi_2O_5$, whereas for 675 and 710-glasses matching of X-ray data was difficult due to the weak intensity and absence of several reflections and a firm identification was deferred. The major exotherm at $\sim 900^\circ\text{C}$ was assigned to the crystallisation of both β -quartz solid solutions viz. magnesian petalite and μ -cordierite. Two separate peaks, corresponding to the formation of the two phases, could not be resolved although the proportions of each phase varied from predominantly μ -cordierite in 675-glass to almost totally magnesian petalite in 750-glass. For samples quenched from the exotherm at $\sim 1050^\circ\text{C}$ the presence of magnesian petalite was undetectable in both 675 and 710-glass whereas in 750-glass, which exhibited no comparable exotherm at this temperature, a sample quenched from 1100°C still contained a small amount of this phase. This may explain the subsequent shift of the last observed exotherm, attributed to crystallisation of cordierite, from 1150°C in 675 and 710-glass to over 1200°C in 750-glass.

It should be pointed out at this stage that the DTA apparatus used was incapable of maintaining a $10^\circ/\text{min}$ heating rate above about 1100°C and a gradual tailing-off in heating rate to $\sim 6^\circ/\text{min}$ at 1250°C occurred

Fig, 3.1 – Determination of T_g by DSC



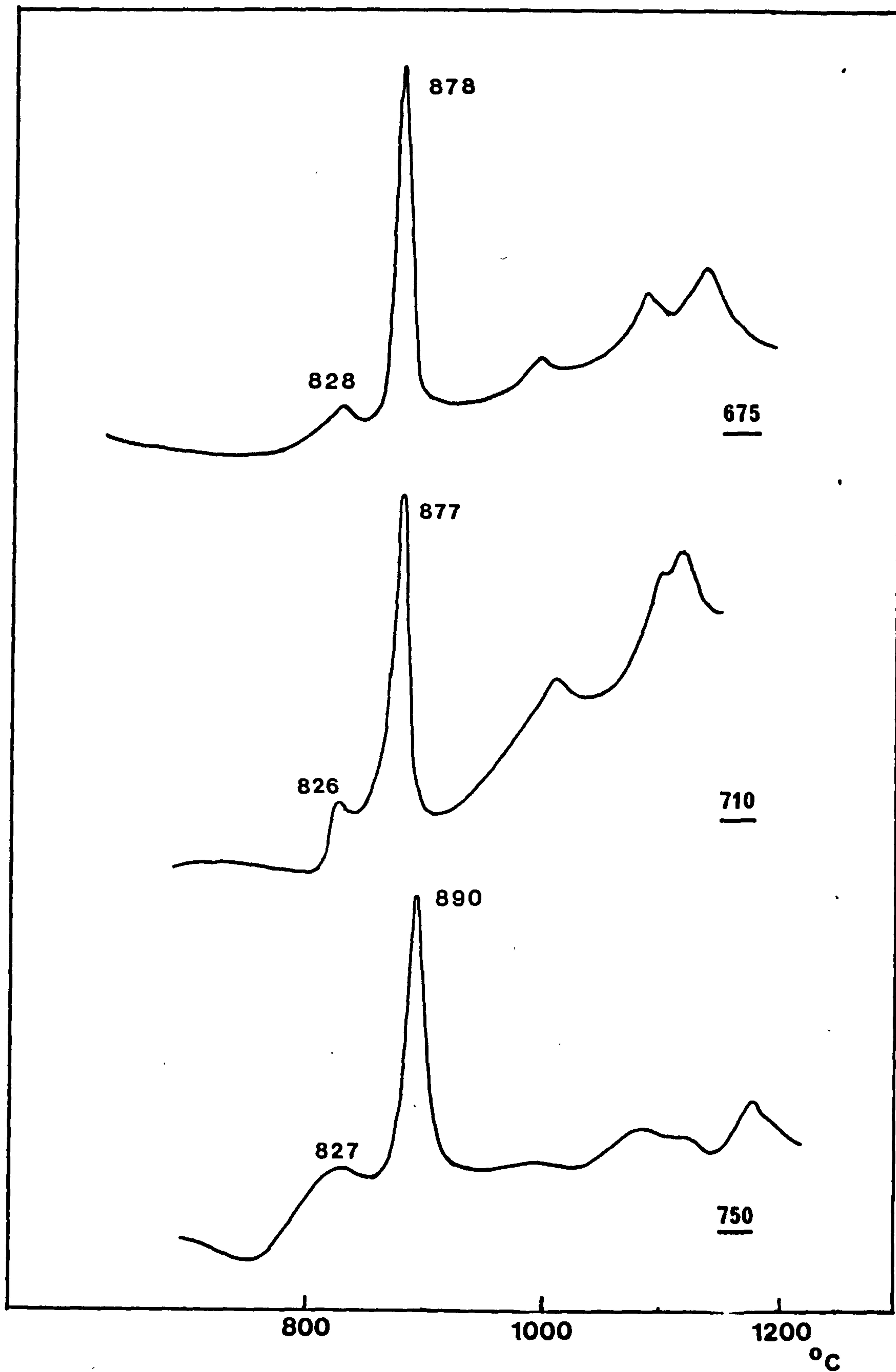


Fig.3,2 - DTA of base glasses at 2°/min

Fig.3.3 - DTA of base
glasses at 5°/min

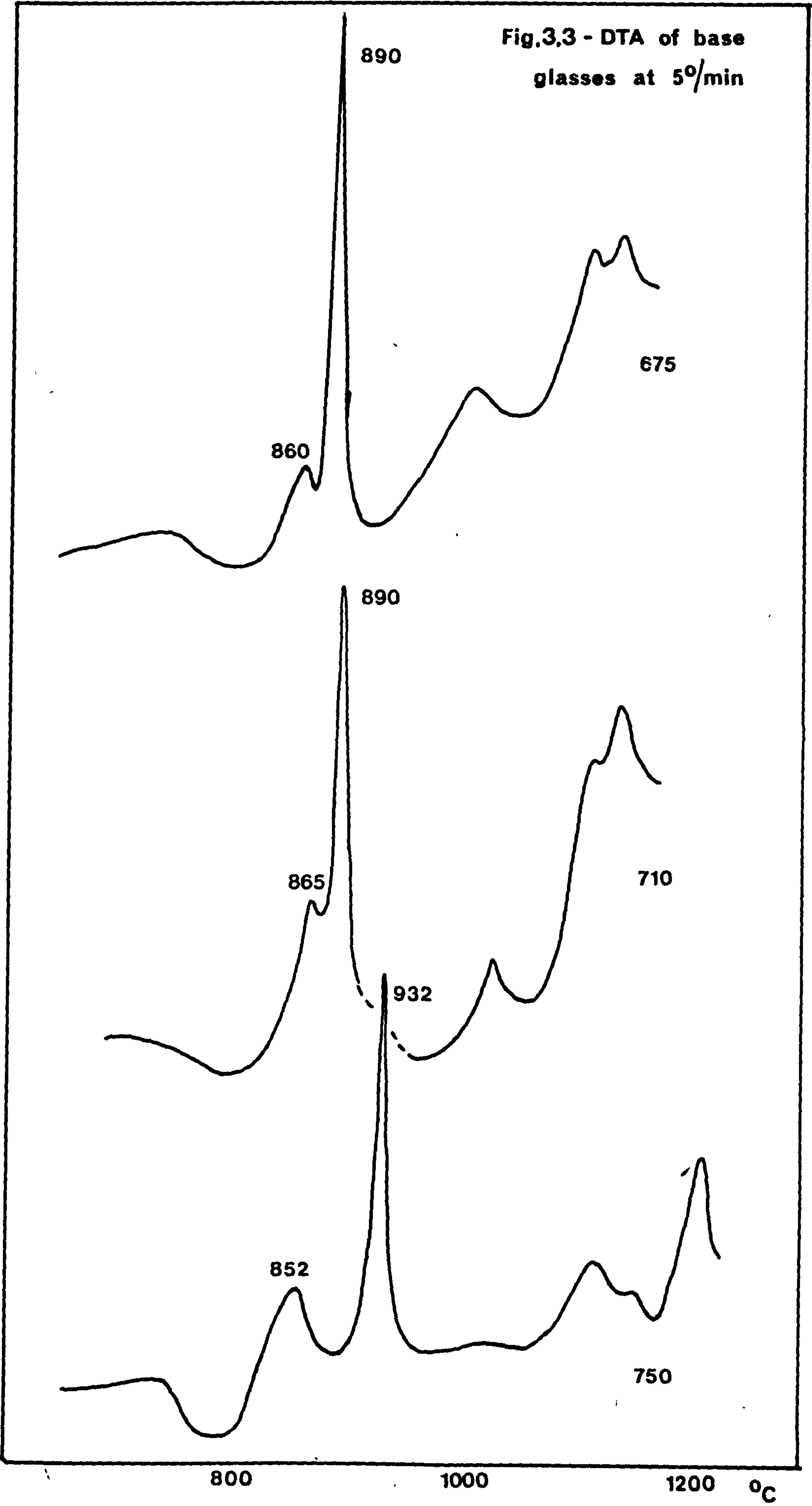
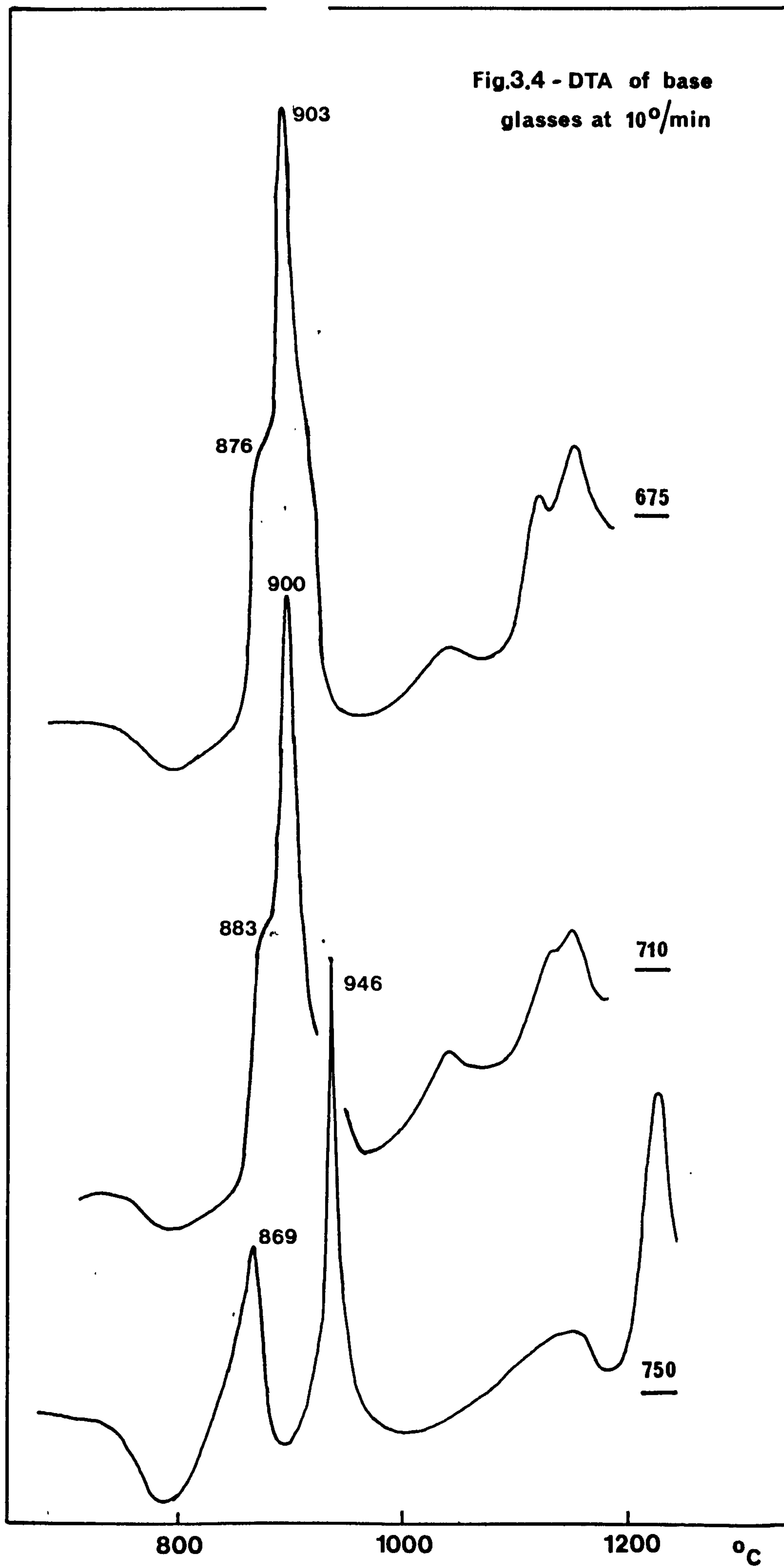


Fig.3.4 - DTA of base glasses at 10°/min



whereupon runs were terminated. In addition, although quenching of specimens yields useful information, the practice should be restrained to prevent excess thermal shock damage to the alumina DTA head. In this case quenching was restricted to one set of runs, i.e. $5^{\circ}/\text{min}$ and an initial drop in temperature of some 200°C was permitted before allowing the head to cool to room temperature at $\sim 15^{\circ}/\text{min}$.

The influence of annealing temperature on the crystallisation characteristics of the glasses under a constant heating rate is clearly mirrored by the variation in shape of the DTA thermograms, especially at heating rates of 5° and $10^{\circ}/\text{min}$. 750-glass is distinguishable from 675 or 710-glass by the lower onset temperature of initial crystallisation and the subsequently higher temperature of bulk crystallisation. However, at a heating rate of $2^{\circ}/\text{min}$ an approach to equilibrium is observed although the major exotherm in 750-glass remains displaced to a higher temperature.

3.3 Calculation of activation energies of crystallisation

Application of the Kissinger method outlined in section 2.6 enabled the activation energies for initial crystallisation to be calculated for the three base glasses (fig. 3.5). For these calculations the value of T in the equation,

$$\ln \left[\frac{H}{T^2} \right] = \frac{-Q}{kT} + c$$

was taken as the peak temperature, T_p , rather than the onset temperature which in the absence of a stable base-line was difficult to assess. An attempt to analyse the formation of the quartz solid-solutions by this method proved unsuccessful with the resulting plots exhibiting considerable non-linearity. This is not unexpected as the Kissinger method is generally only applicable to approximately first order reactions whose kinetics to a large extent obey the Johnson-Mehl-Arrami equation. The seemingly simultaneous crystallisation of magnesium petalite and μ -corderite from an

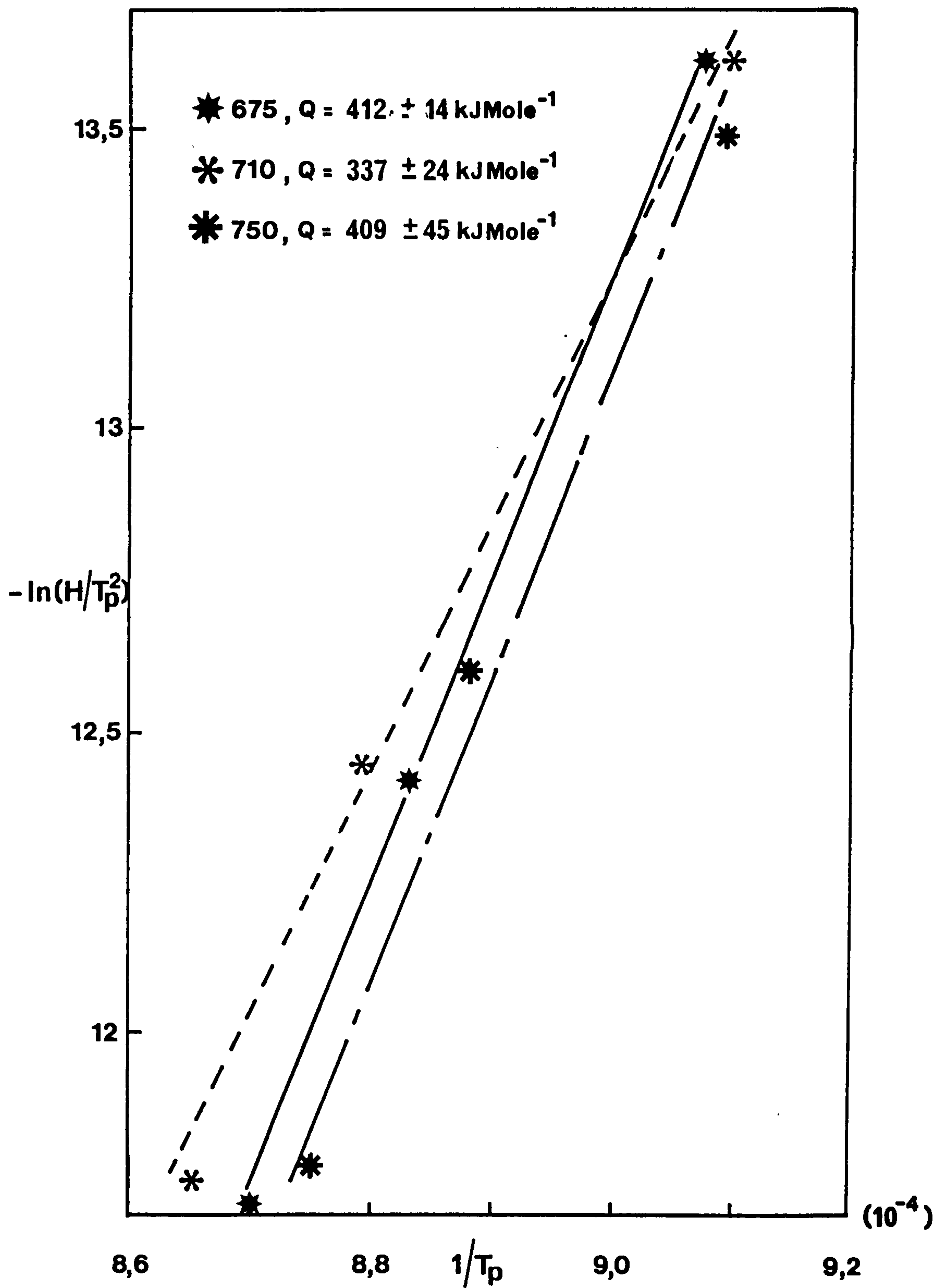


Fig.3.5 – Kissinger plots for crystallisation of MgTi_2O_5 in base glasses

already nucleated system, and at temperatures well above T_g , may have several complicated rate-determining processes operating.

Within experimental error the calculated activation energies (fig. 3.5) for $MgTi_2O_5$ crystallisation are the same for 675 and 750-glasses. The lower value of Q for 710-glass may be a consequence of its slightly higher TiO_2 content as will be shown in sections 4.1 and 4.2. The conditions for a successful application of the Kissinger method are generally determined empirically with reference to observed crystal growth from a pre-nucleated system. The results of fig. 3.5 may not be valid with the appearance of linearity being purely fortuitous. A full discussion of this topic with particular reference to the suitability of the Kissinger method is given by Henderson (60).

3.3.1 Heat-treatment schedule and resulting XRD

On the basis of results from DTA (section 3.2) a schedule of heat-treatments was devised as tabulated in table I for 675, 710 and 750 glasses.

| Temperature °C | Holding times (hrs) |
|-------------------|------------------------|
| 775 | 50 |
| 800 | 1,2,4,8,16 |
| 825 | 1,2,3,8 |
| 875 | 1,4 |
| 925 | 1,4 |

TABLE I. Heat-treatment schedule.

Specimens from the above heat-treatments were subjected to X-ray diffraction (XRD) and in addition to the residual glassy phase three principal crystalline phases were identified, namely:

- (1) magnesium dititanate ($MgTi_2O_5$) which is a pseudo-brookite structure (94,95) with an orthorhombic space group. Incontrovertible identification

of this phase is hindered by its ability to form a whole range of solid solutions with aluminium titanate, Al_2TiO_5 (96) all of which have similar principal reflections

(2) magnesian petalite; a stuffed β -quartz derivative which is capable of existing over a range of compositions in the $\text{MgO-Al}_2\text{O}_3\text{-SiO}_2$ system (see Chapter 1, p.14-15)

(3) μ -cordierite; a metastable β -quartz structure with hexagonal symmetry and the composition of cordierite, $\text{MgAl}_4\text{Si}_5\text{O}_{18}$. For convenience the principal reflections, relative intensities and corresponding d-spacings are summarised in table II.

| Phase | Reflection (hkl) | Angle ($^{\circ}2\theta$) | Intensity I/I_1 | d-spacing (\AA) |
|---------------------------|--|--------------------------------|----------------------|-------------------------------|
| MgTi_2O_5 | 110 | 26.02 | 100 | 3.51 |
| | 023 | 34.02 | 60 | 2.75 |
| | 200 | 55.21 | 60 | 1.87 |
| m-pet | space group not listed in powder file | 23.98 | 20 | 3.79 |
| | | 24.67 | 100 | 3.69 |
| | | 25.48 | 25 | 3.58 |
| μ -cord | 100 | 19.97 | 20 | 4.51 |
| | 101 | 26.52 | 100 | 3.45 |
| | 112 | 55.92 | 30 | 1.86 |

TABLE II

Fig. 3.6(a) illustrates the differences in visual appearance between 675 and 750-glasses for selected heat-treatments. Clearly there is no readily observable difference for the base glasses but at 775/50, where the emergence of MgTi_2O_5 crystallites is observed, the 675-glass exhibits a brown colouration in transmission with a slight blue appearance in reflection. In contrast, 750-glass has a brown/blue colour in both transmission and reflection.

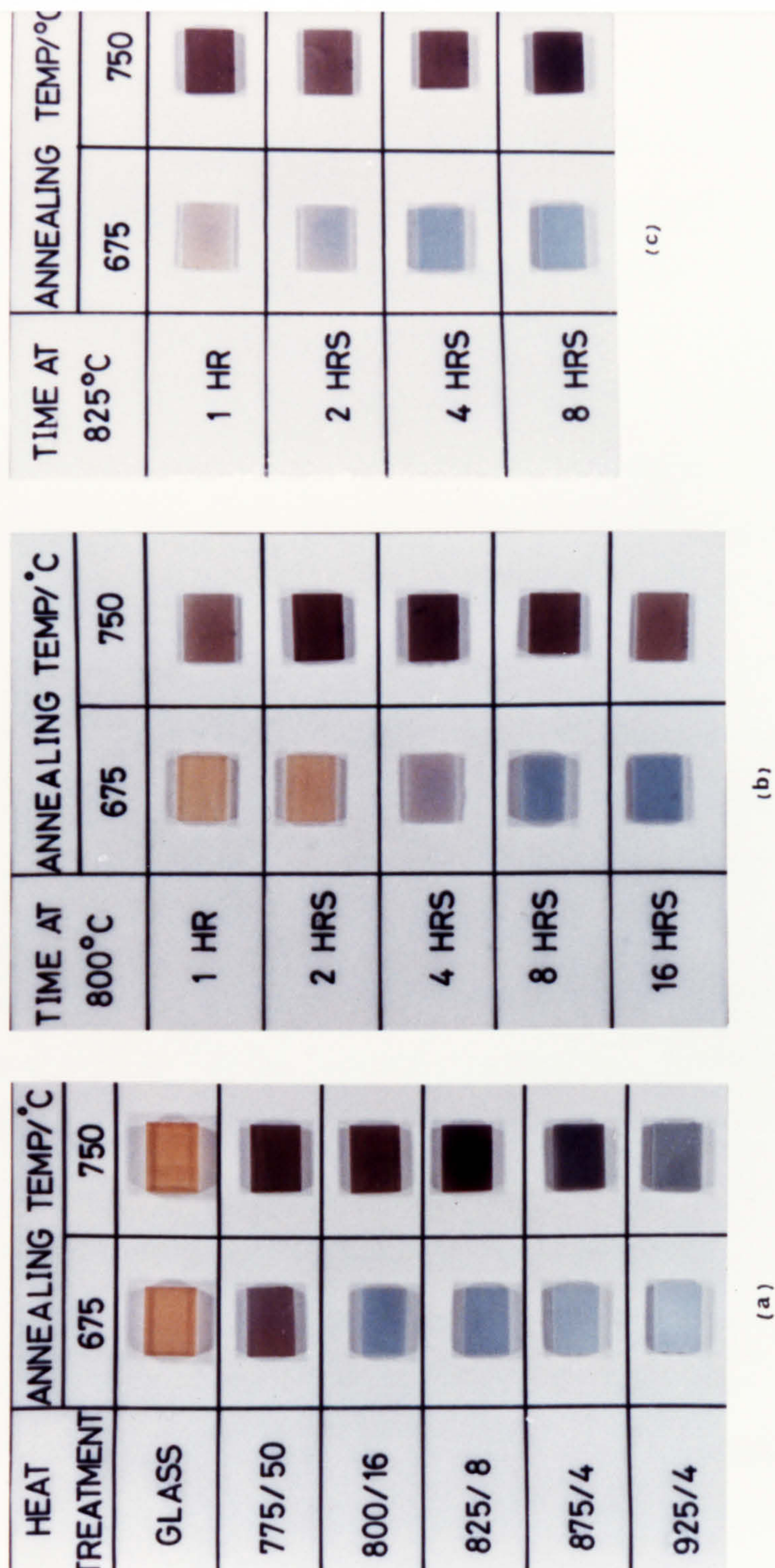


Fig. 3.6 - Visual appearance of heat-treated samples

Although not represented in fig. 3.6., 710-glass was similar in appearance to 750-glass after this heat-treatment.

Fig. 3.6 (b) and (c) show the change in visual appearance of 675 and 750-glasses as a function of time at holding temperatures of 800 and 825°C respectively. The appearance of 710-glass was the same as that of 675-glass and their phase development and visual properties at these temperatures may be summarised as follows. For short holding times there is a darkening in transmission of the originally amber glass coupled with a slight blue appearance in reflection and MgTi_2O_5 is detectable. At prolonged times darkening increases and ultimately the crystallisation of both magnesian petalite and μ -cordierite results in a light blue glass-ceramic with magnesian petalite as the major crystalline phase. For any given heat-treatment the amount of crystallinity present for 710-glass is consistently lower than that for 675-glass.

In the case of 750-glass there is a considerable difference in visual appearance for the same set of heat-treatments. Firstly, the crystallisation of MgTi_2O_5 is observed after only one hour at both 800 and 825°C, with the sample appearing grey/brown in both transmission and reflection over the whole range of treatments. For extended times the appearance of magnesian petalite is observed (800/16) followed by μ -cordierite as a very minor phase (825/8). Fig. 3.7 highlights the differences in phase development for the three glasses at 800/16.

At 875°C and 925°C crystallisation proceeds rapidly and specimens are predominantly crystalline after only 1 hour. Figs. 3.8 and 3.9 illustrate the differences in the relative proportions of magnesian petalite and μ -cordierite and for 675 and 710-glasses the growth in μ -cordierite in preference to magnesian petalite is observed with increasing temperature, whereas in 750-glass magnesian petalite persists as the major phase. It would appear that the ratio of these phases determines the visual appearance of the materials, i.e. from a light-blue glass-ceramic (675/925/4) which

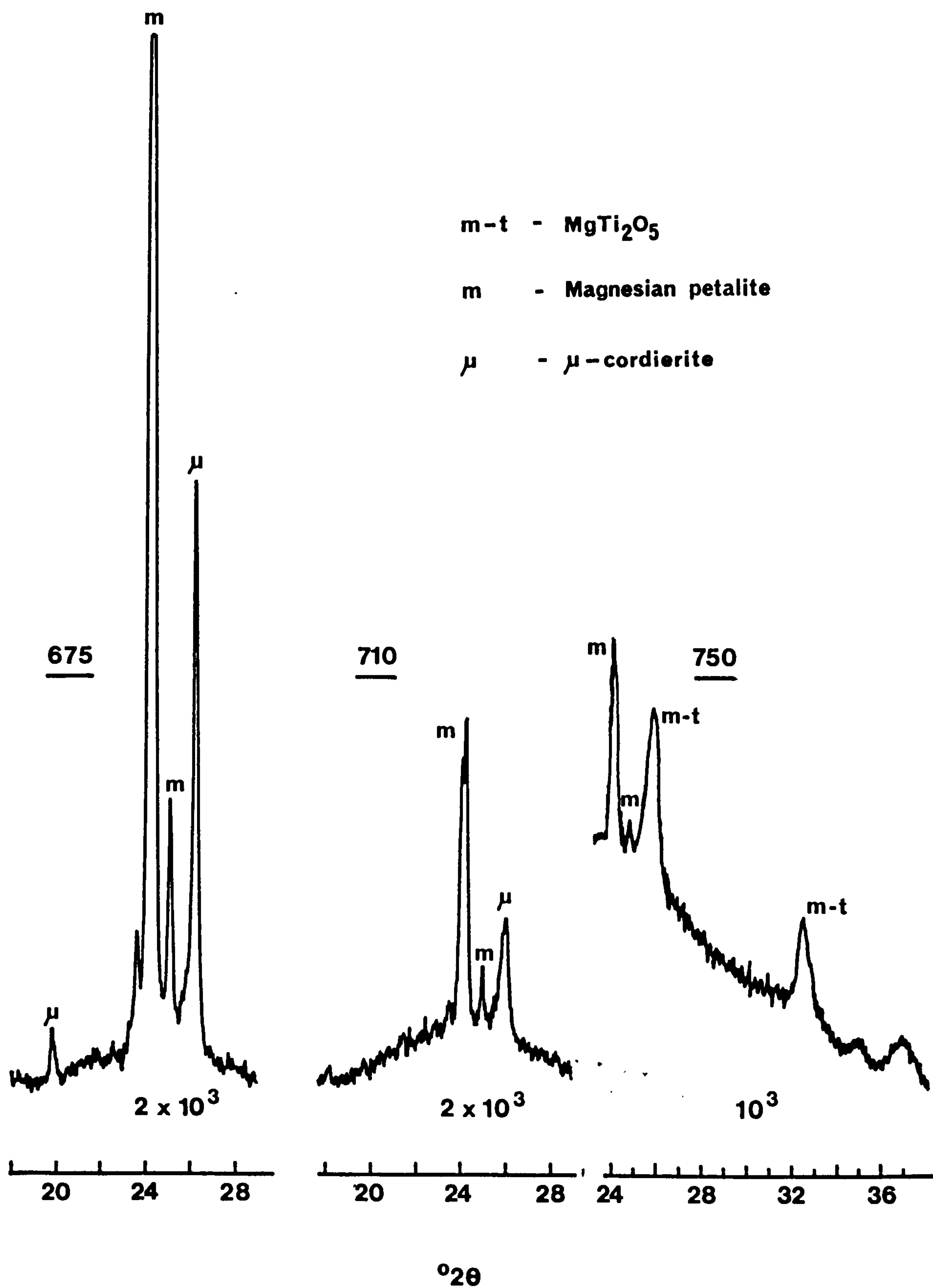


Fig.3.7. - Heat-treatment at 800°C - 16 hrs

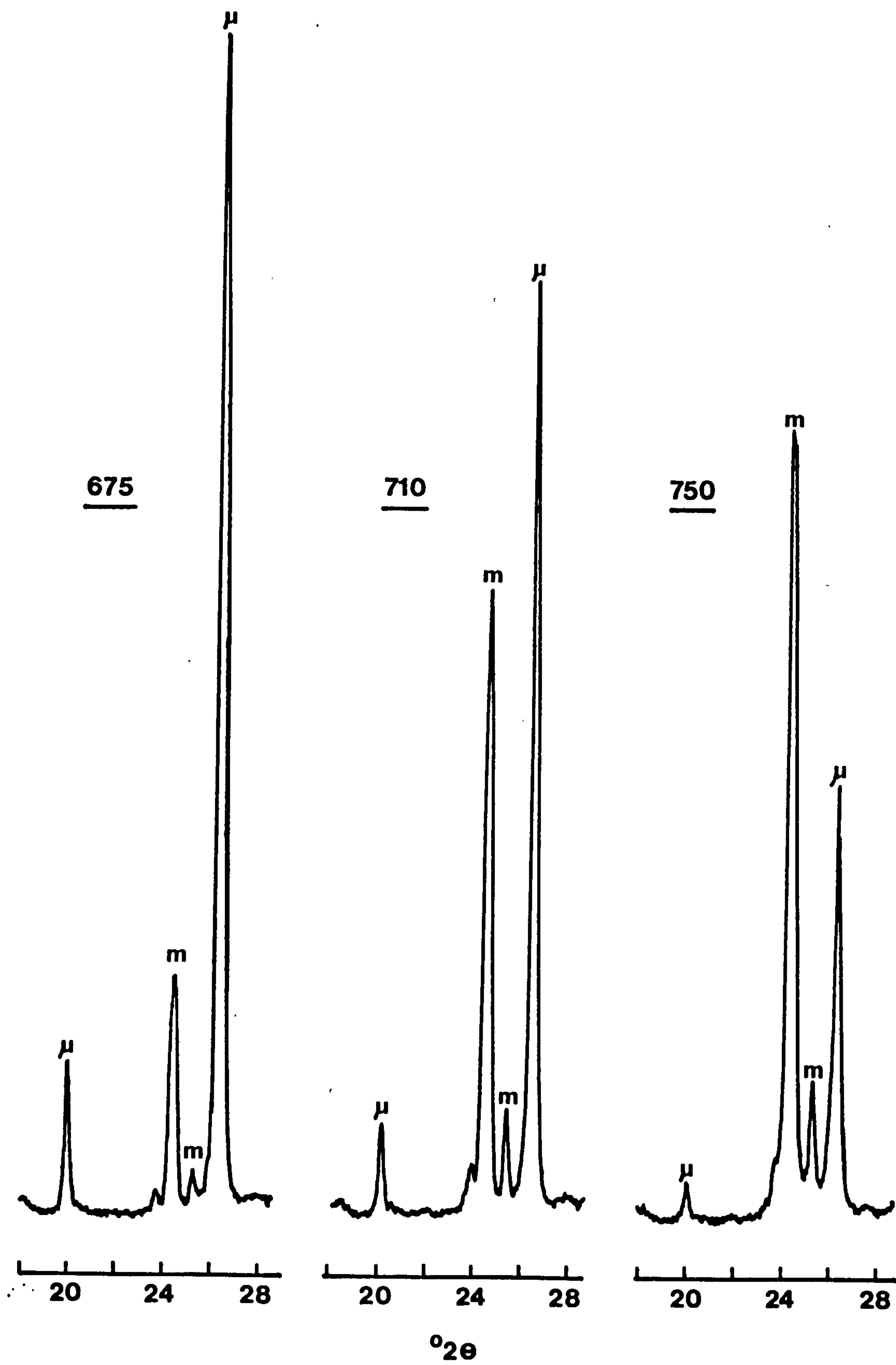


Fig.3.8 - Heat-treatment at 875°C - 4 hrs

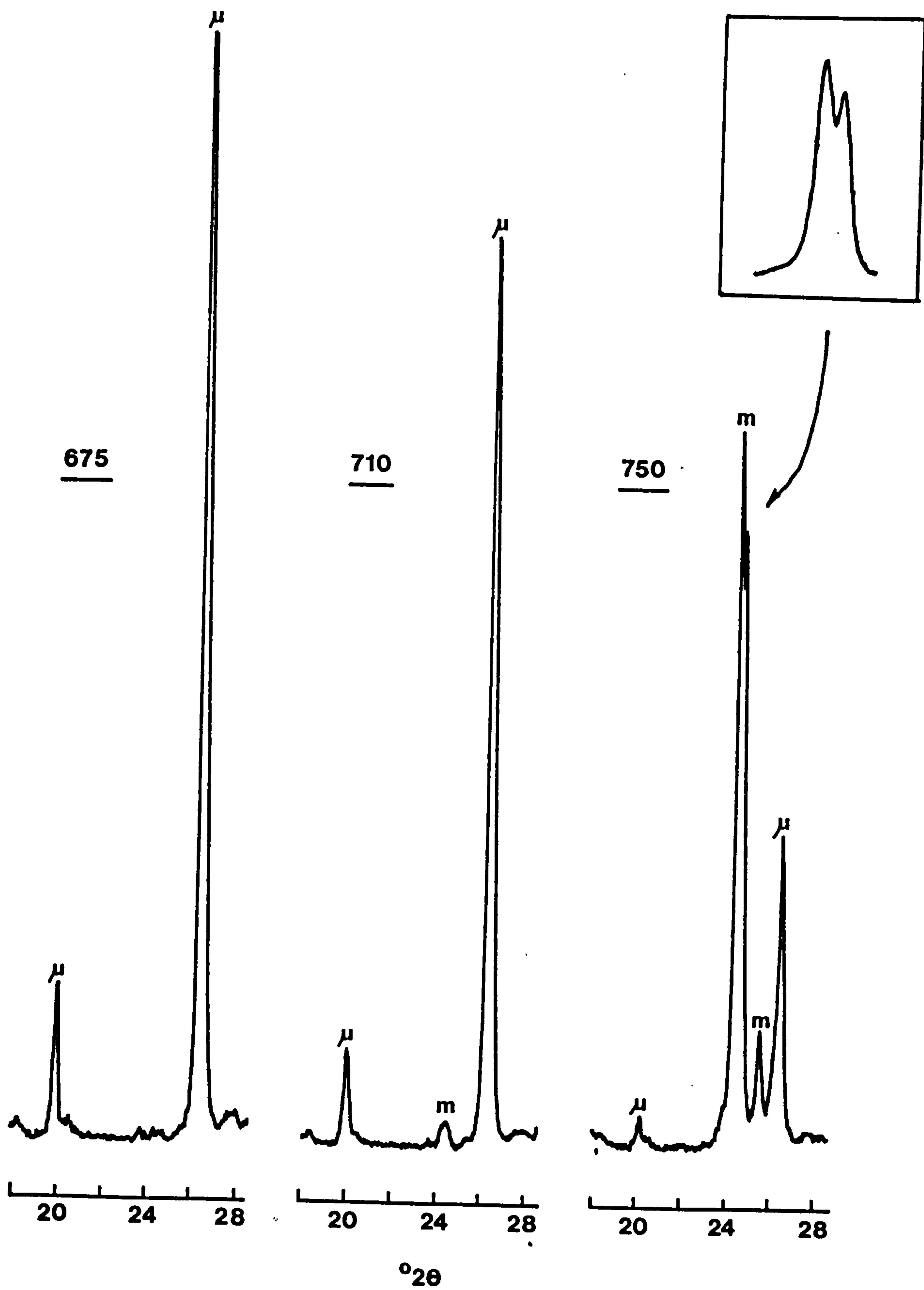


Fig.3.9 - Heat-treatment at 925°C - 4 hrs

is almost totally μ -cordierite to a grey, semi-transparent material (750/875/4) which has a high proportion of magnesian petalite (Fig. 3.6(a)). In fig. 3.9 the magnesian petalite reflection at $24^\circ 2\theta$ clearly exhibits a degree of peak splitting which is partially resolved at slower scanning rates (inset). This was a commonly observed phenomenon for this particular peak and is discussed in more detail in chapter 5.

3.3.2 Determination of crystallite size by line-broadening

The observation of small crystallites of MgTi_2O_5 in several heat-treated specimens prompted a determination of their size by the line-broadening technique outlined in section 2.5.1. Broadening was measured on the three strongest reflections, summarised in table III.

| Peak No. | hkl | $^\circ 2\theta$ | $\cos \theta$ | d(Å) |
|----------|-----|------------------|---------------|------|
| 1 | 110 | 25.4 | 0.9755 | 3.51 |
| 2 | 023 | 32.6 | 0.9598 | 2.75 |
| 3 | 200 | 48.6 | 0.9114 | 1.88 |

TABLE III. Principal reflections in MgTi_2O_5

Crystallite size as a function of heat-treatment is summarised in table IV. The main source of experimental error was in the accuracy of measurement of specimen line broadening which was typically $\pm 0.025^\circ$ in 2θ or $\sim 5\%$ in terms of crystallite size, D. It must be stressed, however, that only a comparison of crystallite sizes was sought and not an absolute determination. These data present little evidence of any major differences in either crystallite size or morphology in the samples heat-treated at 775°C and therefore the contrast in light-scattering properties of 675-/775/50, compared with 710/775/50 and 750/775/50, cannot be explained purely on this basis. There is an expected increase in crystallite

| Heat treatment | Crystallite dimensions for reflections ($^{\circ}$ A) | | |
|----------------|--|----------------|-----|
| | 110 | 023 | 200 |
| 675/775/50 | 263 | 170 | 250 |
| 710/775/50 | 239 | 147 | 250 |
| 750/775/50 | 175 | 140 | 140 |
| 750/800/1 | 175 | 133 | 231 |
| 750/800/16 | 210 | 134 | 242 |
| 750/825/4 | 223 | 165 | 190 |
| 675/825/1 | 112 | not measurable | |
| 675/825/2 | 325 | 217 | 315 |

TABLE IV. MgTi_2O_5 crystallite dimensions
in selected samples.

size with time in the 750-glass samples and the only interesting point is the rapid rate of initial crystallisation, i.e. crystallites of appreciable size ($\sim 200\text{\AA}$) are formed in less than one hour at both 800 and 825°C , whereas in 675 and 710-glass samples heat-treated at these temperatures the growth of MgTi_2O_5 is relatively slow. This might be expected when considering the DTA data presented in section 3.2.

3.4 Summary

The data presented in this chapter clearly show the marked effect of annealing temperature on initial crystalline phase development in this system. Although there is some diversity in behaviour between 675 and 710-glasses, in that crystallisation seems to be slightly retarded in 710-glass, the essential contrast is between these glasses and 750-glass where possibly crystallisation proceeds by a somewhat different mechanism. On the basis of these preliminary observations, three main areas of investigation become apparent, viz;

1. Possible compositional or structural variations in the three base glasses (Chapter 4).
2. The effects of prolonged heat-treatments and heat-treatments at elevated temperatures on the stability of the β -quartz, solid solutions, magnesian petalite and μ -cordierite (Chapter 5).
3. Microstructural development of these metastable solid solutions (Chapter 5).

Chapter 4 - Identification of possible physical and chemical
differences between the base glasses

The following sections are the results of investigations to identify any possible physical or chemical changes brought about during annealing. It should be pointed out at this stage that only the 675 and 750 glasses were prepared from the same batch melt: 710 glass was prepared at a later stage and may well vary slightly in composition. This will be considered when making direct comparisons of physical phenomena which may be strongly composition-dependent.

4.1 EDAX analysis in SEM

For each of the three base glasses, spectra were obtained from 10 sampling points across each specimen and the calculated chemical compositions are presented in table V. Standard errors (α) were calculated from the formula

$$\alpha = \frac{\sigma}{\sqrt{n}}$$

where σ is the standard deviation of a sample population of size n . Values were typically ~ 0.1 which as a measure of compositional variation suggests good homogeneity.

| Specimen | Chemical composition (weight % oxides) | | | |
|-----------|--|--------------------------------|------|------------------|
| | SiO ₂ | Al ₂ O ₃ | MgO | TiO ₂ |
| 675-glass | 50.7 | 21.2 | 17.6 | 10.3 |
| 710-glass | 50.2 | 21.0 | 17.5 | 11.3 |
| 750-glass | 50.6 | 21.1 | 17.6 | 10.3 |
| Nominal | 56.0 | 20.0 | 15.0 | 9.0 |

TABLE V - Chemical composition of base
glasses determined by EDAX

Assuming that the nominal composition was accurately made up and that the glasses are stable under melting conditions, the limitations of the EDAX technique in terms of absolute determination of chemical composition can be readily appreciated. However, a comparison of chemical composition of the three glasses - analysed under identical conditions - indicates a difference in the TiO_2 content of 710-glass of $\sim 1\%$. Both 675 and 750- glasses were prepared from the same batch melt and the expected lack of a significant discrepancy in their chemical compositions is confirmed by this technique. In an effort to confirm this compositional variation, the method for TiO_2 analysis outlined in section 2.12 was employed, the results of which are presented in the following section.

4.2 Chemical analysis by absorptiometric methods

The TiO_2 and Fe_2O_3 content of base glasses was determined using an absorptiometric method (section 2.12). Two assays were performed in each case and showed good agreement (table VI).

| Specimen | Composition by weight of: | |
|-----------|---------------------------|-------------------------|
| | TiO_2 | Fe_2O_3 |
| 675-glass | 9.03 | 0.02 |
| 710-glass | 9.21 | 0.02 |
| 750-glass | 9.03 | 0.02 |

TABLE VI - TiO_2 and Fe_2O_3 content
of base glasses.

This method is considerably more accurate than EDAX and although there is a discrepancy in the TiO_2 content of 710-glass its magnitude is reduced to $\sim 0.2\%$. These results, along with those from EDAX, confirm

that there is no compositional variation between 675 and 750- glass and therefore their subsequent behaviour may be considered without recourse to possible compositional fluctuations. The presence of Fe_2O_3 as an impurity may be used to discuss the optical properties of these glasses (section 4.5).

4.3 Additional heat-treatments.

Annealing times for the base glasses were extended up to 100 hours and although no visible or other change was detected for 675-glass the presence of phase separation and MgTi_2O_5 crystallites was observed in the other glasses. TEM studies and u.v-visible and infra-red spectroscopy showed a change in properties with extended annealing time. In 710-glass a gradual darkening was noticed and after 100 hours phase separation was observable: in 750-glass the emergence of MgTi_2O_5 after only 40 hours is confirmed by XRD. The results of density measurements, u.v. visible, infrared and EPR spectroscopy are presented in the following sections.

4.4 Density measurements

The densities of both 675 and 750- glasses were determined from measurements on four samples of each, ranging in mass from 3-30g. The mean density was calculated and these values, along with standard error determinations, are summarised in Table VII.

| Glass | Mean Density g/cm^3 | Standard error |
|-------|------------------------------------|-------------------|
| 675 | 2.635 | 0.002 |
| 750 | 2.647 | 0.001 |

TABLE VII - Densities of base glasses.

A temperature variation of 0.3°C was recorded throughout the experiments. In comparing the two results and assessing the significance of the overall change in density $\Delta\rho/\rho$, sources of experimental error must be considered. The accuracy of $\pm 0.1\text{mg}$ in weighing means that the largest error, i.e. for the smallest weight determined ($\sim 2\text{g}$), can be only $\sim 0.05\%$. Another source of error is in the exact determination of the weight loss of the cradle in water. This was overcome to a certain extent by adjusting the level of the immersion fluid to coincide with a small mark on the cradle's vertical support. For a variation of 1mm in immersion depth an error of $\sim 0.002\%$ can be calculated based on a mass per unit length of $4.6 \times 10^{-4}\text{g/mm}$ for the wire. These minor errors are far outweighed by that introduced as a result of temperature variations in the immersion fluid. Bell (97) has put a practical limit on $\Delta\rho/\rho$ of 10^{-5} assuming a temperature uniformity of within 0.01°C . Clearly, for the variation of at least 0.3°C encountered in these experiments, an accuracy of at best $\sim 0.03\%$ can be expected. In these terms the observed difference in density of $\sim 0.5\%$ may be considered significant.

In addition to the above measurements the densities of several heat-treated specimens were determined as shown in table VIII.

| Specimen | Density (g/cm^3) |
|------------|-----------------------------|
| 675/775/50 | 2.664 |
| 710/100 | 2.652 |
| 750/18 | 2.648 |
| 750/40 | 2.657 |
| 750/100 | 2.658 |
| 675/100 | 2.642 |

TABLE VIII - Additional density measurements

Fig.4.1

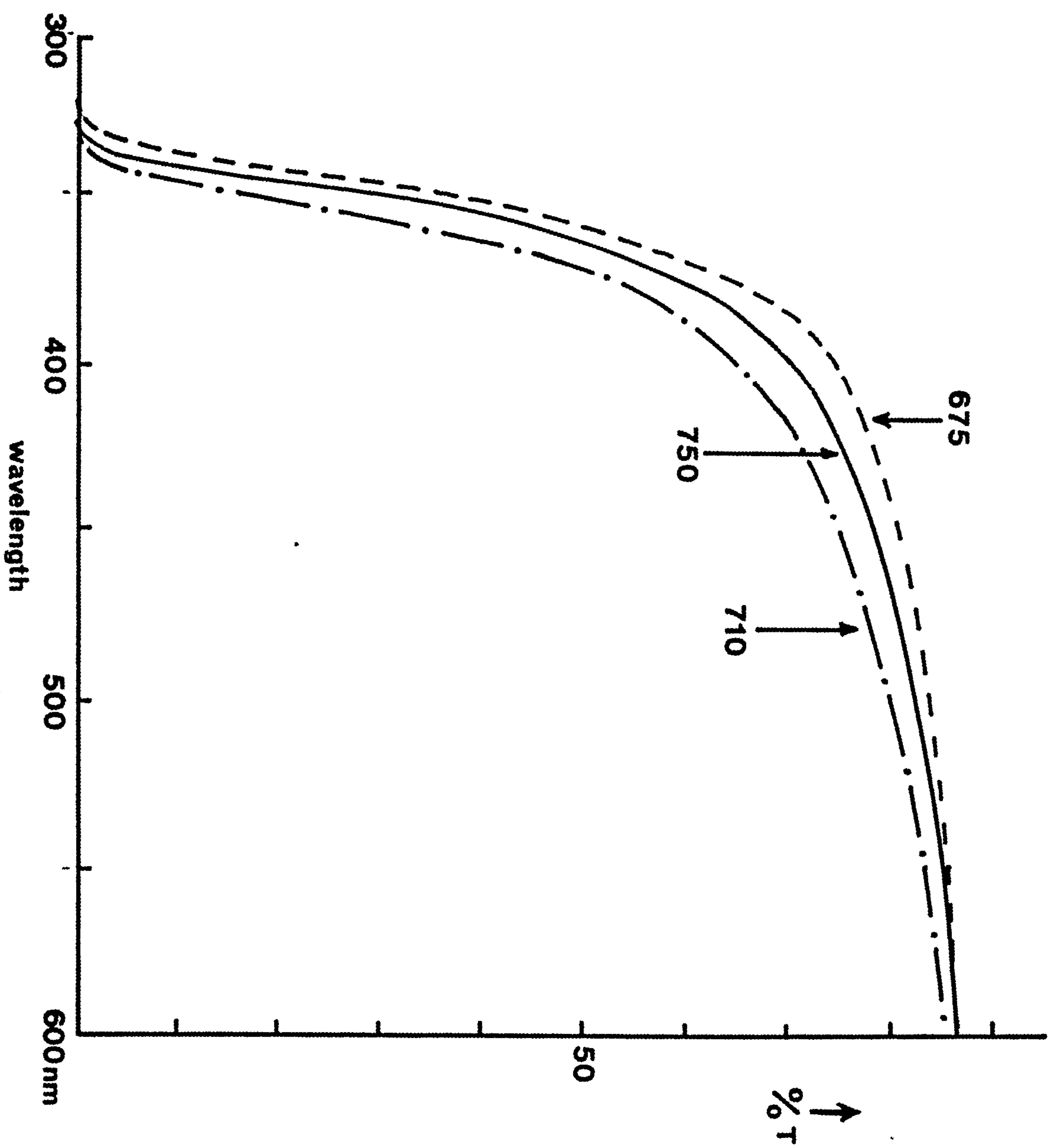
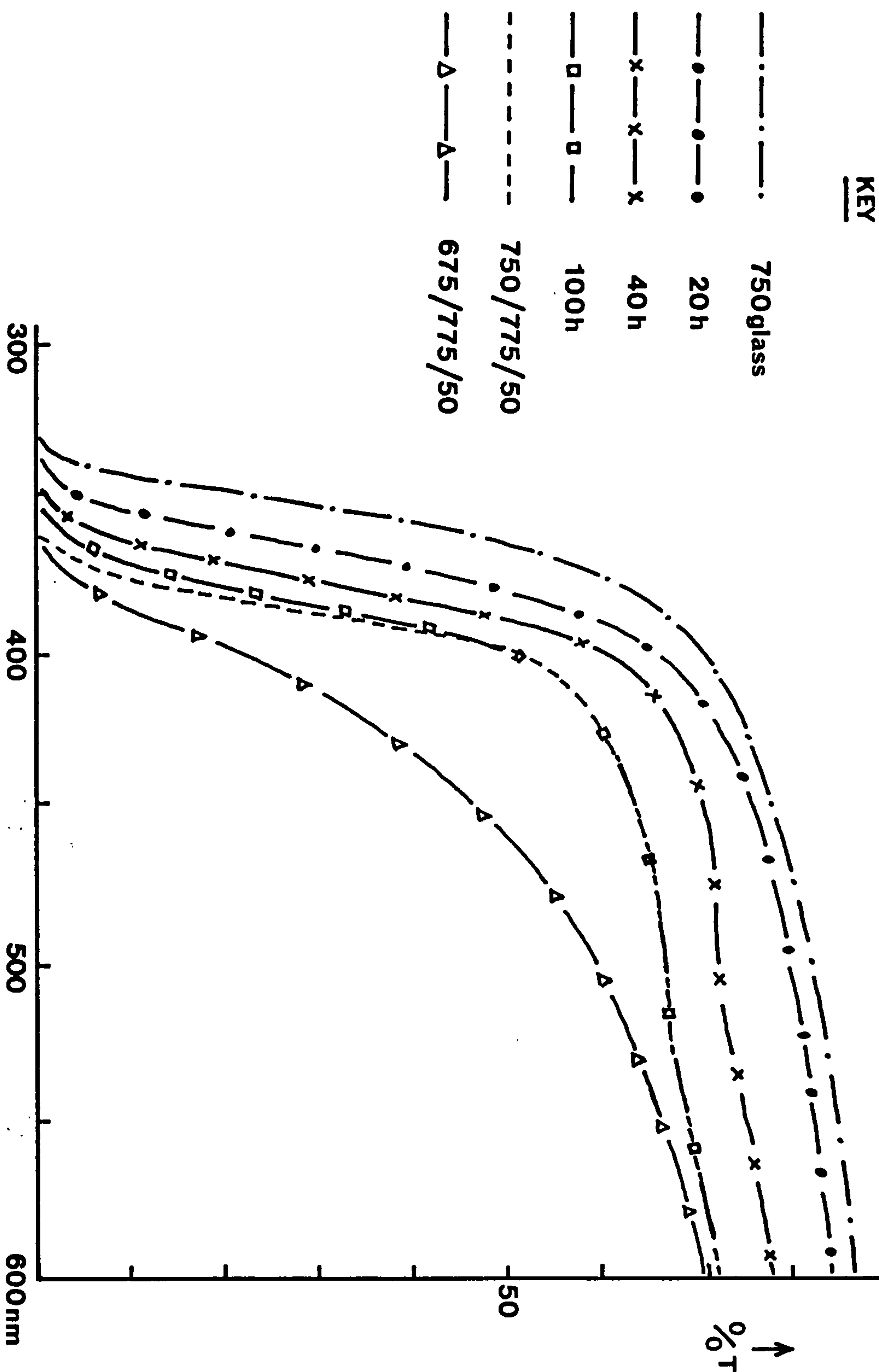


Fig.4.2



Although these results are for a single measurement on samples of typically 2g mass and their accuracy is somewhat reduced, the general trend of increasing density on heat-treatment is apparent and in agreement with observations on $\text{TiO}_2\text{-SiO}_2$ glasses (98) where an increase in density was noted as the glass partially crystallised.

4.5 U.V - Visible spectroscopy of glassy specimens

Optical absorption measurements in the u.v- visible spectrum were performed on parallel, polished specimens standardised to a thickness of $900\mu\text{m}$, (section 2.10) and therefore any observed effects do not require additional absorption coefficient or surface reflection corrections and direct comparisons may be made.

In fig. 4.1 the transmission curves for base glasses over the range 600-300nm are shown. Appreciable variation in transmission between 400 and 500nm is noted as well as slight shifts in the u.v. edge. The inconsistent trend may be explained on a compositional basis as chemical analysis (sections 4.1 and 4.2) has shown 710- glass to have a slightly higher TiO_2 content than 675 or 750- glass which may strongly influence optical absorption at these frequencies.

A comparison of 675 and 750- glass shows a divergence in their transmission curves at $\sim 560\text{nm}$ and a resulting edge shift.

Fig. 4.2 presents the transmission curves for 750- glass heat-treated at 750°C for 20, 40 and 100 hrs respectively, along with 750/775/50 and 675/775/50. In addition to an overall darkening of the glasses with time a very broad absorption band is developing at around 500nm. Phase separation is observable in 750/20 and in 750/40 and 100 the presence of MgTi_2O_5 is detectable by XRD; a certain amount of attenuation may be expected from light scattering at these centres.

In both 675/775/50 and 750/775/50, MgTi_2O_5 crystallites are present. However their visual appearance (section 3.3) and absorption characteristics differ considerably. This may be explained by considering the microstructures of these specimens which are presented as part of the overall microstructural development in section 5.3.

4.6 Infra-red spectroscopy of glassy specimens

Transmission curves for selected glassy specimens are presented in fig. 4.5 over the frequency range $1400\text{--}400\text{cm}^{-1}$. Essentially, the three traces represent single phase glassy specimens (base glasses and 675/100) (A) phase-separated glass (710/100, 750/20) (B) and glasses containing MgTi_2O_5 crystallites with and without additional phase-separated structure (750/40, /100 and all glasses /775/50) (C). The important features to note are the increasing absorption at $\sim 1085\text{ cm}^{-1}$, 790 cm^{-1} and 460 cm^{-1} with a relative decrease at $\sim 950\text{ cm}^{-1}$ as phase separation and initial crystallisation occur. On the basis of calculations by Langer and Schreyer (99) from an empirical relationship (100), the peaks at 1085 cm^{-1} and 950 cm^{-1} may be assigned to the stretching vibrations of SiO_4 and AlO_4 tetrahedra respectively.

These absorption bands were observed in a glass of cordierite composition whereas an absorption at $\sim 1080\text{ cm}^{-1}$ in alkali-silicate glasses with increasing alkali content has been assigned to vibrations of SiO_4 groups in which two of the oxygens are non-bridging (78). The band in the region $400\text{--}500\text{ cm}^{-1}$ is generally accepted as the O-Si-O bending mode vibration. There is some confusion over the origins of the small band at $\sim 800\text{ cm}^{-1}$. Some authors (101, 102) have assigned this vibration to the symmetric stretching of SiO_4 tetrahedra which would in principle be i.r. inactive. However, a slight deviation from symmetry, as observed by Wyckoff (103) in high purity quartz, causes an asymmetric, and hence I.R.-active,

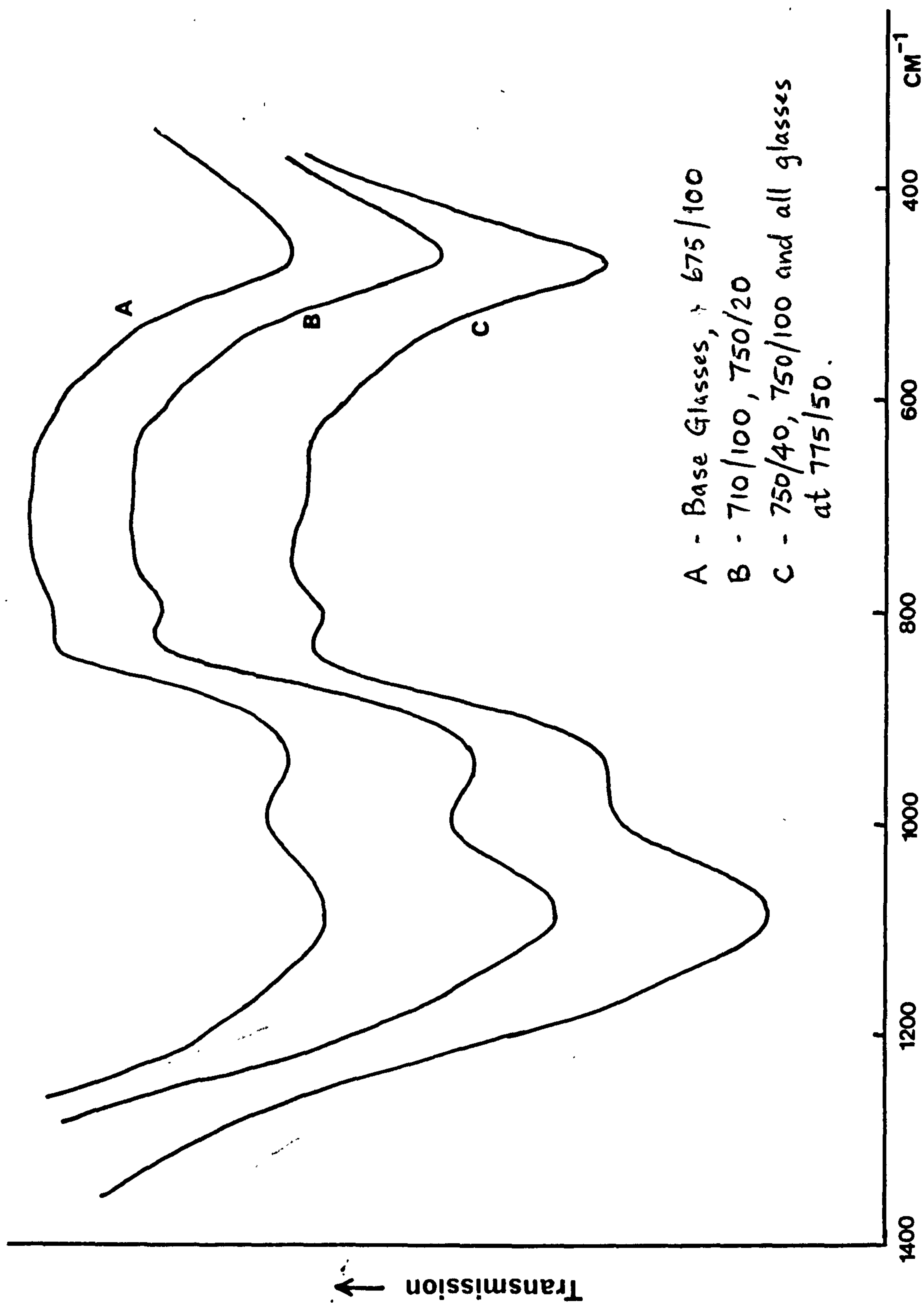


Fig.4.3 - Infra-red spectra of glassy specimens

vibration. On the other hand this band has been assigned (104) to a bond-bending type of motion in which a bridging oxygen vibrates approximately at right-angles to the Si-O-Si bond and in this plane.

4.7 Electron paramagnetic resonance (EPR)

The EPR spectra of selected samples were recorded primarily to investigate the presence of Ti^{3+} which for a silicate glass has a typical g-value of ~ 1.9 (78). More particularly, Garif'yanor (105) assigned a g-value of 1.94 with a peak to peak breadth (ΔH) of 120G. for Ti^{3+} at room temperature in a TiO_2 -containing magnesium aluminosilicate glass melted in a reducing atmosphere. Samples of equal mass (0.5g) were analysed under a consistent set of operating conditions and with the inclusion of a standard which gave a sharp signal at $g=2$. As a control a glass of the base composition but without TiO_2 was prepared (A). The response of the above sample, along with those of the base glasses (B) and a sample containing MgTi_2O_5 crystallites (750/825/2) (C) are presented in fig. 4.6 over the range $g=2.5$ to 1.6.

In addition to the standard peak at $g=2$ there is some evidence of a response at around $g=1.95$ in both the base glasses and 750/825/2 which represents a significant shift from $g=2$. ΔH -values of these lines are ~ 60 -70G. It should be stressed that these spectra were recorded at maximum apparatus sensitivity at which the limit for detection of Ti^{3+} is $\sim 10^{15}$ atoms which in a sample of 0.5g represents a concentration of about 1ppm. In the absence of a much more detailed and rigorous study the absence of Ti^{3+} may not be firmly concluded. However, if present, a concentration of 1ppm can be given as an upper limit.

At a reduced apparatus sensitivity an appreciable response for Fe^{3+} was noted in all of these specimens (fig. 4.7) at $g = 4.5$. These high g-values have been shown to correspond to tetrahedrally coordinated Fe^{3+}

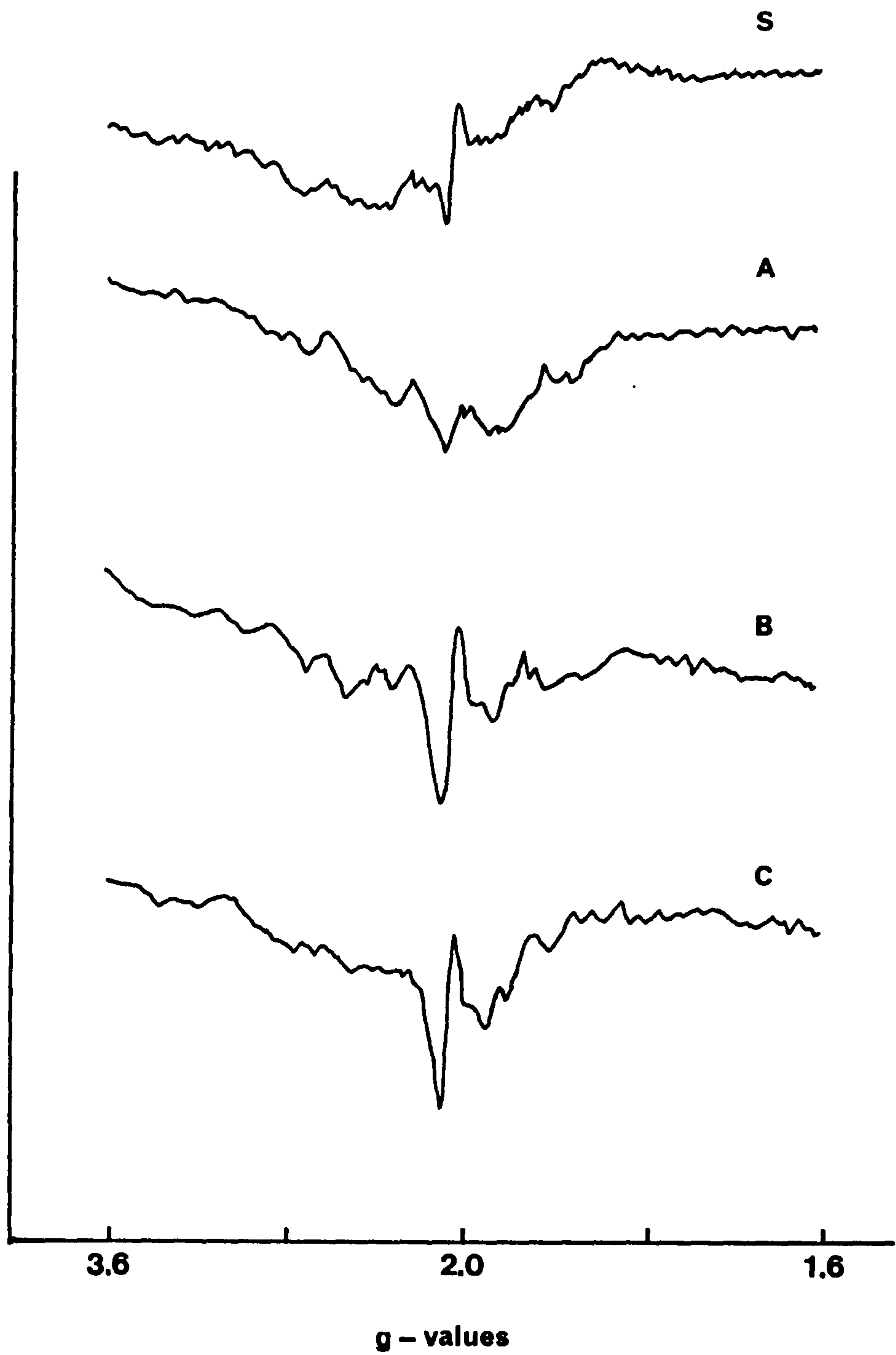


Fig.4.6 - EPR spectra at $g \approx 2$

- S - Standard**
- A - Glass without TiO₂**
- B - Base glasses**
- C - 750/825/2**

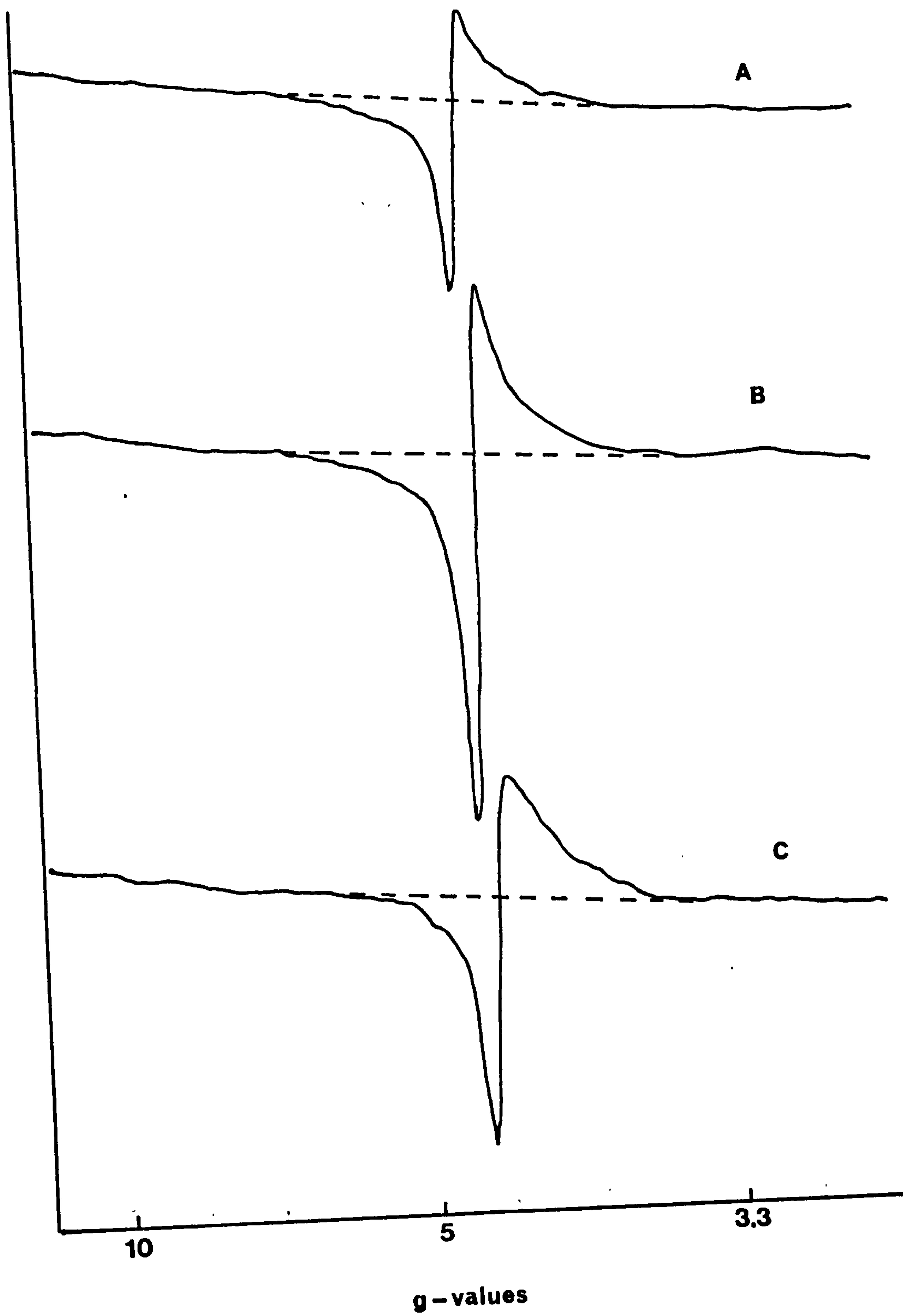


Fig.4.7 - EPR spectra of Fe^{3+}

ions exhibiting high crystal field splitting (106). Elementary analysis of the line shape reveals symmetry variations between the samples, detailed analysis of which may give useful information about the local environment of the Fe^{3+} ion and changes in this on subsequent crystallisation of the glass. However the complexity of such analyses rendered further study of this phenomenon beyond the scope of this thesis. Fe^{2+} has a d^6 electronic configuration and is therefore not detectable by EPR techniques.

4.8 Discussion

Before discussing the implications of the results of the previous sections in terms of changes in the structure of the glass, it may be beneficial to postulate a possible model for the base glass system. As molar percentages, the composition of the base glass is; SiO_2 - 58%, Al_2O_3 - 12%, MgO - 23% and TiO_2 - 7%. If we assume a fundamental network of SiO_4 tetrahedra with tetrahedral AlO_4 groups joining this network in substitutional sites, then from charge balance considerations;



and therefore ~ 6 mole % of the Mg^{2+} ions present will be required to occupy interstitial sites in close proximity to the Al^{3+} ions. The remaining Mg^{2+} may act as a network modifier in which case non-bridging oxygens (n.b.o's) will result. To complete the picture let us assume that some of the TiO_2 will enter the network in fourfold coordination - the remainder occupying octahedral modifying sites resulting in further n.b.o's - and that the small amount of iron impurity will be present as network forming FeO_4 units.

The origins of the amber colour of these base glasses and many other TiO_2 -containing glasses are not fully understood. The colouration is generally coupled with a shift in the u.v. edge to longer wavelengths and has been attributed to either (a) a reduction in strength of the overall

silicate network by the formation of n.b.o's in the presence of network modifiers or (b) the existence of transition ion chromophore centres. In the latter, absorption may occur by either of two mechanisms; (i) intra-ionic transitions whereby an incoming photon causes excitation of a d-electron to a higher degenerate energy level brought about by crystal field splitting or (ii) charge transfer in which an electron is transferred between the central transition ion and a ligand or vice versa. This involves movement of an electron through a considerable distance which results in a high absorption intensity and a strong dependence of absorption energy on ion-ligand (or donor-acceptor) distance.

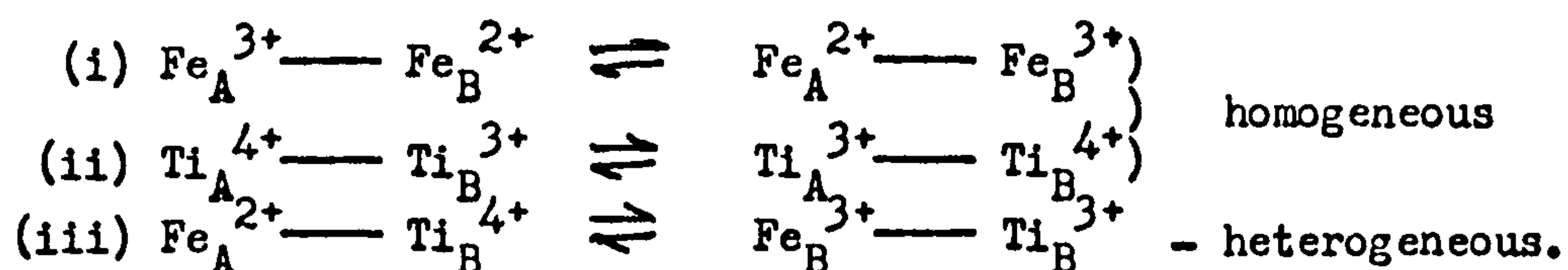
For a series of alkali-trisilicate glasses the presence of ferric iron and titanium in concentrations of \sim 1ppm were found to have a greater influence on the absorption edge than n.b.o's, giving cut-off at 280nm (107). The presence of these elements in the base glasses used in the present work is of much larger proportions and would therefore be expected to exhibit the dominant effect on edge shifts.

For a glass system containing ferrous and ferric iron and titanium in both 3^+ and 4^+ states there exist the following absorption mechanisms;

(a) d-d transitions in split-field Fe^{2+} , Fe^{3+} and Ti^{3+} ions

(intraionic) and

(b) charge transfer between the following redox pairs



In all cases the absorption band energy will depend on the particular ligand environment of the transition ions. For such a complex, multicomponent system as encountered here theoretical calculations of expected absorption are beyond the scope of this thesis. It is sufficient, however, to appreciate

that any small structural changes within the glass may have an observable effect on the optical properties, in addition to compositional variations.

For the u.v.-visible data presented in fig. 4.1. the shift in u.v. edge and increased absorption of 710-glass is almost certainly due to its increased TiO_2 content (sections 4.1 and 4.2) showing agreement with Baiburt et.al. (108) who observed such a shift in cut-off with increasing TiO_2 content in a $\text{MgO-Al}_2\text{O}_3\text{-SiO}_2$ glass. For the case of 675 and 750- glasses which were prepared from the same batch melt and have been shown to have identical compositions (section 4.1 and 4.2) the observed variation in absorption at the u.v. edge may be explained in structural terms. Smith and Strens (109) have shown the dependence of absorption energies on the donor-acceptor distance in various Fe-Ti chromophore centres for several minerals and concluded that a reduction in this distance results in shifts of the u.v. edge to longer wavelengths. Varshal (110) has suggested that dissolution of Ti and Fe in the alumina rich phase of a phase separated cordierite glass also reduces this distance to give observed edge shifts. Although phase-separation is not identified in the base 750-glass, a degree of ordering may be taking place in which ions in the glass rearrange themselves prior to phase separating in a way which causes a reduction in the Ti-Fe distance. The increased density of 750-glass ($\sim 0.5\%$) may be explained by a relaxation of the silica network due to viscous flow as observed in many silicate glasses (111). On the basis that this would increase the average chemical bond strengths, a shift in the u.v. edge to shorter wavelengths would be expected (81). The small variation noted between 675 and 750- glasses may result from a combination of these two opposing factors.

On phase separating the formation of a silica-rich phase would be expected and has indeed been observed (112). The other phase would therefore have a higher proportion of Fe_2O_3 , TiO_2 and MgO with the

possibility of Al_2O_3 enrichment not excluded. In addition to reducing the distance between Fe-Ti pairs as previously discussed, the effect of removing Ti^{4+} and Mg^{2+} from network modifying positions would strengthen the network in the SiO_2 -rich phase which is consistent with I.R. data (fig. 4.5) if we assign the decreasing band at 960 cm^{-1} to n.b.o. vibrations and note the increased absorption at 450 cm^{-1} due to O-Si-O bending.

The subsequent crystallisation of MgTi_2O_5 is not well understood and by no means conclusive with possible variations existing between 675 and 750- glasses. It may be the case that once phase separation has occurred TiO_2 crystallises out as a magnesium titanate or even a magnesium aluminotitanate third phase and plays no further part in the crystallisation process. Alternatively total crystallisation of the TiO_2 -rich phase may take place as proposed by several authors (Chapter 1). The I.R. data for crystallite-containing samples suggest a further reduction in the n.b.o. density which could be brought about by either of the above processes.

To summarise, some local ordering of ions in the glass structure at annealing temperatures at and above T_g (710 and 750- glasses) may be sufficient to enhance widespread phase-separation of these glasses on subsequent heat-treatment e.g. $775^\circ\text{C}/50\text{ hrs.}$ and that although phase-separation may occur in 675-glass it will be to a much lesser extent. The subsequent chemical compositions of the separated phases may determine which of the β -quartz solid solutions will preferentially crystallise and hence the relative proportions of the two as a function of temperature and time.

Chapter 5 - The stability of magnesian petalite and microstructural development in 675- and 750- glasses

In the following chapter the results of additional heat-treatments on 675 and 750- glasses are discussed with particular reference to the magnesian petalite phase. Selected micrographs are presented which illustrate the essential features of the microstructures encountered and, where possible, explanations are offered for the different morphological characteristics.

5.1 Transformation of 675- glass to 750- glass

To provide additional evidence that the effects of "annealing" the base glass at 750°C are real, samples of 675- glass were heat-treated at 750°C for 3 hours. These, together with untreated samples of both 675- and 750- glass, were subjected to selected heat-treatments of 825°C - 8 hrs and 925°C - 4 hours respectively. All samples were subsequently analysed using XRD and for both of the above heat-treatments the resulting visual appearance and phase composition of the 675/750/3 glass showed close similarity with 750- glass; 675- glass continued to exhibit the differences previously observed (section 3). It can therefore be concluded that annealing of the base glass at 750°C can be regarded rather as a heat-treatment during which the properties of the base-glass are in some way altered.

5.2 The stability of the magnesian petalite solid solution

The appearance of magnesian petalite over a wide range of heat-treatment temperatures and times has been observed (section 3.3) and in order to assess the limits of its stability a series of heat-treatments (Table IX) was performed on samples of 675/825/8, 710/825/8 and 750/825/8 in which magnesian petalite is present as the major crystalline phase.

| Temp ($^{\circ}\text{C}$) | Time (hrs) |
|-----------------------------|------------|
| 825 | 20 |
| 825 | 40 |
| 925 | 4,10 |
| 1000 | 5 |
| 1100 | 4 |
| 1200 | 2 |

Table IX - Heat-treatments on 825/8 samples

At 825°C magnesian petalite remained the predominant phase (fig. 5.1) and little change in the magnesian petalite: μ -cordierite ratio was observed in any of the base-glasses over 40 hours. At no stage was splitting of the principal magnesian petalite reflection observed although a general broadening of this peak was noted. In contrast, all samples heat-treated at 925°C

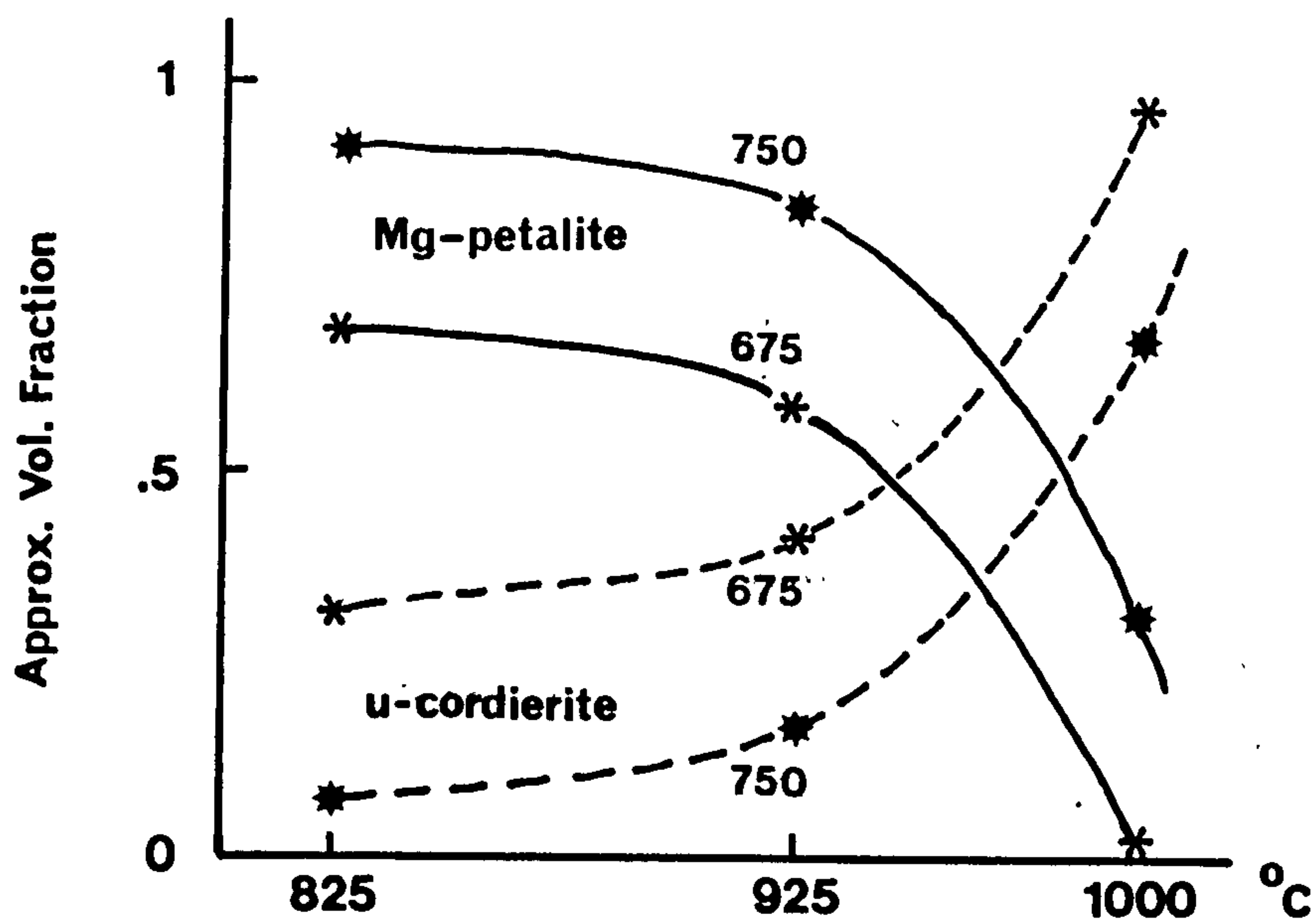


FIG. 5.1

exhibited splitting of this peak: magnesian-petalite remained the major phase with an increase in the magnesian-petalite: μ -cordierite ratio from 1.3 in 675-glass to 5.25 in 750-glass (fig. 5.1). It should be noted that in base-glasses heat-treated at 925°C - 4 hours only (fig. 3.9) μ -cordierite was the predominant phase. For heat-treatment at 1000°C - 4 hours a marked difference was observed between 675/710-glasses and 750-glass: magnesian petalite was not present in the 675-glass specimen which comprised mainly μ -cordierite with some cordierite. In the 750-glass specimen magnesian petalite remained the second major phase after μ -cordierite and the appearance of enstatite (MgSiO_3) was noted: a large degree of splitting occurred in the principal magnesian petalite reflection.

At 1100°C the emergence of cordierite dominates and at 1200°C all glass-ceramics exhibit remarkable similarity in phase constitution with cordierite as the major phase. Although a discussion of the final crystallisation of cordierite is relevant, insufficient time was available for an in-depth study. Much work already exists in this area and attention was therefore confined to the earlier stages of crystallisation, particularly of β -quartz solid solutions.

Possible explanations of peak splitting observed in magnesian-petalite (fig. 5.2) are as follows:

- i) the development of an additional phase having a strong reflection at $3.69\overset{\circ}{\text{\AA}}$ which could effectively split the magnesian-petalite peak by overlapping. However, no additional peaks were recorded in these spectra which would be weaker reflections from the additional phase and no change in intensity of the overall peak at $\sim 3.69\overset{\circ}{\text{\AA}}$ ($24.2^{\circ} 2\theta$) relative to other magnesian-petalite peaks was observed for specimens exhibiting peak-splitting.
- ii) small distortions of the magnesian-petalite lattice resulting in a reduced multiplicity of reflections. Magnesian-petalite was so named

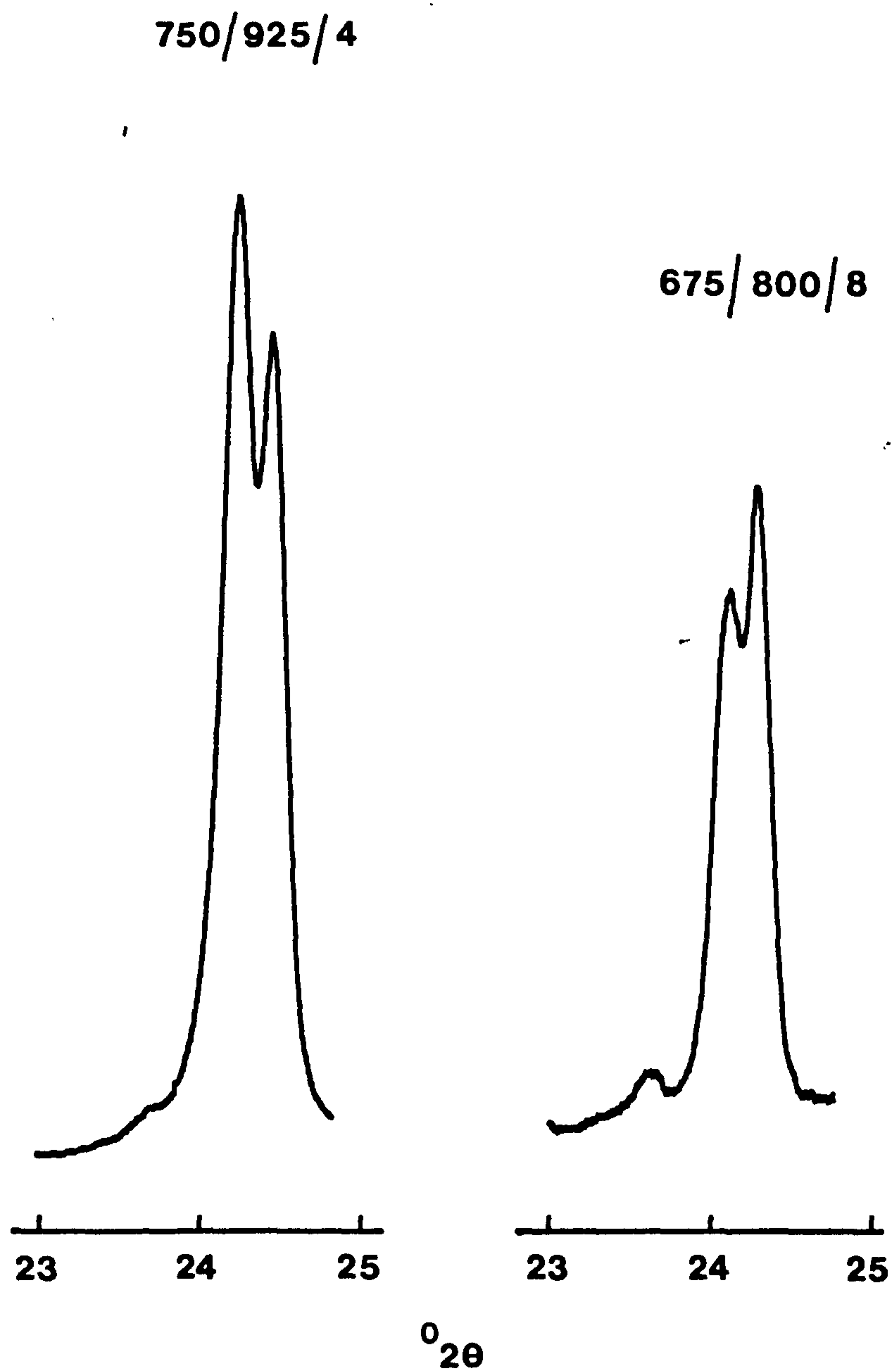


**Fig. 5.2 - Examples of peak-splitting
in principal magnesian petalite
reflection**

because of its structural likeness to the natural mineral ($\text{LiAlSi}_4\text{O}_{10}$) and has been assigned a monoclinic cell (113): petalite exhibits a multiplicity of reflections at both 3.67\AA and 3.73\AA . The breadth of an unsplit magnesian-petalite peak (750/825/8) suggests a grain size of $\sim 500\text{\AA}$ from line-broadening calculations (section 3.3.2); however, TEM studies of 750/825/8 indicate a grain size of $\sim 1000\text{\AA}$ (fig. 5.6) which suggests that the broad, yet unsplit, peak in this specimen may indeed be caused by the overlapping of two reflections. The degree of splitting typically observed (fig. 5.2) represents a change of only $\sim 0.03\text{\AA}$ in lattice spacing which could well be brought about by either a small distortion or change in parameters of the unit cell of the magnesian-petalite lattice; this explanation is therefore favoured.

5.3 Microstructural development of magnesian-petalite and μ -cordierite.

TEM was employed to investigate the microstructure of selected specimens of heat-treated 675- and 750- glass. Phase composition was considered with a view to choosing those specimens which highlighted the difference in properties of the base-glasses as observed in chapters 3 and 4. Table \bar{X} lists the specimens studied and summarises the principal phases identified by XRD.

TEM studies of these materials were generally hindered by both the fine scale of some microstructural features and the propensity of the magnesian-petalite phase to disorder over relatively short times (~ 10 - 20 secs.) of illumination. The generally small scale of microstructure results in a large degree of overlay which at the tilt angles required for EDAX analysis severely limited the spatial resolution of this technique in all but the thinnest regions of a specimen; the resulting X-ray count-rate was insufficient for reliable analysis of such areas. Use of this technique was therefore restricted to the scanning transmission mode (STEM) whereby a reduced probe of $\sim 50\text{\AA}$ diameter allowed some confirmation of the

| Base glass and heat-treatment | Phase composition |
|-------------------------------|--|
| 750/20 | None detectable. Blue coloration. Glass-in-glass phase separation suspected. |
| 675/775/50 | MgTi ₂ O ₅ crystallites. |
| 750/775/50 | MgTi ₂ O ₅ crystallites. |
| 675/825/4 | Mainly magnesian-petalite, some μ -cordierite. |
| 750/825/8 | magnesian petalite. |
| 675/925/4 | μ -cordierite |
| 750/925/4 | magnesian petalite and μ -cordierite |
| 675/775/50/1000/5 | μ -cordierite, enstatite |
| 750/1000/4 | μ -cordierite, magnesian-petalite, some enstatite. |
| 750/775/50/1000/5 | magnesian petalite, enstatite, some μ -cordierite. |

Table X. Specimens studied by TEM.

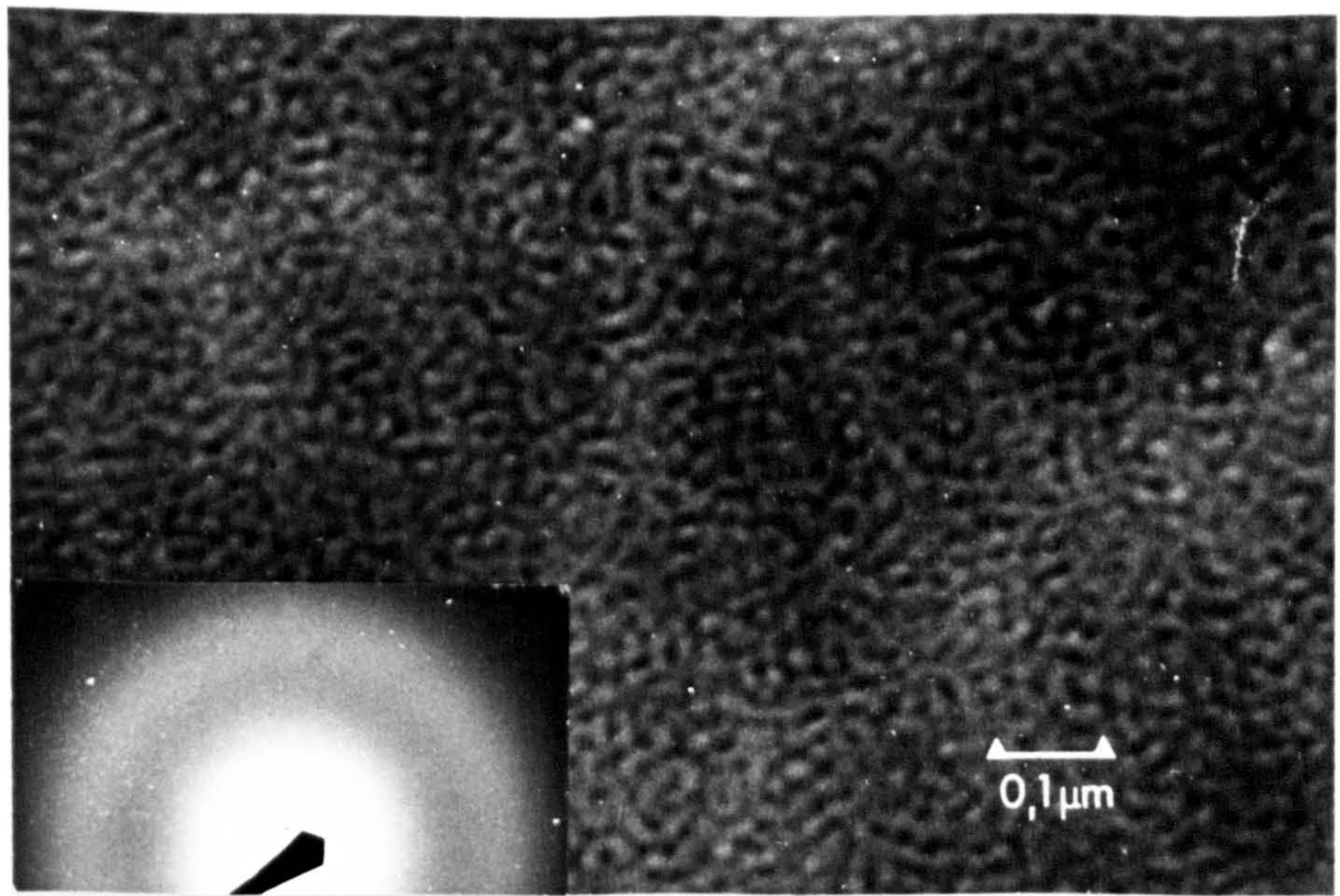
composition of MgTi₂O₅ crystallites: i.e., that they contained significantly more Mg and Ti than the surrounding glass or crystalline silicate phase. Attempts were made to compositionally resolve these silicate and glass phases but as a result of the above considerations data were generally unreliable and inconsistent.

The phenomenon of disordering is commonly observed in metastable silicate compounds resulting in a visible loss of crystallinity. Additional radiation damage may cause cavitation of glassy phases. Disorder of the magnesian petalite phase was commonly observed and attempts were made to study specimens containing this phase with a 200keV microscope for which the reduced beam current significantly increases stability times. Theoretically, a higher accelerating voltage should improve resolution. However the 200keV instrument was found to be optically inferior with much loss of image sharpness. The

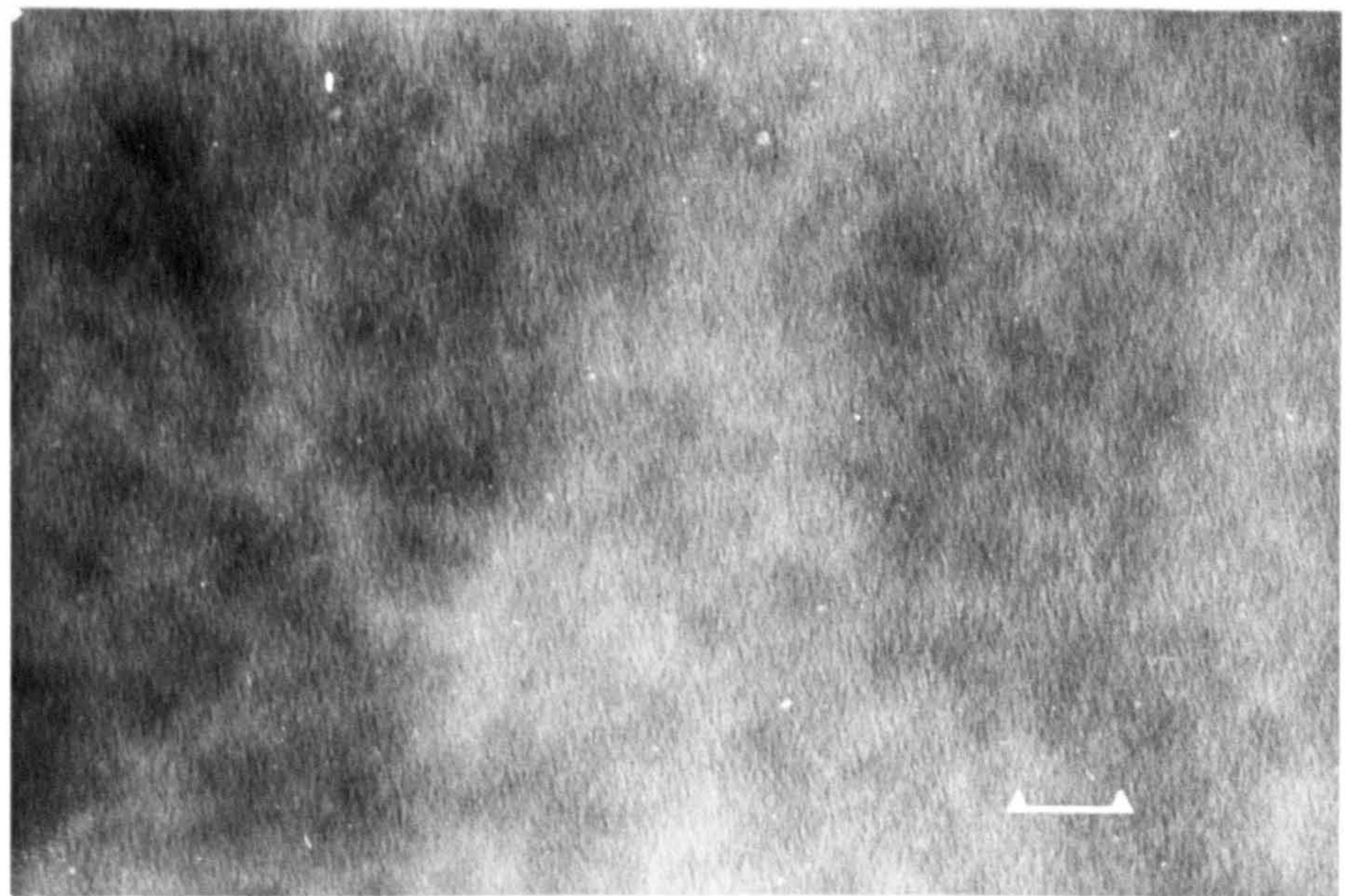
disordering problem was sufficiently reduced in the 100keV microscope by reducing the spot size, inserting additional condenser apertures and reducing the beam current at source. This had the effect of extending stability times to many minutes with an overall improvement in image sharpness and contrast.

In fig. 5.3. glass-in-glass phase separation of 750/20 is shown (a) compared with the typical "microstructure" observed in untreated 675 and 750- glass (b). The fine scale of separation ($\sim 100\text{\AA}$), high interconnectivity and lack of sharp delineation between the phases are all indicative of spinodal decomposition wherein the chemical composition of the phases varies gradually from one to another in the absence of a well defined interface. After initial suspicions that this structure may be an artifact introduced by the carbon-coating process, both 750/20 and the base-glasses were rethinned and coated simultaneously. The question of defocus is also ruled out as a through focus series of micrographs was recorded of which fig. 5.3(a) represents the "sharpest". From absorption contrast considerations one would expect the darker of the two phases to contain a higher proportion of TiO_2 . Clearly such microstructure is not evident in the untreated glass samples which were thinned using the same apparatus.

Figures 5.4(a) and (b) are micrographs of 675/775/50 and 750/775/50 respectively and in both cases MgTi_2O_5 was the only crystalline phase identified by XRD. In fig. 5.4(a) the growth of MgTi_2O_5 would appear to be of a spherulitic nature and the residual glass shows little evidence of additional contrast, i.e. phase separation. This is markedly different to fig. 5.4(b) in which smaller and approximately spherical crystallites of MgTi_2O_5 appear to grow in the darker, TiO_2 -rich glass phase. In both cases there is some correlation between observed crystallite size and that determined by XRD line-broadening (section 3.3.2). The variation in size and morphology of these crystallites is evidence that different nucleation and growth mechanisms may be operating in 675- and 750- glass.

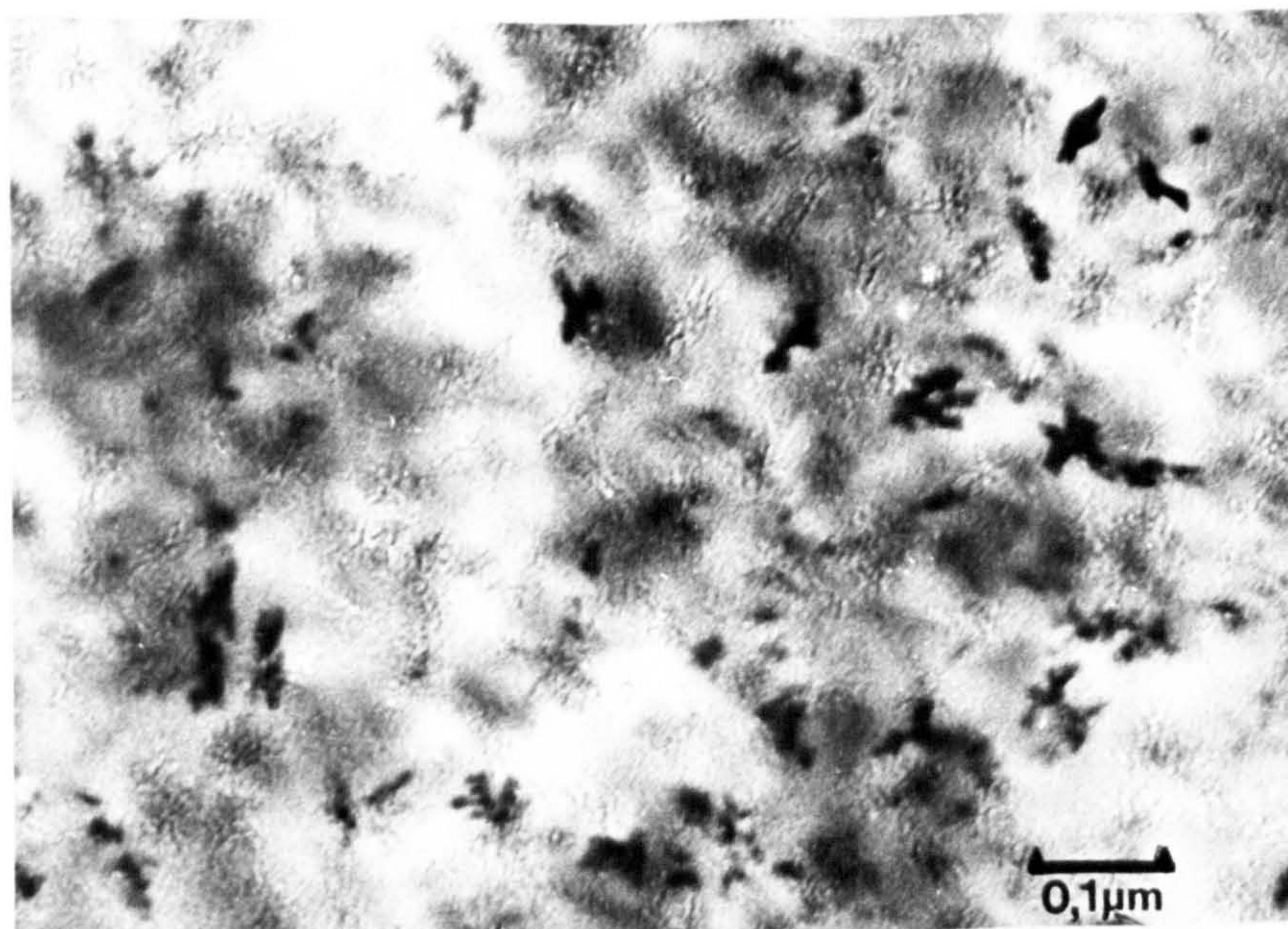


(a) phase separation

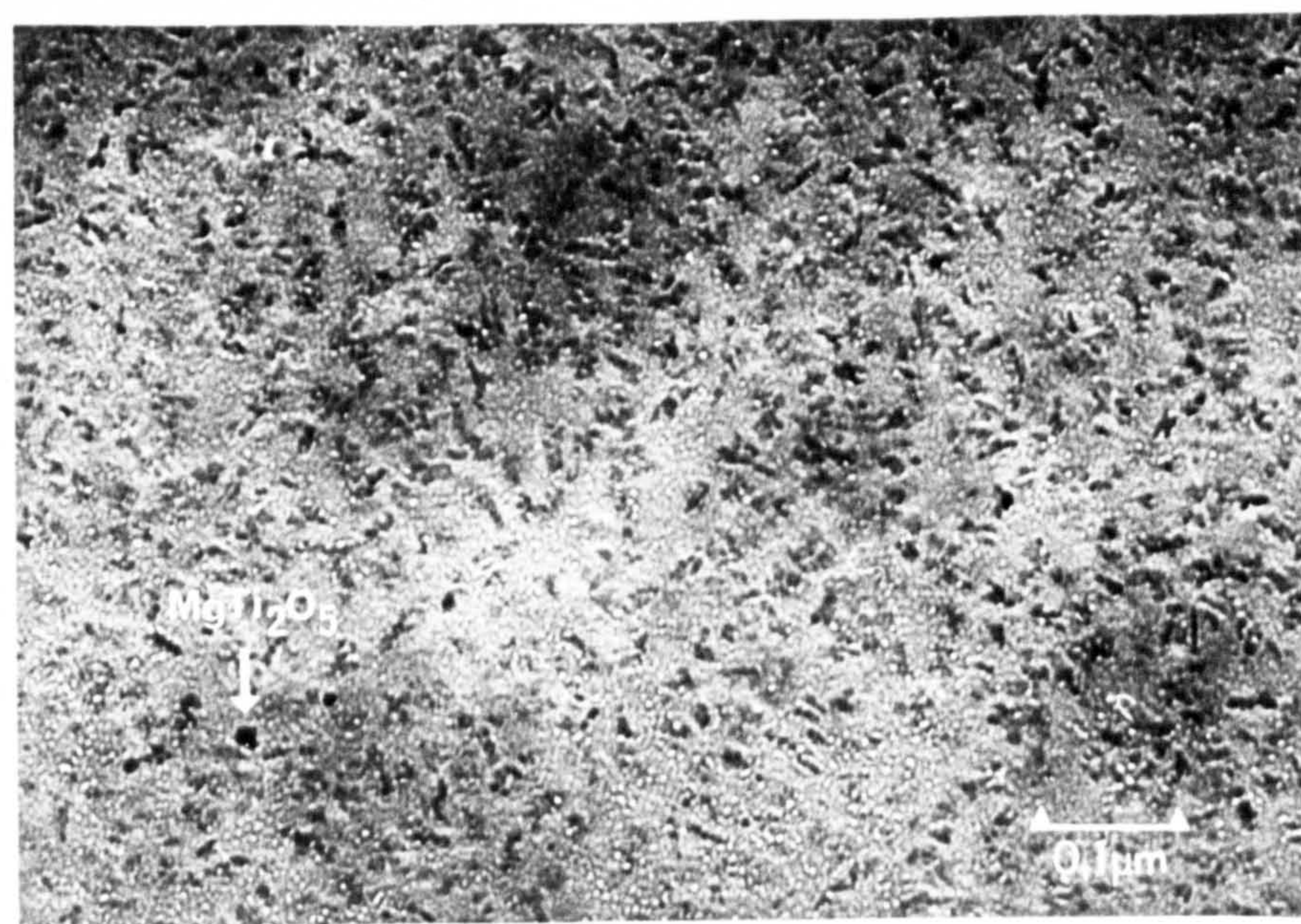


(b) base glass

FIG. 5.3



(a) 675/775/50



(b) 750/775/50

FIG. 5.4

In 675/825/4 the emergence of magnesian-petalite and μ -cordierite was observed and fig. 5.5(A) and (C) illustrate the typical microstructure of this specimen. In fig. 5.5(B) and (E) a single crystal of magnesian-petalite is identified by selected-area electron diffraction and confirmed by dark field imaging (fig. 5.5(D)). Crystallisation of magnesian-petalite has occurred in the glass matrix between the MgTi_2O_5 spherulites as observed in fig. 5.4(a) and growth of the spherulites has been furthered. The additional satellite spots in figs. 5.5(B) and 5.5(E) (inset is an enlargement) indicate that a degree of long-range ordering is taking place of the magnesian-petalite lattice with an estimated periodicity of $\sim 30\text{\AA}$ i.e. several unit cell dimensions. In the absence of much additional diffraction data and an accurate knowledge of the unit cell dimensions and symmetry, a calculation of the exact periodicity and direction of ordering was not attempted. Calculation of lattice plane d-spacings assuming the monoclinic cell of Leng-Ward (113) i.e. $a = 11.78\text{\AA}$, $b = 4.94\text{\AA}$ and $c = 7.62\text{\AA}$ with $\beta = 112^\circ$ could not be rationally matched to the data included here. It was therefore concluded that the magnesian-petalite phase in 675/825/4 possessed a unit cell of different dimensions from the above; possibly a consequence of compositional variations. The presence of μ -cordierite in this specimen was confirmed by XRD but could not be identified in the microstructure.

In 750/825/8 (fig. 5.6) crystallisation of magnesian petalite has taken place from one of the separated, amorphous phases, although which of these phases is not immediately obvious. Consideration of the simplified phase diagram (fig. 5.7) suggests that if the initial glass composition decomposes to the sub-phases indicated then the SiO_2 -rich phase would lie in the theoretical phase-field for magnesian-petalite formation (48) and would therefore be expected to precipitate from this phase preferentially. The resulting microstructure is that of a fine-grained

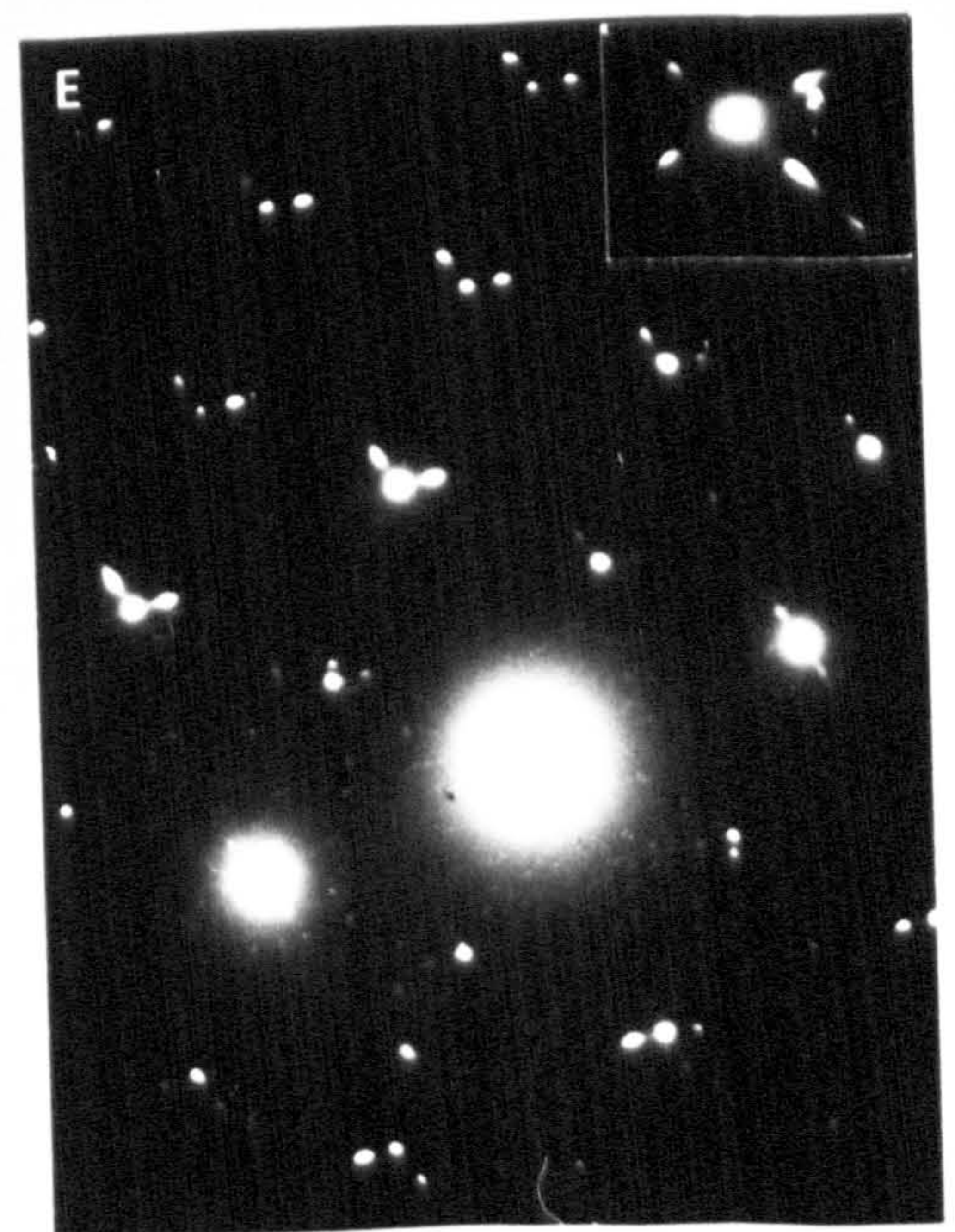
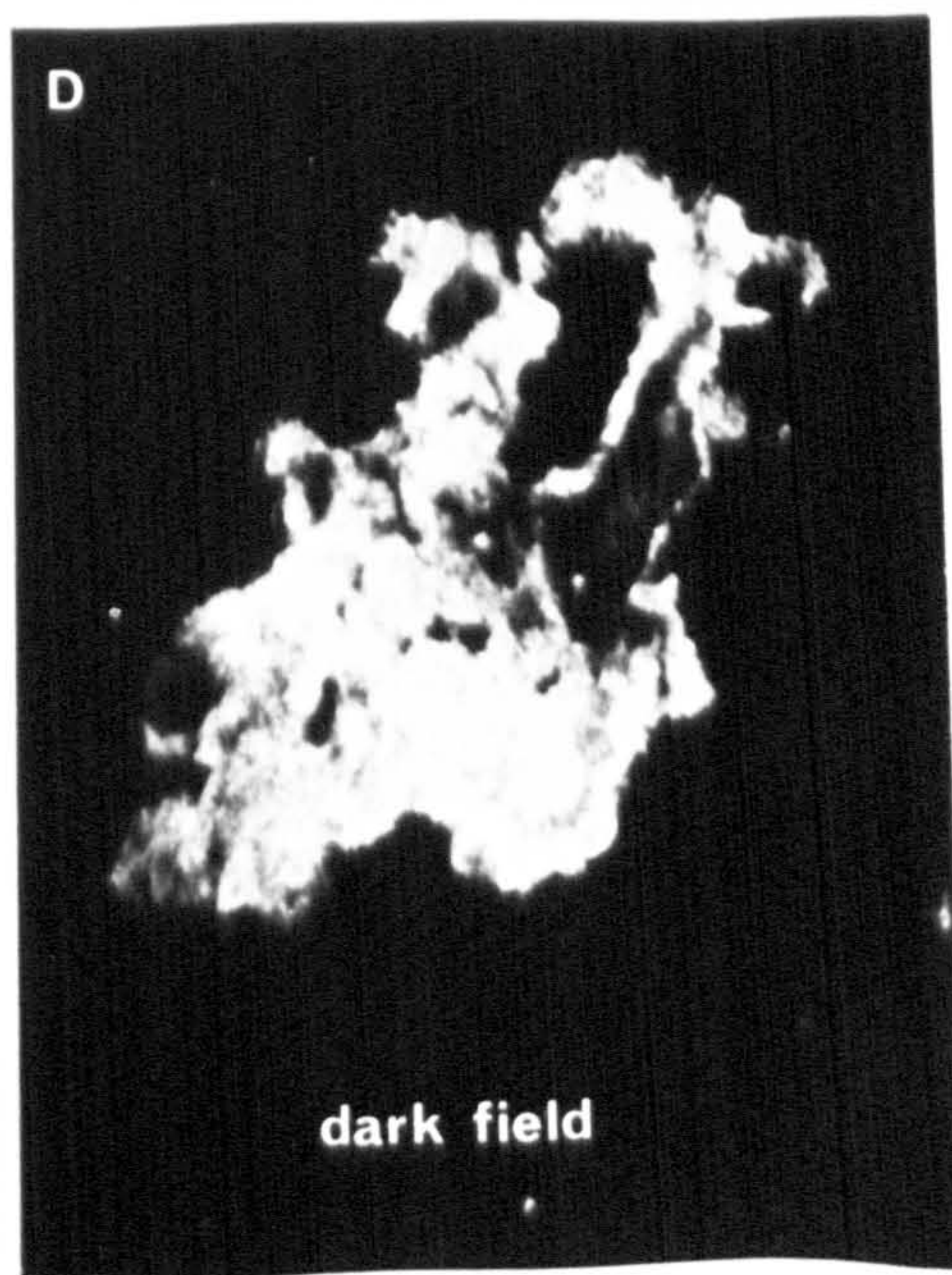
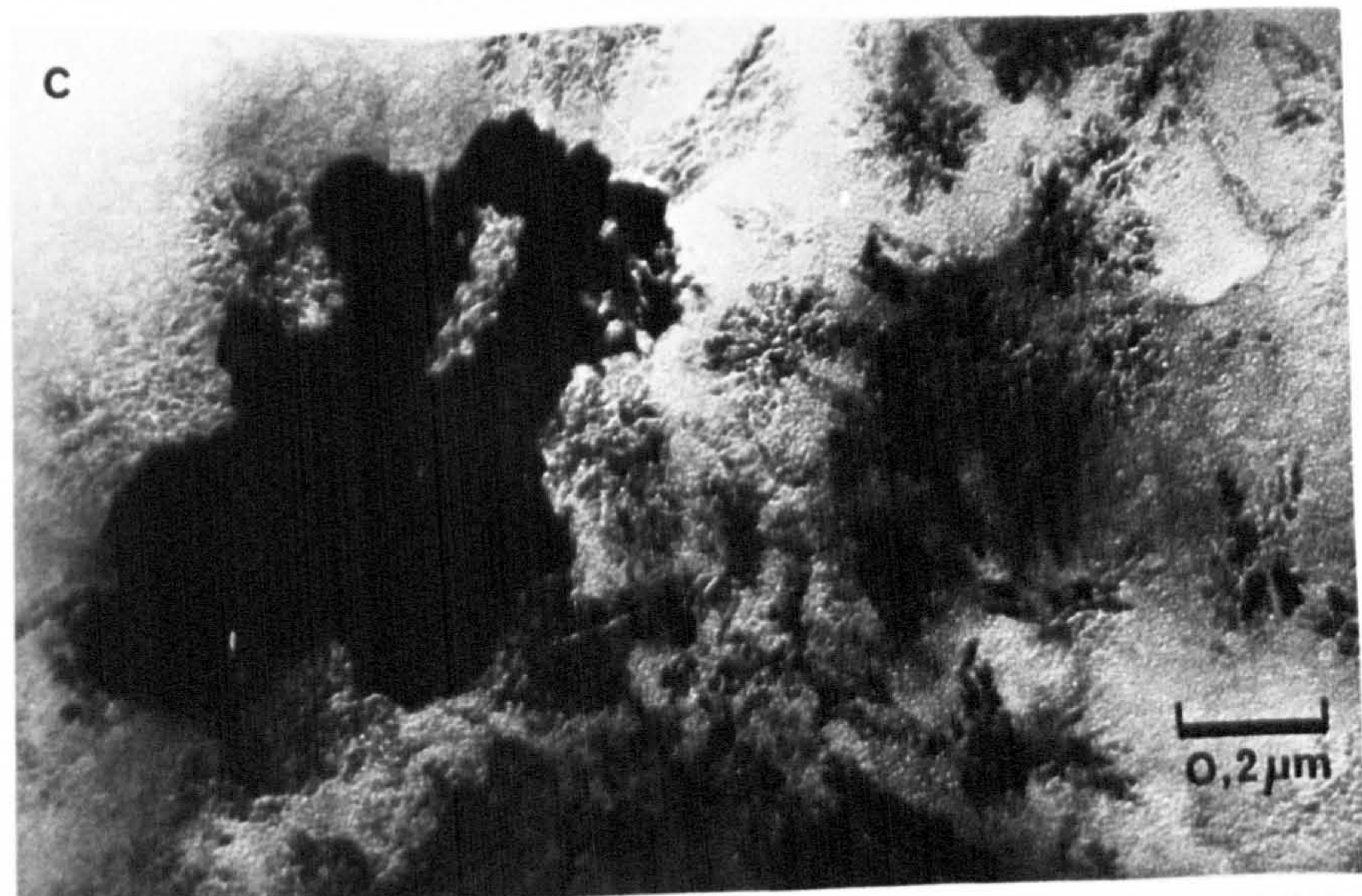
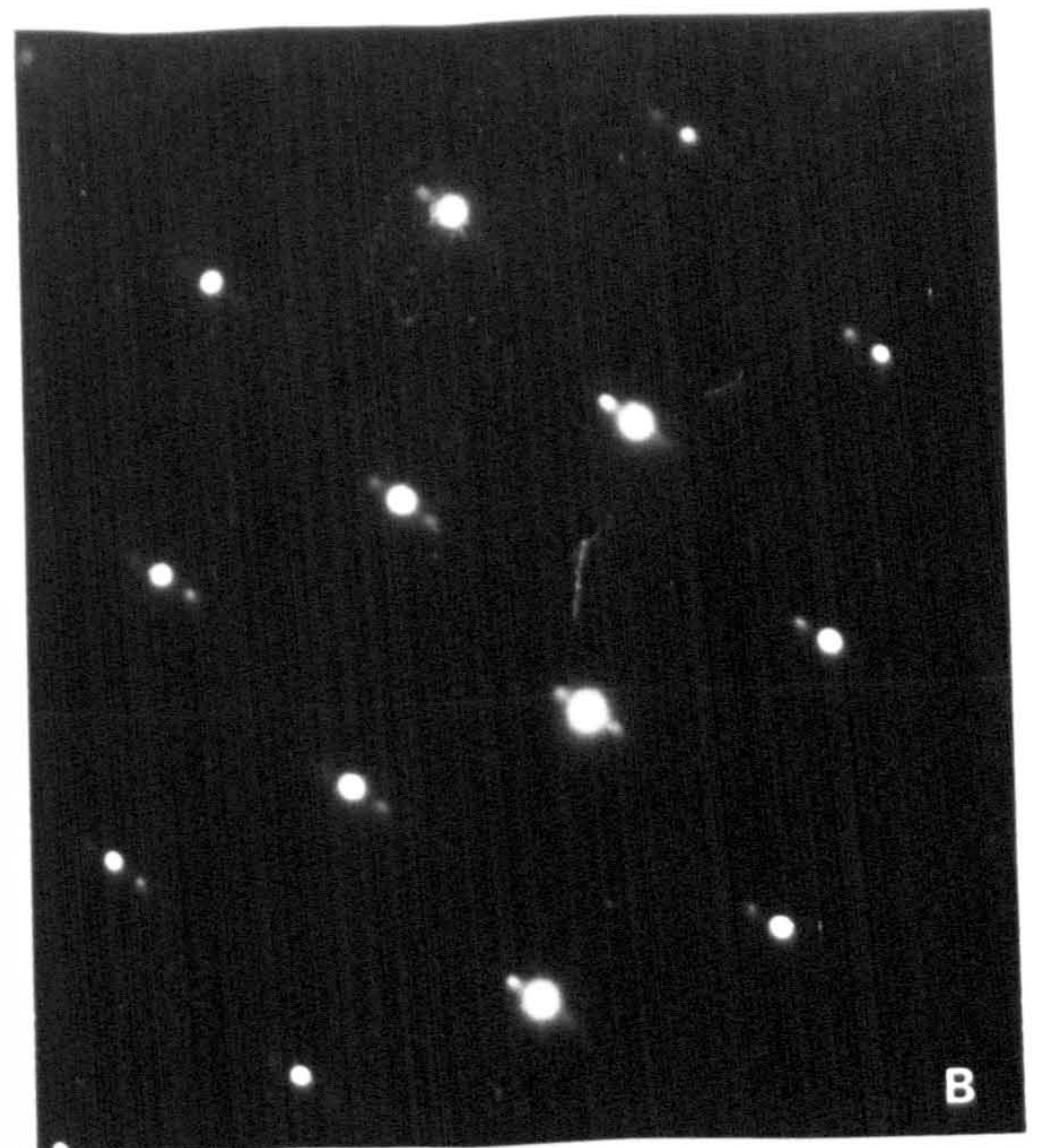
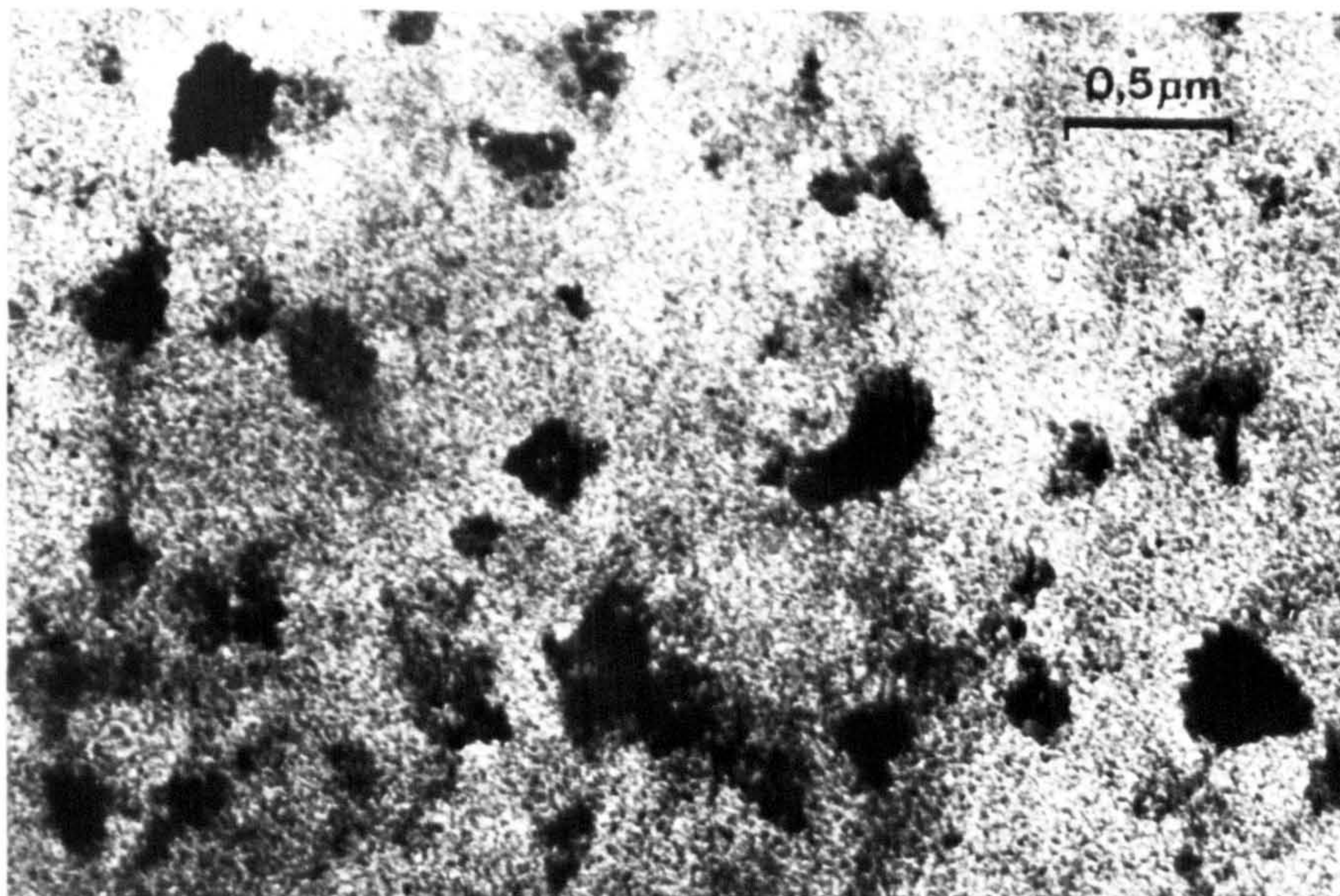
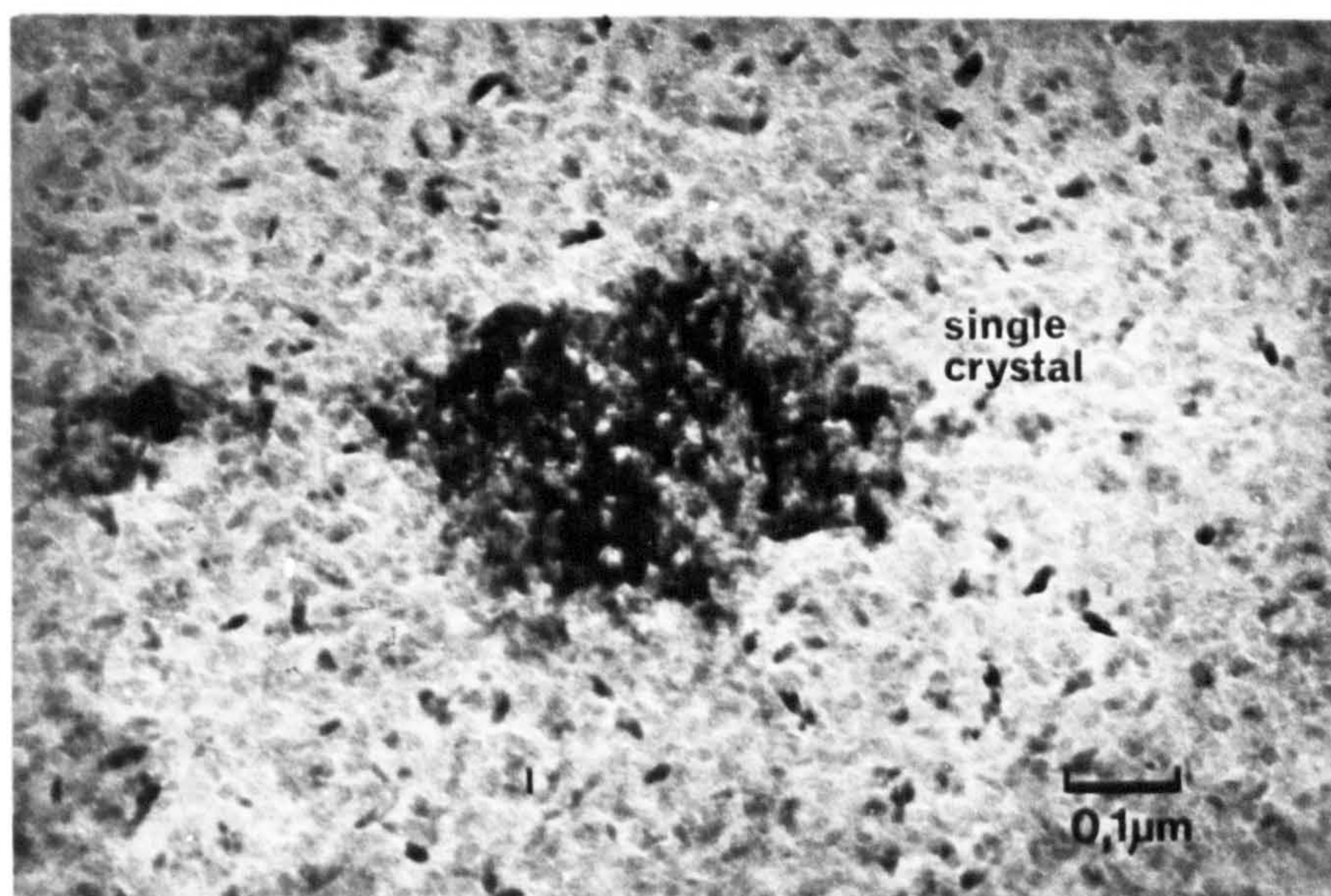


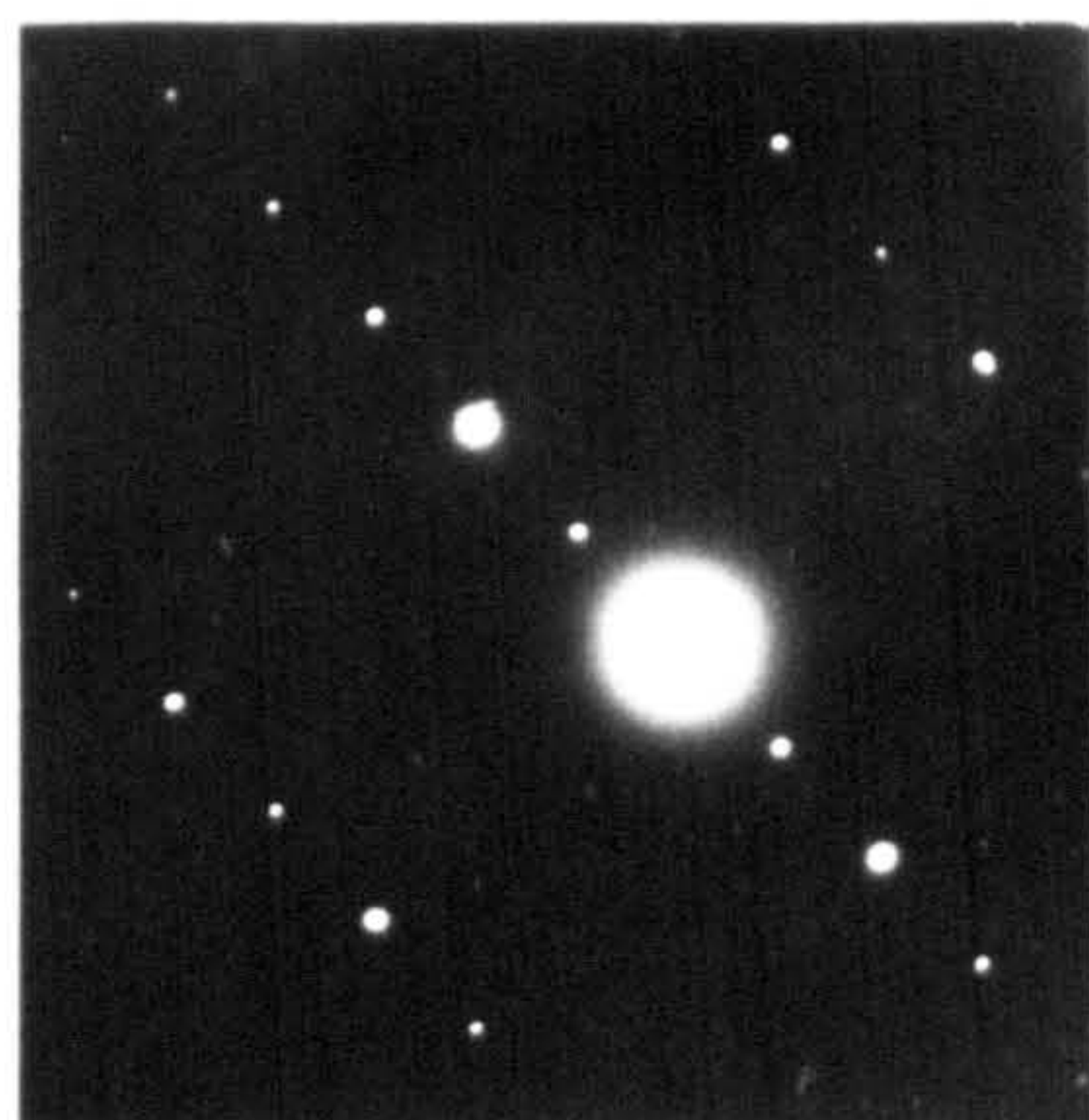
FIG. 5.5 - 675/825/4



A



B



C



FIG. 5.6 - 750/825/8

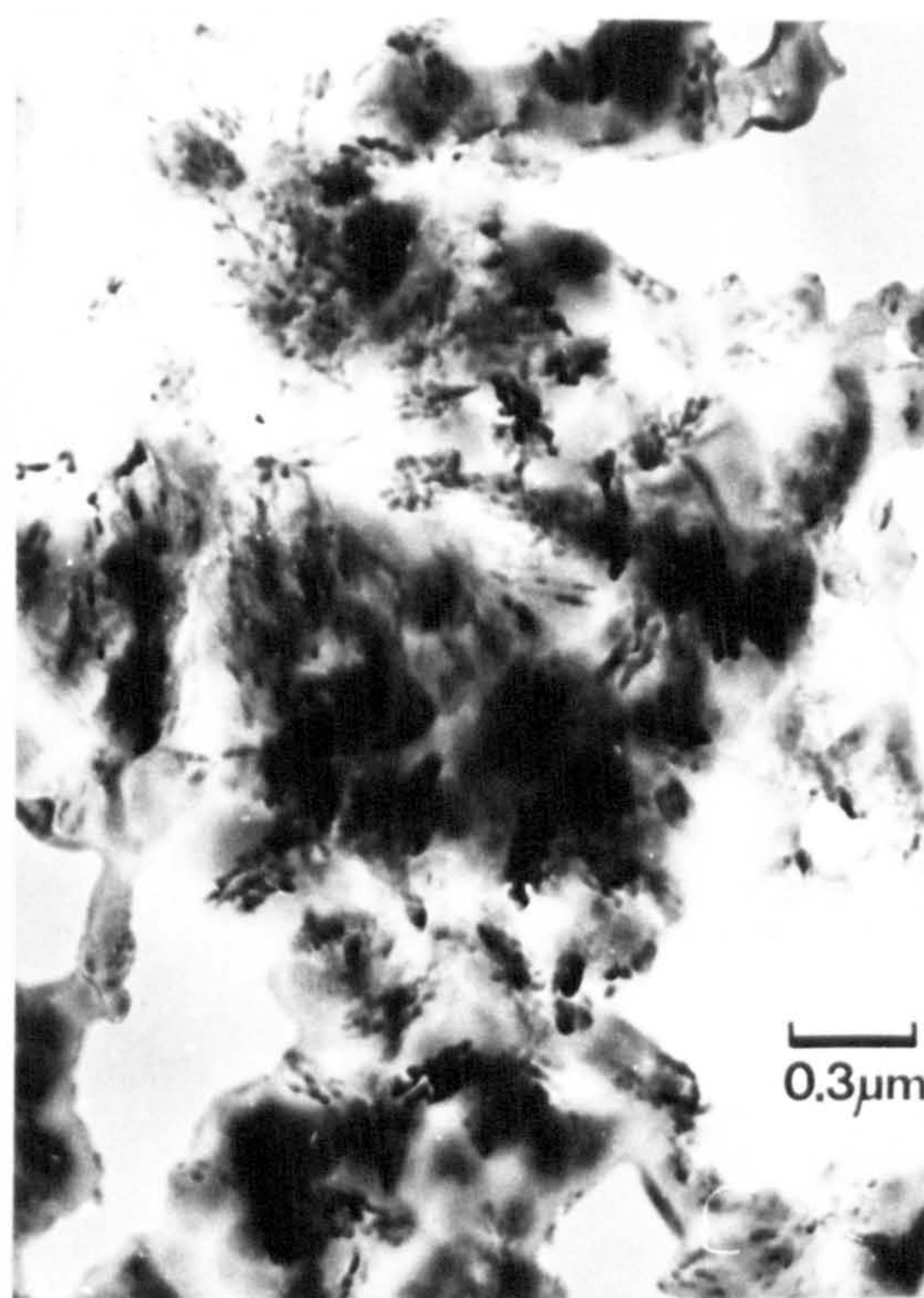
polycrystalline material in which single crystals have grown through a phase-separated structure to impingement (fig. 5.6(A) and (B)). This was observed more clearly at a lower magnification (A) by tilting the specimen whereby the whole area under illumination could be mapped out by such single-crystal regions as they came in and out of diffraction contrast.

Clearly crystallisation of magnesian petalite from 675- glass (fig. 5.5) and 750- glass (fig. 5.6) exhibits considerably dissimilar growth characteristics which are a result of the different nucleation environments initiated (fig. 5.4). Growth through the phase-separated structure (750- glass) has been retarded, resulting in a reduced average grain size.

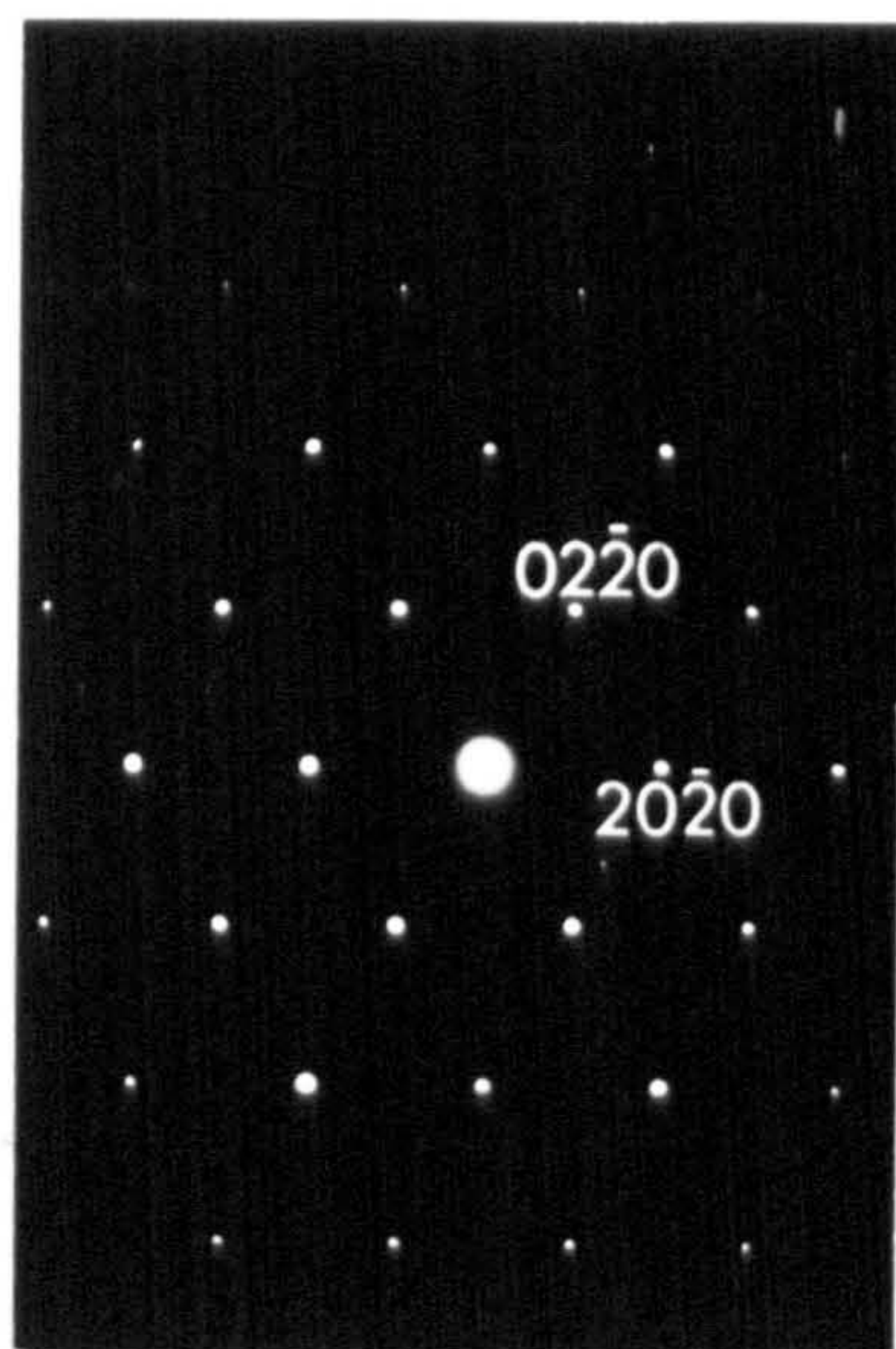
Single crystals of μ -cordierite are evident in 675/925/4 (fig. 5.8) in which this phase was the only one identified by XRD (fig. 3.9). A background structure of MgTi_2O_5 spherulites is again observed as in fig. 5.4(a) and the inclusion of these within a μ -cordierite crystal has caused considerable strain as shown by the bend contours in fig. 5.8(A). Tilting away from a strongly diffracting condition clearly reveals the distribution of MgTi_2O_5 crystallites. Figs. 5.8(C), (D) and (E) are single crystal diffraction patterns for the three zone axes indicated and are sufficient to define the μ -cordierite unit cell. The additional weaker spots on patterns D and E are indicative of an ordered superlattice with a doubling-up of the unit cell for both a- and c- axes: indexing of the principal reflections is made on this basis and a systematic absence of the $10\bar{1}0$ reflection is noted. μ -cordierite is a β -quartz derivative having a hexagonal cell in which Al^{3+} substitutes for Si^{4+} with Mg^{2+} present to maintain charge neutrality. Schulz et al (47) investigated a whole range of such derivatives with $\text{MgO}:\text{Al}_2\text{O}_3:\text{SiO}_2$ ratios of 1:1:6 to 1:1:2 (μ -cordierite represents 1:1:2.5) and observed super-cells with an overperiod which varied as a function of both heat-treatment temperature and composition: ordering was not observed for a 1:1:2 compound in which



A

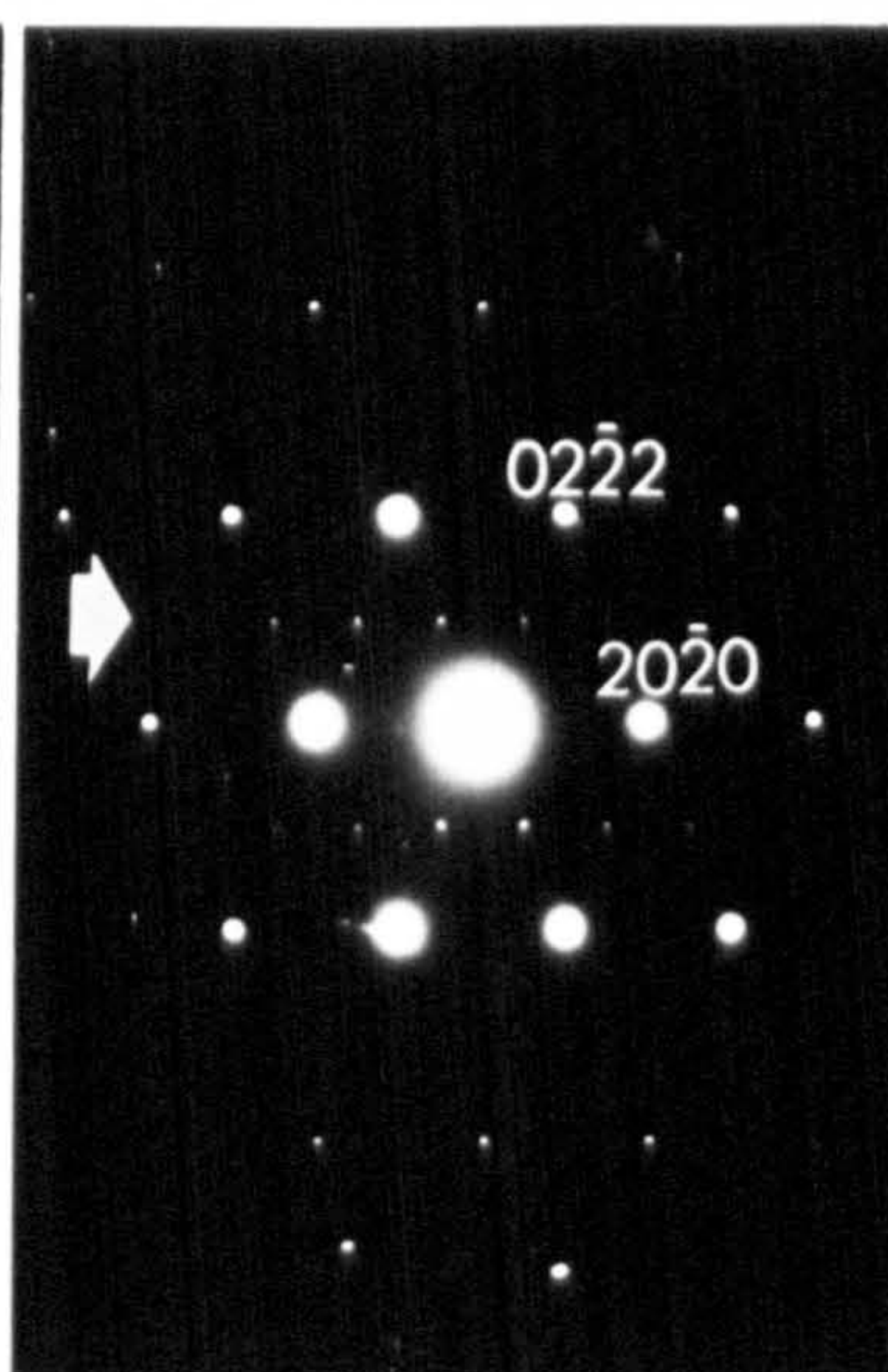


B



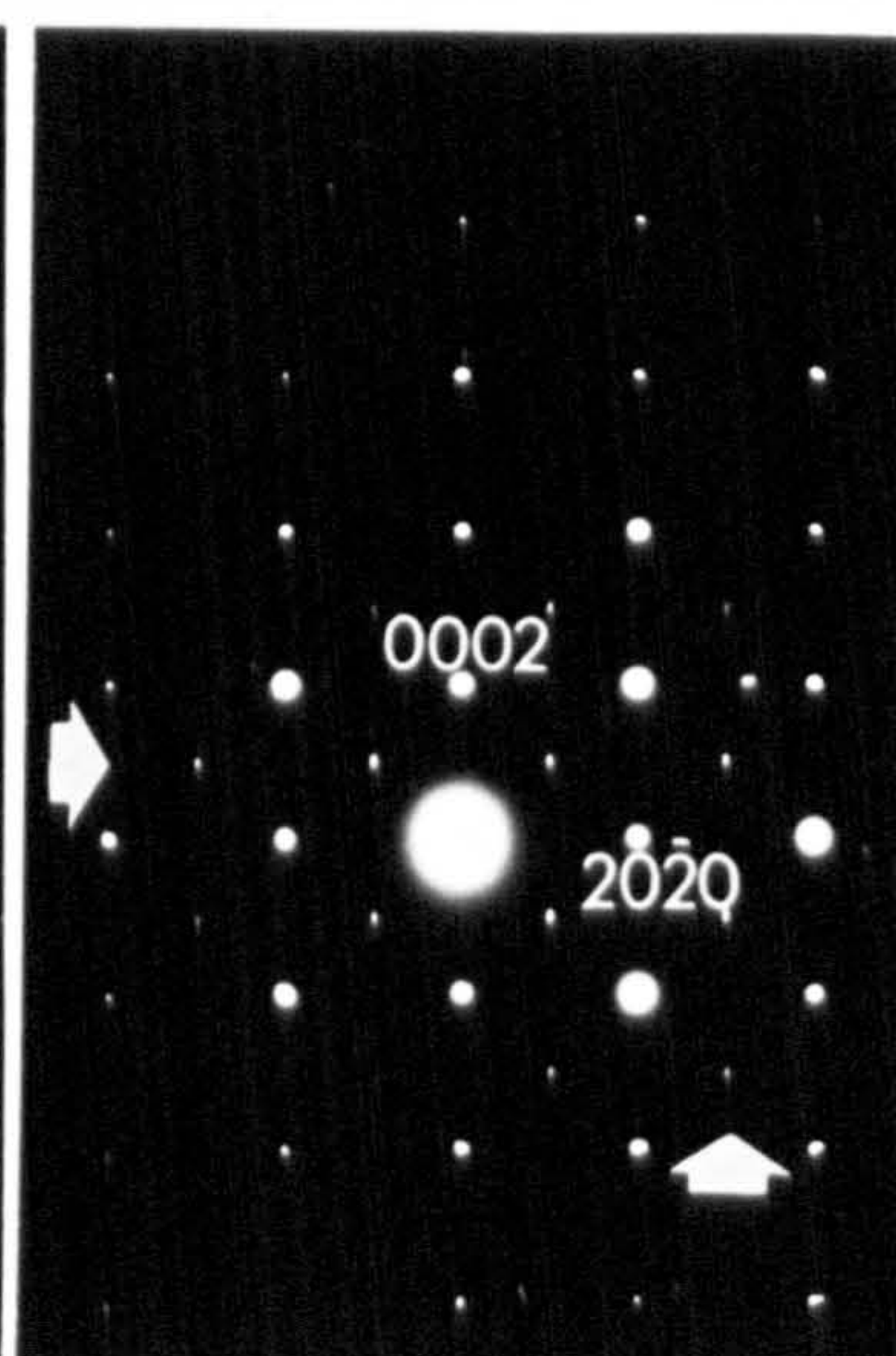
C

[0001]



D

[0101]



E

[0100]

Indexing based on doubled unit cell.

FIG. 5.8 - 675/925/4

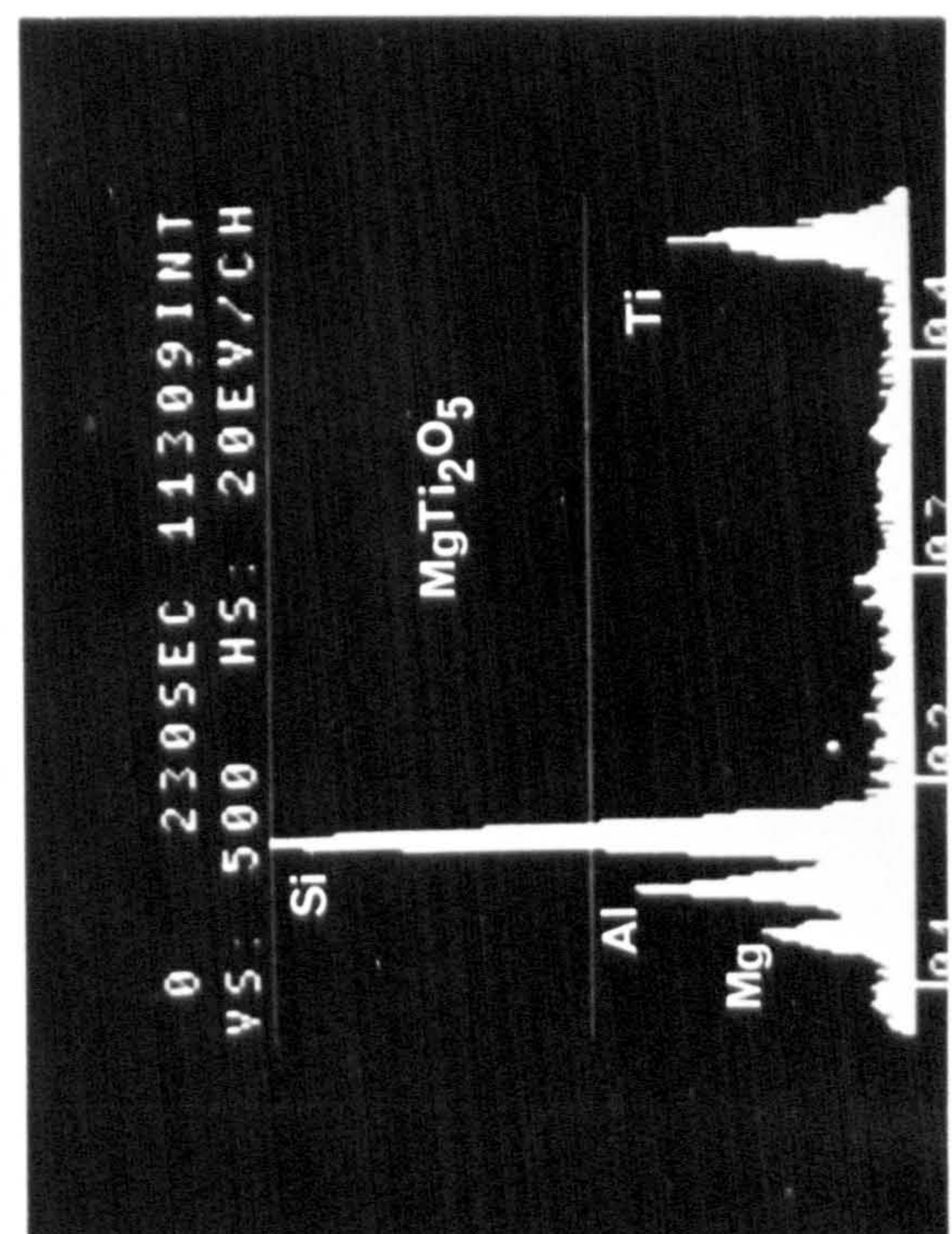
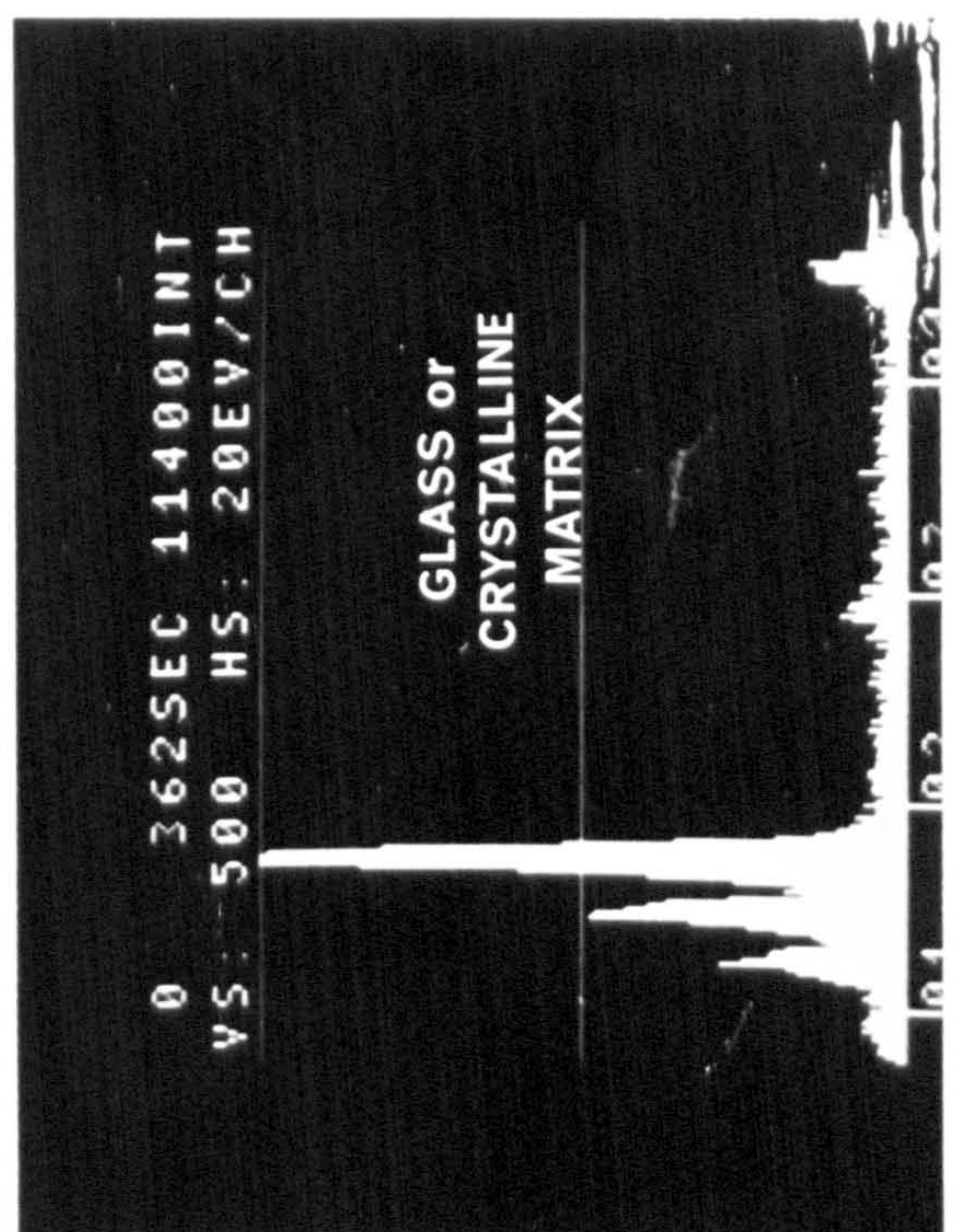


FIG. 5.9

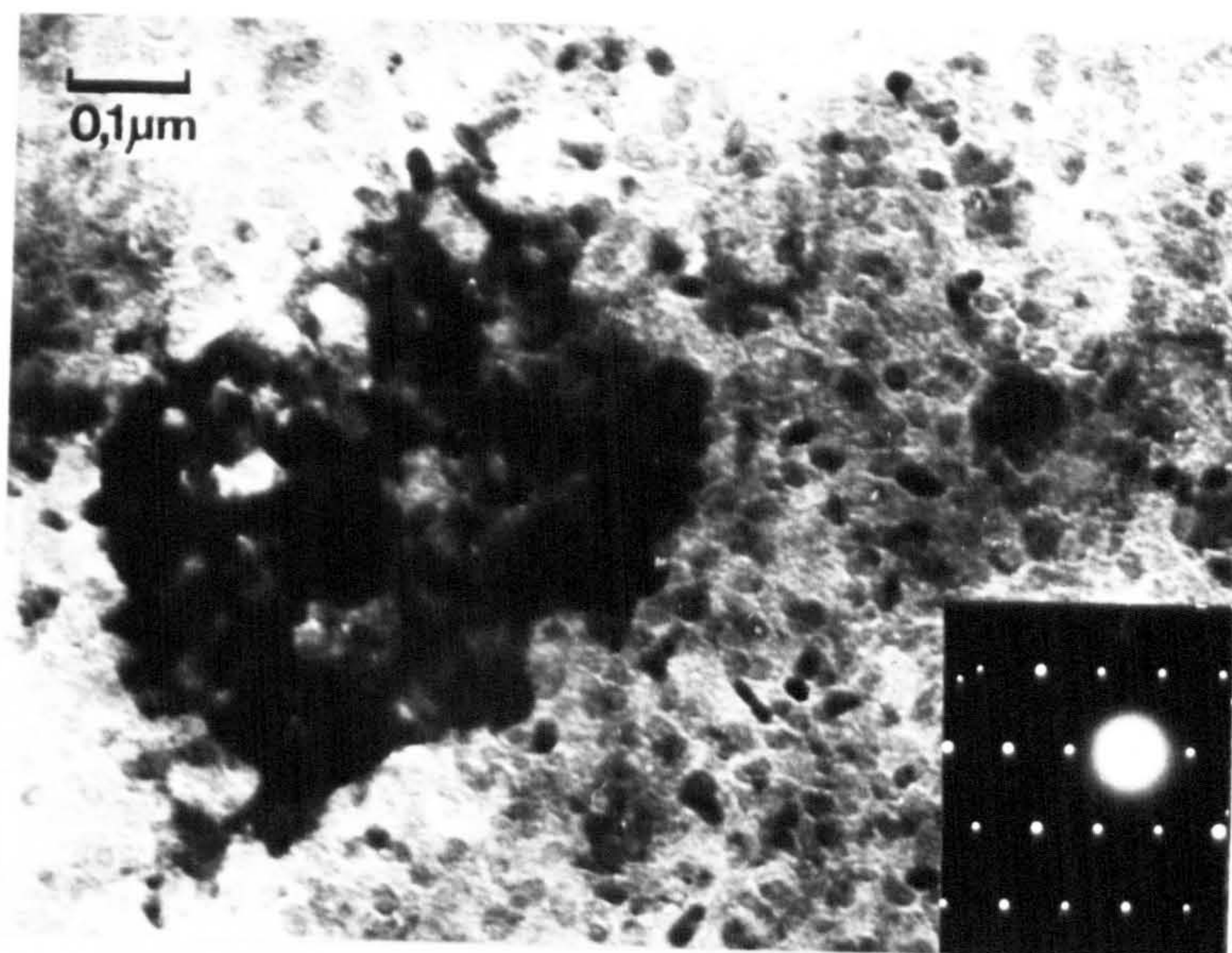
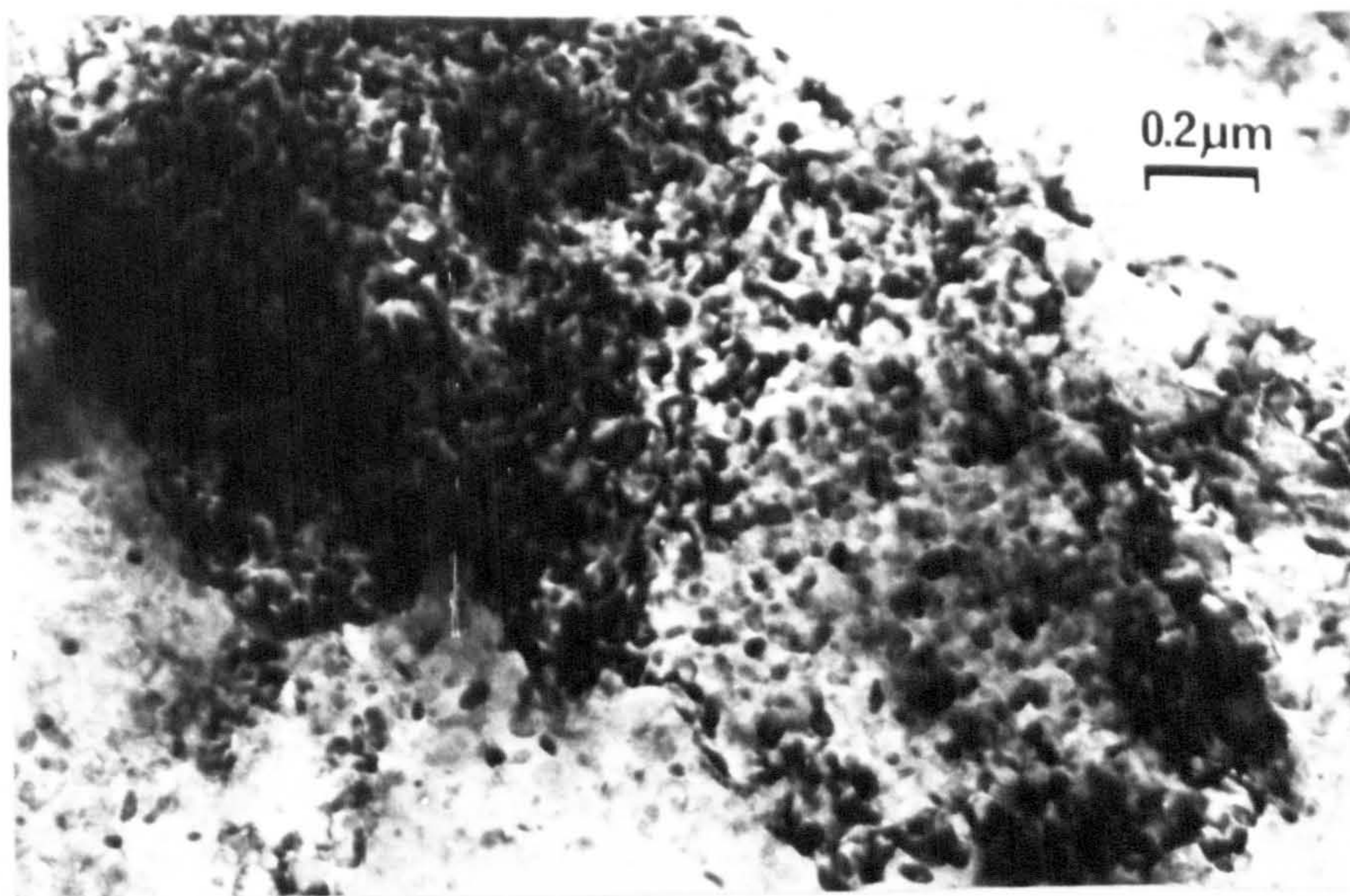
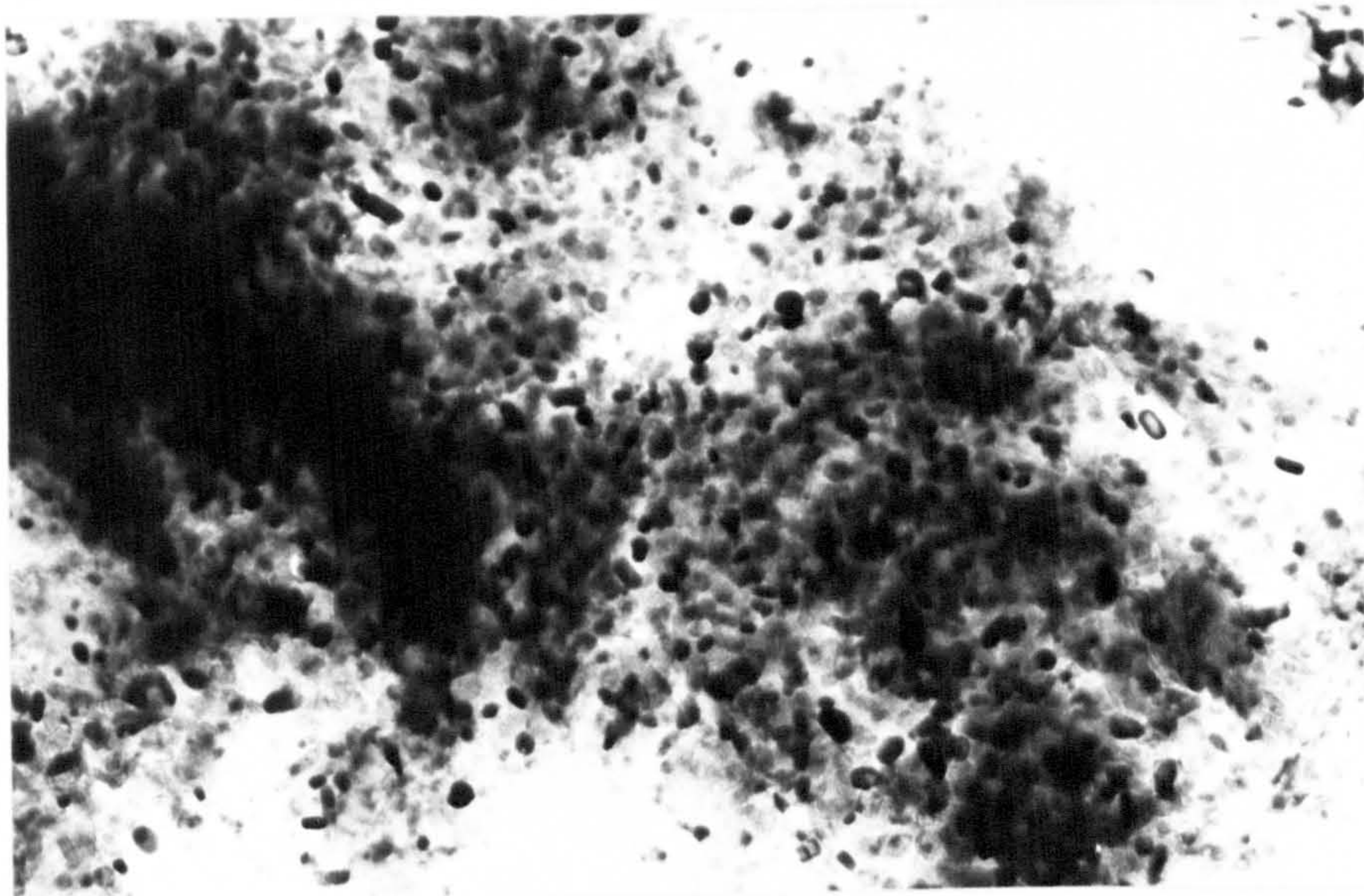


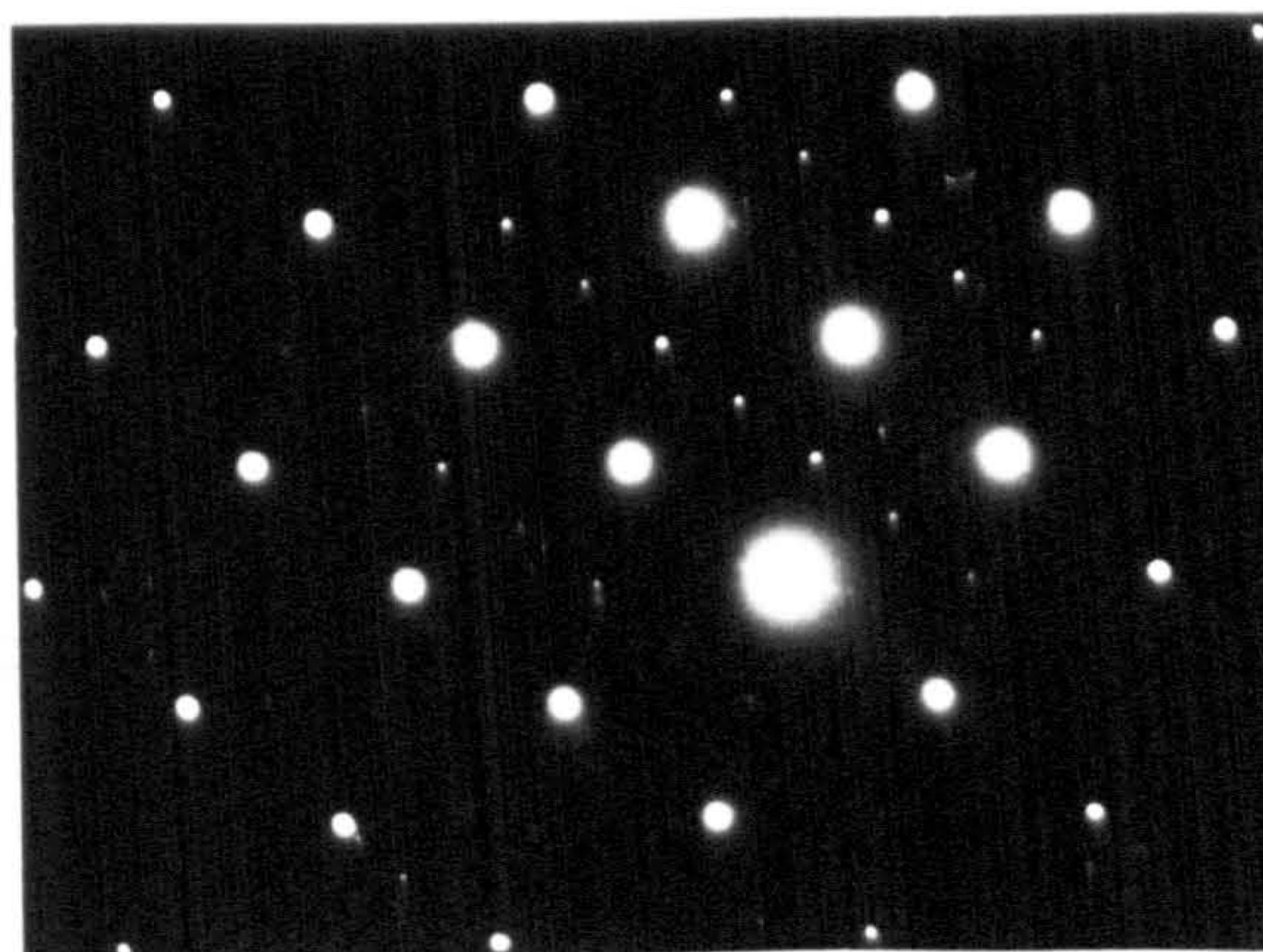
FIG.5.10 – 750/925/4



A



B



C

FIG. 5,11 - 750/1000/4

phase development samples of 675/775/50 and 750/775/50 (fig. 5.4) were heat-treated at 1000°C for 5 hours and the crystalline products determined by XRD. A marked difference in phase composition was noted for the two specimens (fig. 5.12); μ -cordierite and small amounts of enstatite in 675/775/50/1000/5(X) as against magnesian petalite, enstatite and some μ -cordierite in 750/775/50/1000/5(Y). Appreciable splitting of the magnesian petalite principal reflection is clear in fig. 5.12(B). The microstructures of specimens X and Y are presented in figures 5.13 and 5.14 respectively. The μ -cordierite phase in X again exhibits long-range ordering of a double periodicity (fig. 5.13(B)). The complexity and fine scale of these microstructures limited phase identification by conventional techniques. Both EDAX analysis and micro-diffraction were attempted using the STEM probe. No consistent data on variations in chemical composition could be collected and micro-diffraction was unsuccessful.

5.4 Summary

The microstructural development of both magnesian petalite and μ -cordierite is considerably influenced by the microstructure present during the "nucleation" stage at around 775°C. The presence of phase separation in 750- glass at this stage appears to have the effect of both limiting the growth of magnesian petalite and subsequent stabilisation of this phase. The role of MgTi_2O_5 as nuclei in both glass systems is not obvious as single crystals of both magnesian petalite and μ -cordierite, with grain sizes larger than the inter-nuclei distance, grow with a coherent orientation in the surrounding glass matrix. This may be in part due to accelerated growth rates or coarsening at elevated temperatures. The transformation of magnesian petalite to μ -cordierite is assumed to take place via the diffusion of both Mg^{2+} and Al^{3+} ions; however, a clearly identifiable growth interface is not evident in these complex micro-

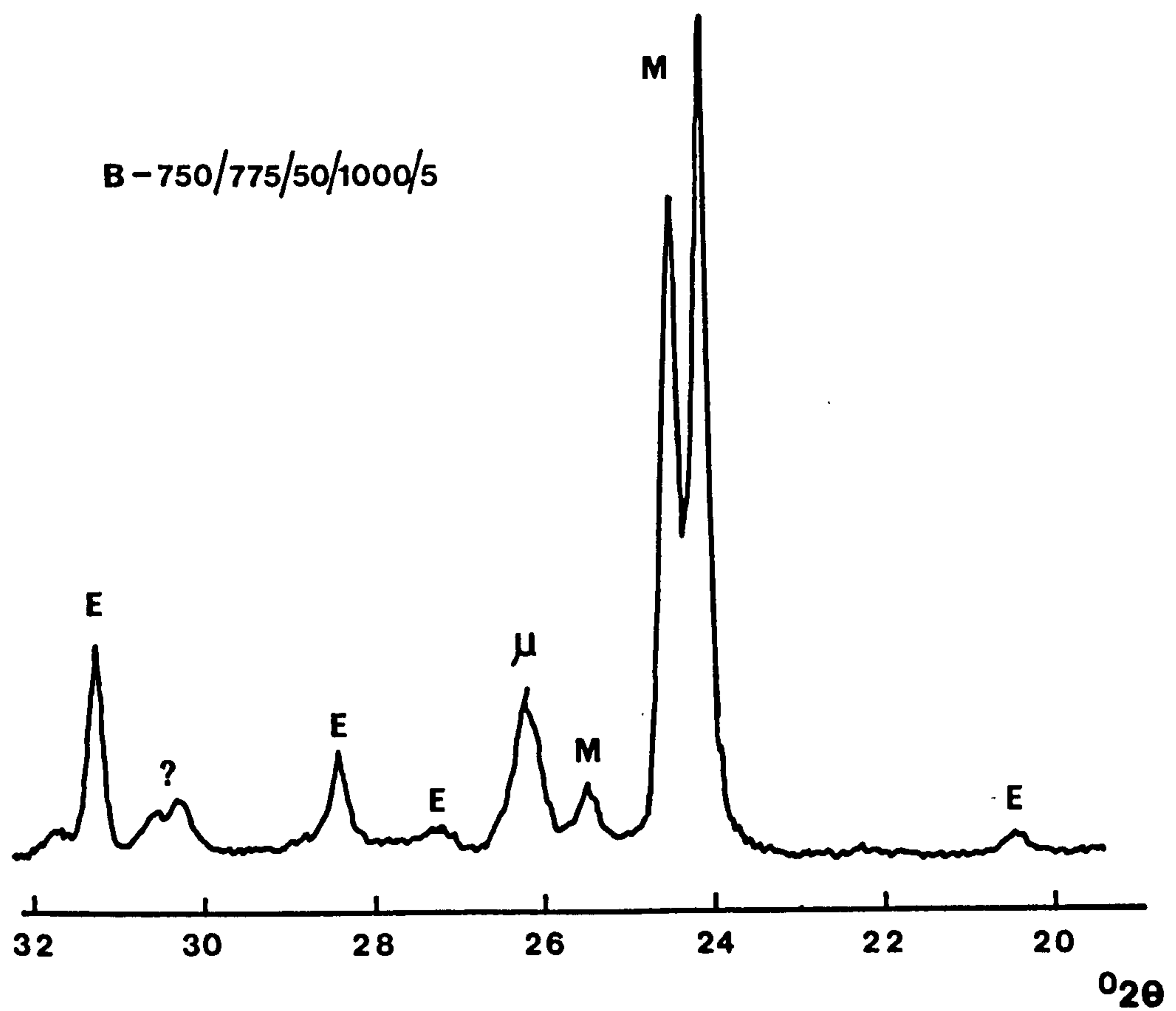
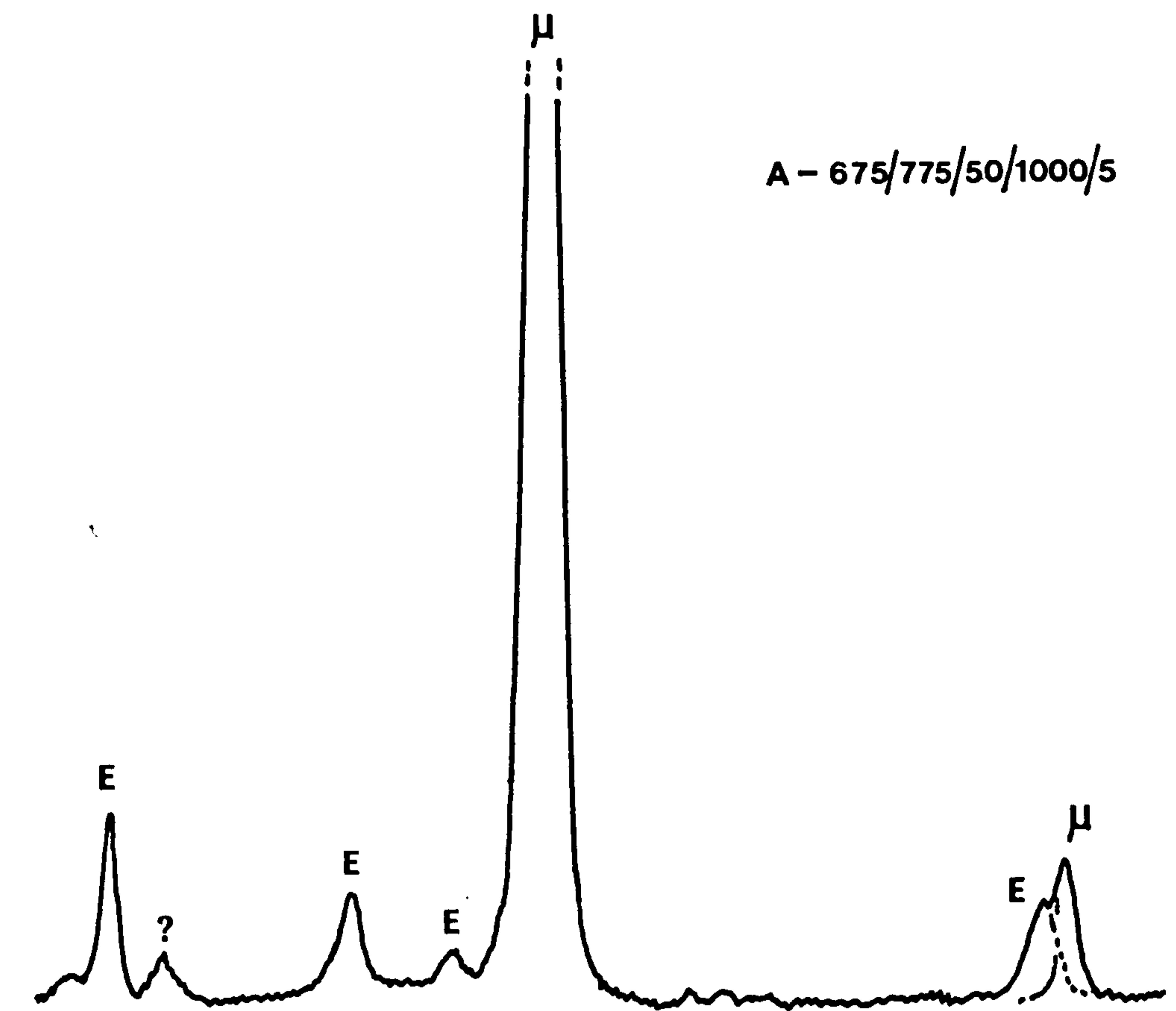
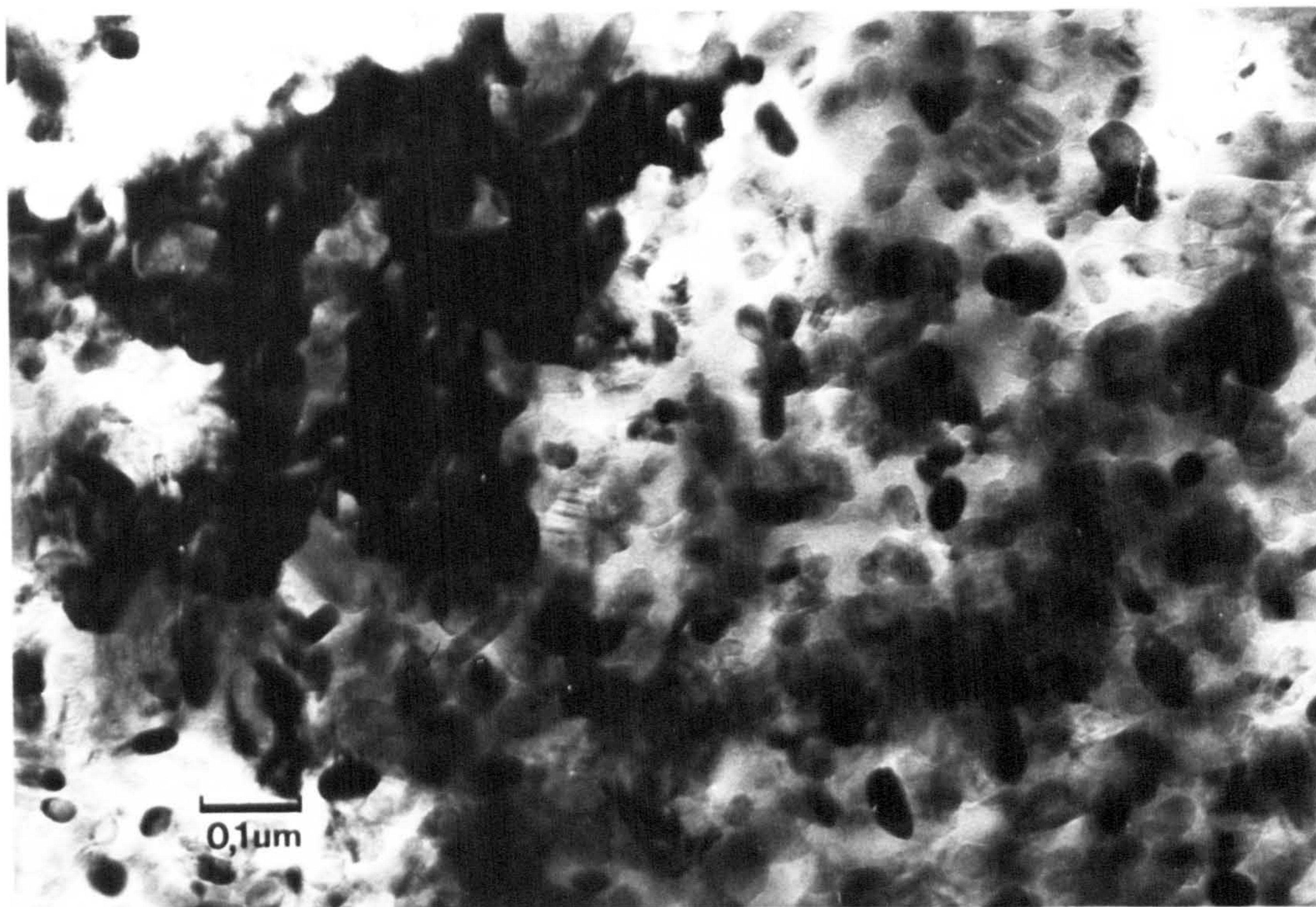
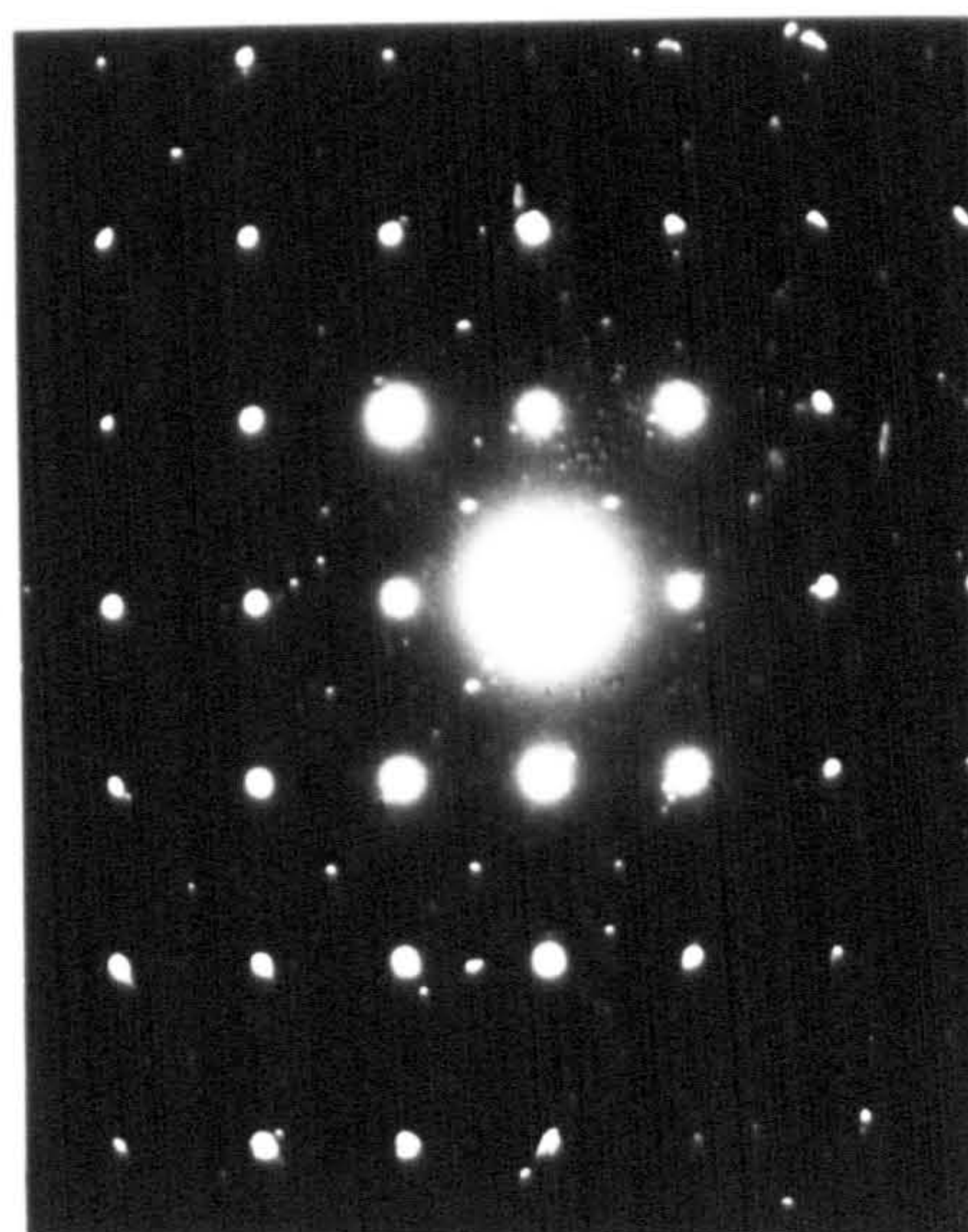


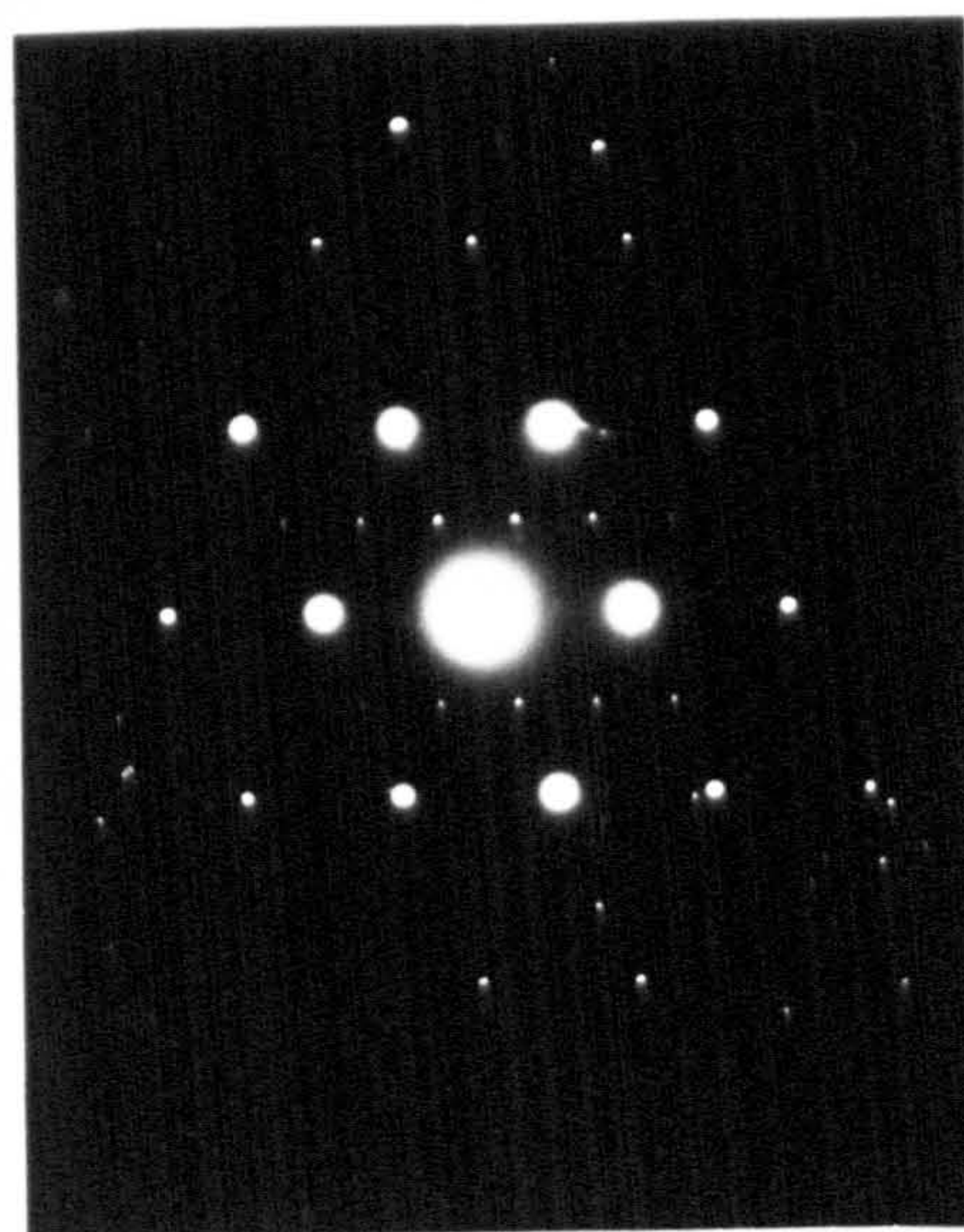
FIG.5.12.



A



B



FIG, 5, 13 - 675/775/50/1000/5

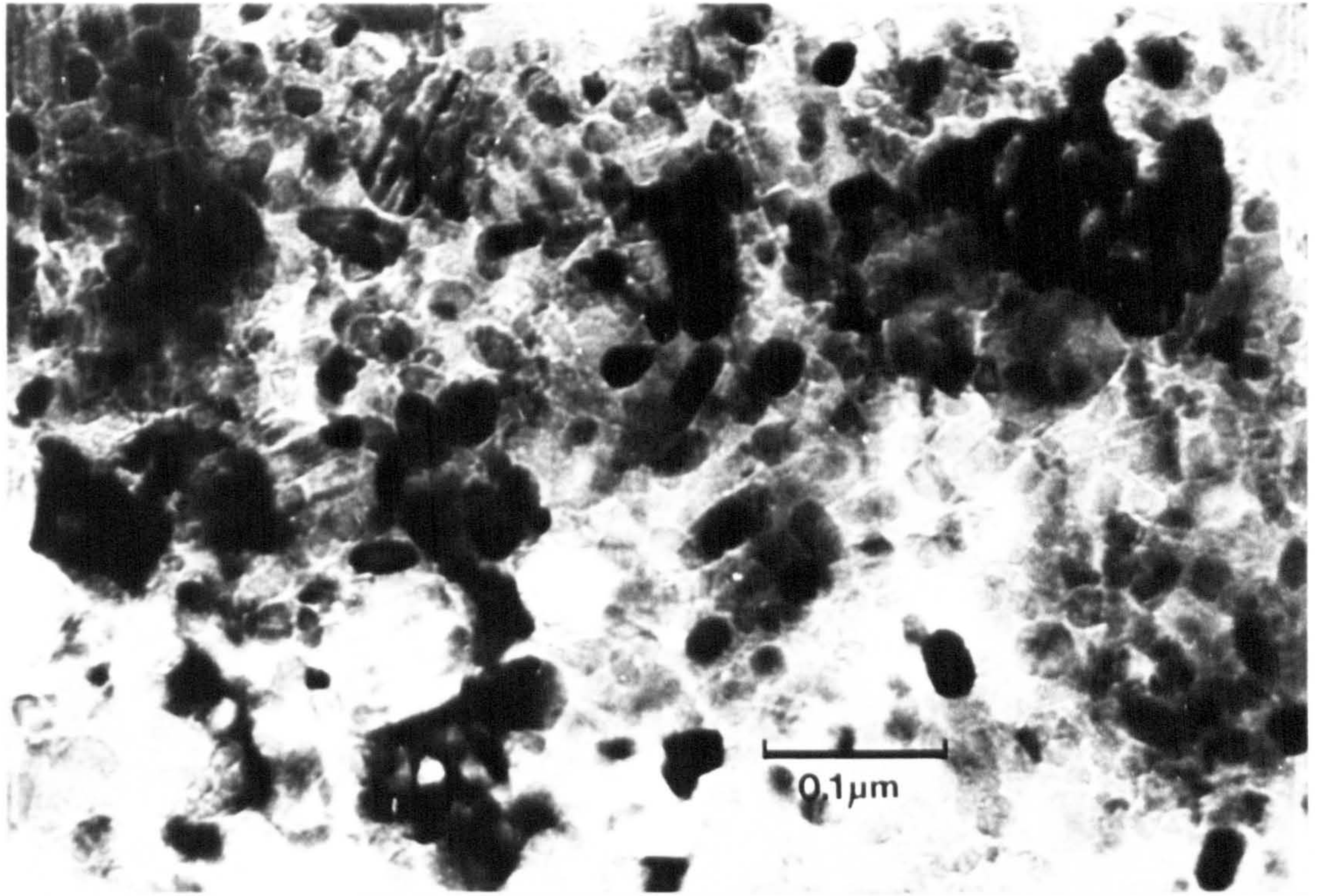


FIG. 5.14 - 750/775/50/1000/5

structures. With the above considerations in mind the development of microstructure prior to cordierite crystallisation will now be discussed in more detail.

Chapter 6 - Concluding discussion

6.1 Discussion

Glass-in-glass phase separation is clearly a precursor to nucleation and growth of MgTi_2O_5 in 750- glass and there is microstructural evidence (fig. 5.3(a)) that segregation of the amorphous phases occurs by spinodal decomposition (see Appendix 1). The possibility of an incipient ordering of this glass after short times at temperatures just above T_g ($\sim 720^\circ\text{C}$) was discussed in Chapter 4. Such an ordering process could be regarded as the initial stages of spinodal decomposition where compositional fluctuations would be sufficiently small to be unresolvable using TEM and thus remain undetected in untreated 750- glass. Subsequent heat-treatment of this glass at temperatures of $\sim 800^\circ\text{C}$ has resulted in phase separation and precipitation of MgTi_2O_5 crystallites in the TiO_2 -rich phase as a preferable route to a lower total free energy state. This is in contrast to direct precipitation of MgTi_2O_5 in the glass matrix as with 675- glass. The resulting differences in microstructure (fig. 5.4) have a profound influence on the subsequent crystallisation of both magnesian-petalite and μ -cordierite in terms of the ratio of these phases at given crystallisation temperatures (Chapter 3) and their growth morphologies (Chapter 5). The occurrence and extent of phase separation may well be an additional factor controlling the overall microstructural development of these particular glass-ceramics.

The pseudo-spherulitic morphology of MgTi_2O_5 in 675- glass can be appreciated by considering the general case in which this growth mechanism is preferred and extending the arguments to the present system. Growth of MgTi_2O_5 nuclei from the base glass will necessitate the rejection of both SiO_2 and Al_2O_3 from this phase which can be represented as "impurities" ahead of the crystal-liquid interface. The possibility of Al_2O_3 inclusion

in magnesium dititanate can not be discounted on the basis that a range of solid solutions exist from MgTi_2O_5 to Al_2TiO_5 as previously mentioned (96). The great similarity in d-spacings and relative intensities of XRD data for this range render conclusive identification of MgTi_2O_5 difficult; however, this phase will be referred to in all further discussion. For simplicity let us therefore consider only SiO_2 to be the rejected "impurity". On the basis that the rate of diffusion of SiO_2 away from the interface will be slow in a high viscosity liquid, then in keeping with the general model for spherulitic growth (114) the concentration of SiO_2 at the interface will be high and decay exponentially as a function of distance (x) away from the interface. As a consequence the degree of undercooling will be low at the interface and increase similarly with x. This phenomenon is known as constitutional supercooling and is represented schematically for this system in fig. 6.1. Under such conditions small perturbations on the interface become unstable with respect to the planar growth front as they reach out into regions of substantially increased undercooling and will grow to form fibrous, cellular projections as seen in figs. 5.4(a), 5.5, 5.8 and 5.9. Growth of the observed fibrils will ultimately be chemically arrested in that most of the TiO_2 in the glass (liquia) phase will be consumed. At elevated temperatures these pseudo-spherulites are seen to recrystallise to give a more faceted morphology (fig. 5.13).

In 750- glass the crystallisation of MgTi_2O_5 takes place in the TiO_2 -rich phase which has resulted from prior phase separation. Spherulitic growth is not observed and may be explained by the expected reduction in viscosity of the TiO_2 -rich phase preventing sufficient build up of SiO_2 which will be present at a reduced concentration. It must be emphasised that the modelling of spherulitic growth has been largely

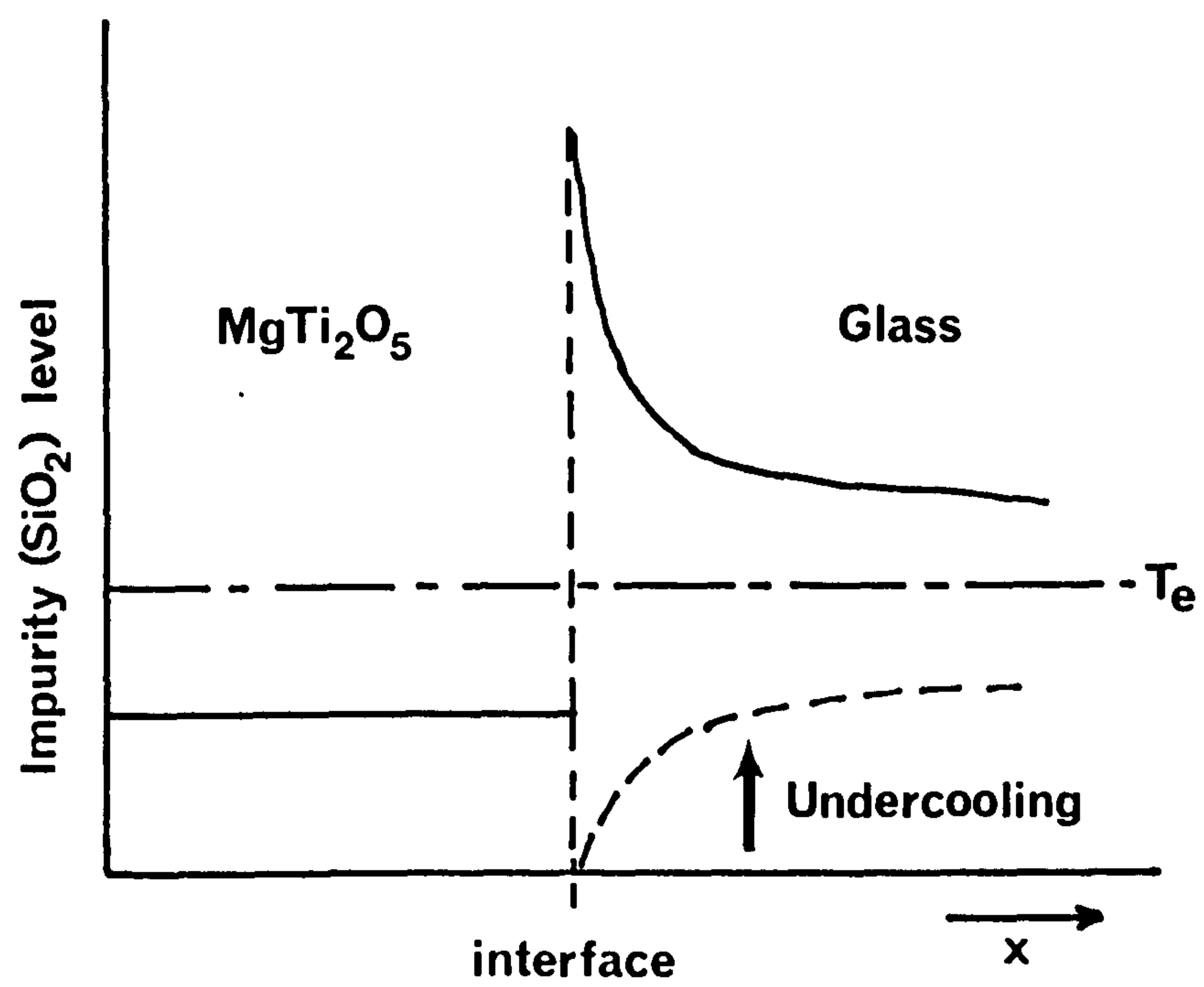
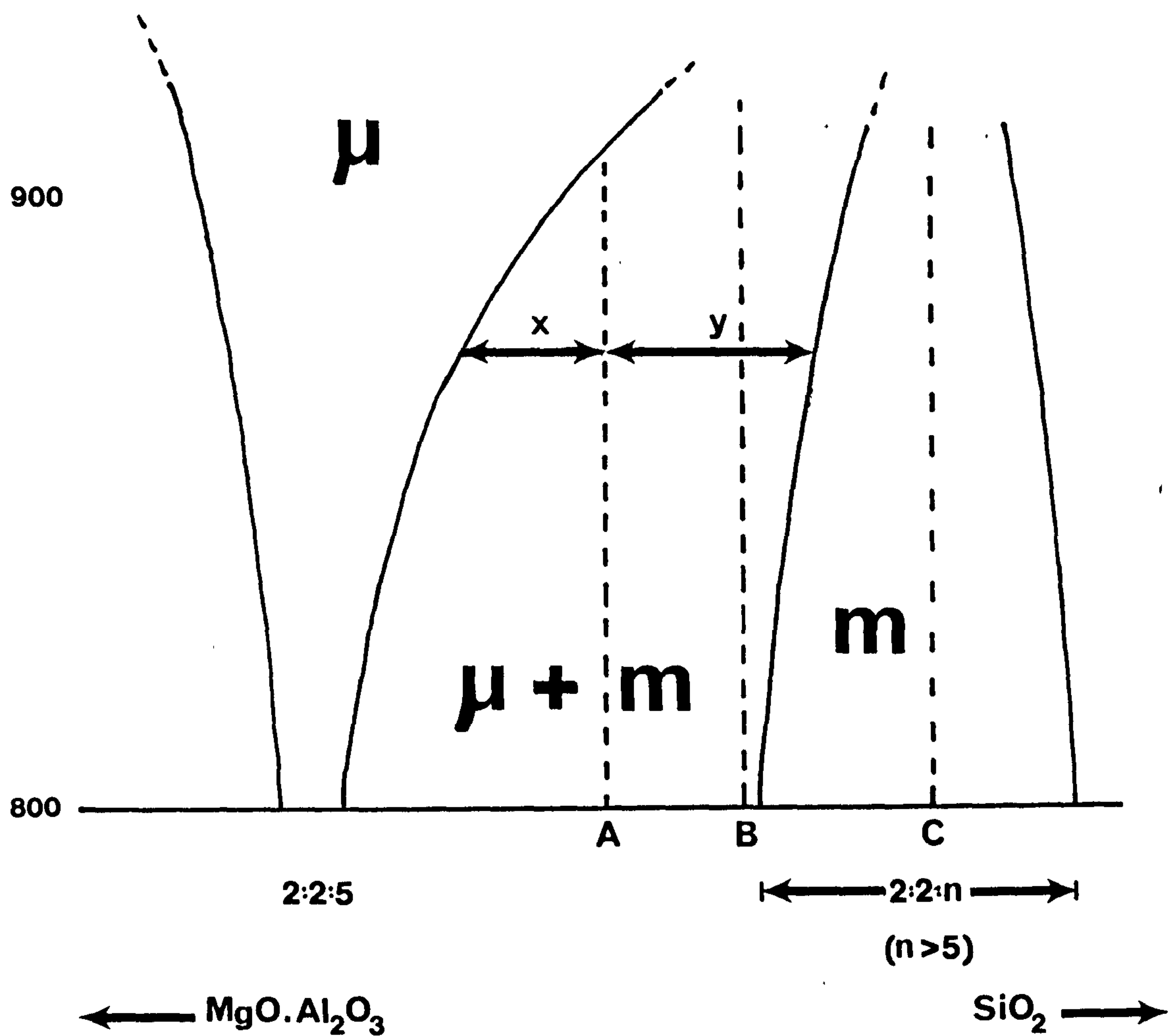


Fig.6,1 – Constitutional supercooling

based on the freezing of binary eutectic alloy systems and crystallisation of binary silicates with low nucleation densities. In this respect the growth of MgTi_2O_5 from a densely nucleated quaternary system cannot be conclusively discussed on this basis; however an attempt has been made to explain the observed phenomena using an extension of classical arguments.

The crystallisation of both magnesian-petalite and μ -cordierite from 675- and 750- glass shows a marked variation in the relative proportions of each phase as a function of both thermal history (i.e. annealing temperature) and heat treatment (section 3.3). This may be explained by considering the composition of the residual glass phase after nucleation of MgTi_2O_5 which in the case of 750- glass is preceded by phase separation. This phase separation would result in a SiO_2 -rich phase and a TiO_2 -rich phase in which the concentration of both Al_2O_3 and MgO may also be increased (Chapter 4). Precipitation of MgTi_2O_5 from 675- glass leaves a residual glass phase which does not differ too greatly in composition from that of the parent glass. Hence, the situation arises whereby the chemical composition of the potentially crystallisable glass phase varies from 675- to 750- glass. The subsequent crystallisation and resulting magnesian petalite: μ -cordierite ratio can be understood by reference to a hypothetical phase diagram as constructed in fig. 6.2. Points A and B represent respectively the residual glass compositions in 675- and 750- glass which will crystallise. The magnesian petalite phase field is shown to narrow in compositional stability with increasing temperature. Conversely, the μ -cordierite phase field is shown to widen. These are reasonable assumptions on the basis of work by Holmquist (49) who showed the formation of a magnesian-petalite phase to be favoured in more siliceous magnesium alumino silicate glasses. The ratio of magnesium

$$\left(\frac{\mu}{m}\right)_A = \frac{y}{x}$$



μ - μ - CORDIERITE
 m - MAGNESIAN - PETALITE

FIG. 6.2

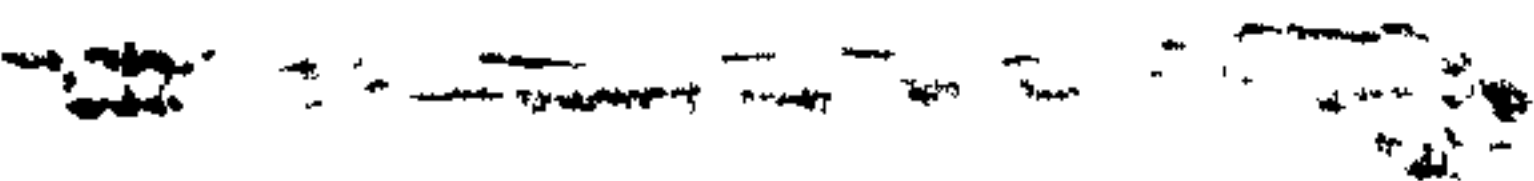
petalite: μ -cordierite can be estimated by the Lever rule and for composition B a ratio >1 exists to higher temperatures than in composition B. This argument may be extended to explain the phase development in samples which have received extended nucleation treatments; i.e. 675/775/50/1000/5 and 750/775/50/1000/5. Assuming a time-dependent segregation of the amorphous phases then the compositional shift of the crystallisable glass phase in 750/775/50 may be even further along the SiO_2 axis to a point (C) where μ -cordierite is only an equilibrium phase at temperatures above 1000°C and therefore has not developed in 750/775/50/1000/5. The limitations of this model are acknowledged in the absence of detailed information about the phase diagram for this system at temperatures well below the liquidus. However, to a first approximation it can be used to account for observed phenomena. It would appear then that the extent of phase separation in terms of compositional segregation controls initial crystalline phase development by shifting the composition of the glass matrix and thereby determining the proportion of equilibrium phases forming at subsequent heat-treatment temperatures.

Transformation of magnesian petalite to μ -cordierite requires a structural rearrangement of the lattice; primarily involving Mg^{2+} and Al^{3+} ions. As such, it will require diffusion of these ions in the solid state to new positions which may be either substitutional or interstitial. Atomic mobility in ceramic phases by a diffusional process is known to be strongly influenced by temperature to an extent that the diffusion coefficient D exhibits an exponential temperature dependence: i.e.

$$D = D_0 \exp \left[-\Delta G/kT \right]$$

where ΔG is an activation energy representing a barrier to the transformation whereby the total free energy of the system will be reduced

as represented schematically in fig. 6.3. The chemical environment of the diffusing species may have an additional influence on the activation energy and hence the diffusion coefficient.

Although not determined, the composition of the magnesian-petalite phase would be expected to be SiO_2 -rich with respect to μ -cordierite (fig. 5.7) and therefore transformation would require the diffusion of both Mg^{2+} and Al^{3+} from the residual glass phase into the crystalline matrix.  In practice a combination of both may occur and so the activation energy, ΔG represents the sum of activation energies for these individual processes.

Attempted EDAX analysis of the magnesian petalite phase in both 675- and 750- glass crystallised at 825°C proved to be inconsistent and unreliable. This was regarded as a limitation of the technique as applicable to these systems and therefore it cannot be assumed that the chemical compositions of the magnesian-petalite phases grown in either of the crystallised base glasses will be the same; this phase may exhibit considerable stability over a range of composition. It is possible, therefore, that the composition of magnesian-petalite grown from 750-glass may be sufficiently different to that grown from 675- glass to cause an increase in the activation energy for diffusion, ΔG . Therefore, at a given temperature the fraction of untransformed magnesian petalite in the 750- glass system would be higher than for 675- glass as observed (section 5.2, fig. 5.1). Additional influences on ΔG could come from differences in the distribution and composition of the residual glass phase.

Long range ordering in both magnesian-petalite and μ -cordierite has been observed using electron diffraction. This phenomenon is commonly encountered in many systems where a deviation from stoichiometry exists. Accommodation of non-stoichiometry occurs by the concentration of excess atomic or molecular species at preferred sites within the host lattice.

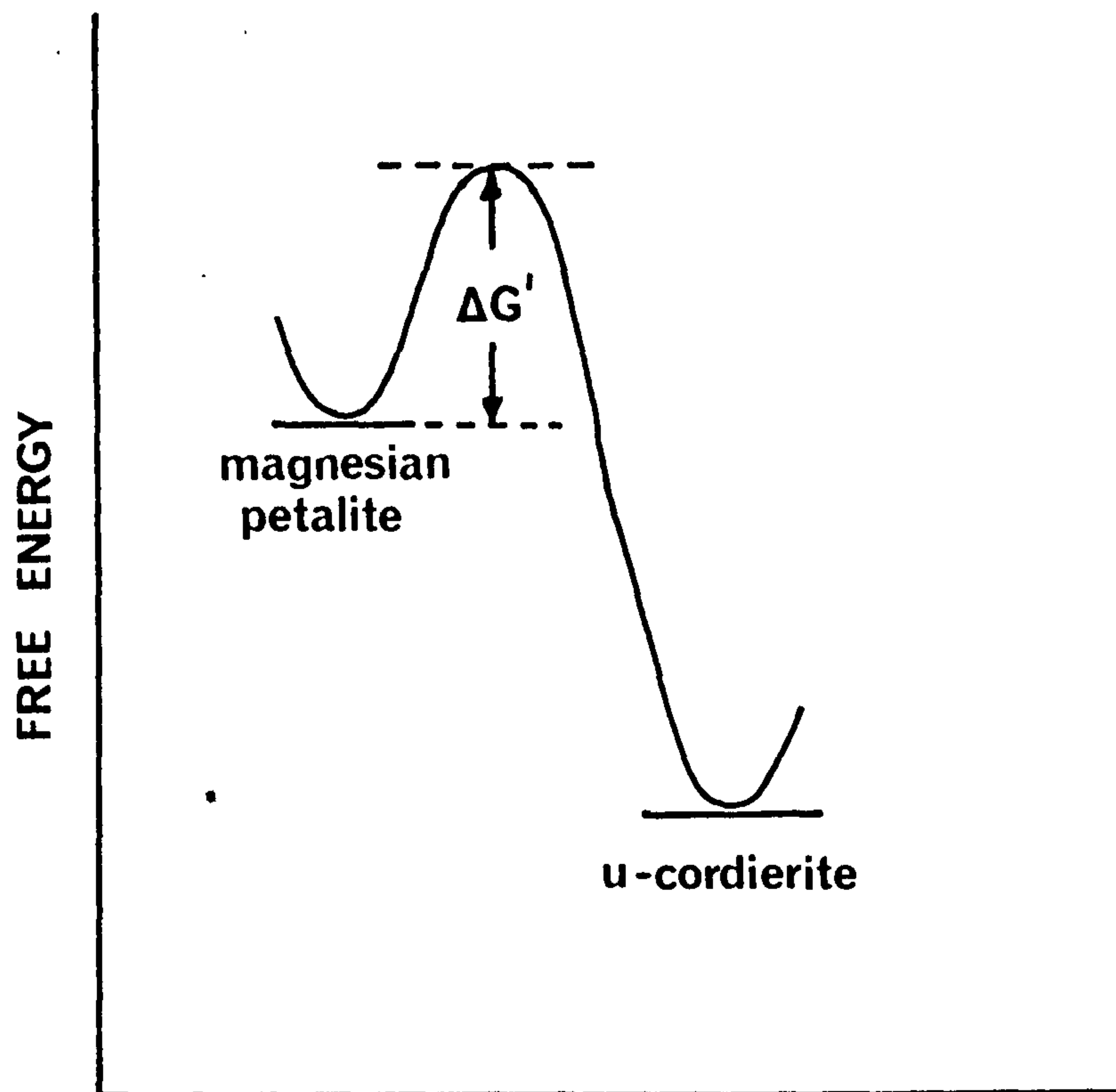


Fig.6,3 - Ionic mobility

The result is a lowering of the total free energy of the system compared to that in which the "impurity" atoms are randomly distributed.

In β -quartz solid solutions the ordering is generally associated with the arrangement of Mg^{2+} ions in a silicate lattice in which Al^{3+} occupies Si^{4+} sites substitutionally. The electron scattering factors of Mg, Al and Si as a function of $\sin\theta/\lambda$ are presented in table XI.

| Element | $\sin\theta/\lambda$ | | | | |
|---------|----------------------|------|------|------|------|
| | 0.10 | 0.15 | 0.20 | 0.25 | 0.30 |
| Mg | 4.29 | 3.14 | 2.33 | 1.79 | 1.45 |
| Al | 5.07 | 3.74 | 2.75 | 2.07 | 1.63 |
| Si | 5.26 | 4.08 | 3.10 | 2.36 | 1.84 |

Table XI. Electron scattering factors for Mg, Al and Si (from "International Tables for X-ray Crystallography (1962).).

For the small values of θ associated with electron diffraction it can be seen that the difference in scattering factor between Mg and Si is considerably larger than that between Al and Si. Hence ordering of Mg atoms would exert greater influence on the structure factor for μ -cordierite than a corresponding over-ordering of Al. Electron diffraction would therefore be more sensitive to planes with a higher or lower Mg population compared to the basic unit cell, resulting in sufficiently intense additional spots on the diffraction pattern. The molar composition of the base glass, i.e. $23 \text{ MgO} \cdot 12 \text{ Al}_2\text{O}_3 \cdot 58 \text{ SiO}_2 \cdot 7 \text{ TiO}_2$ deviates considerably from the stoichiometric μ -cordierite composition, $2 \text{ MgO} \cdot 2 \text{ Al}_2\text{O}_3 \cdot 5 \text{ SiO}_2$; being essentially MgO-rich. Some of the excess Mg could conceivably be accommodated in the μ -cordierite lattice and result in a doubling of the unit cell as observed. The remainder would react

with excess SiO_2 at elevated temperatures ($\sim 1000^\circ\text{C}$) to form enstatite (fig. 5.11). Ordering in the magnesian petalite phase is less well understood but would be expected to occur by a similar mechanism. The lower symmetry of the magnesian petalite cell requires that much additional work be carried out to clarify the mode of ordering in this phase.

6.2 Conclusions

On the basis of the work presented in this thesis and the subsequent discussion, the following conclusions may be drawn pertaining to the general glass composition studied:

1. The general microstructural and phase development in this system proceeds in a complex manner.
2. Glass-in-glass phase separation, as a precursor to nucleation and growth of metastable β -quartz solid solutions, can be initiated by an incipient local ordering of the glass structure during heat-treatment for short durations just above the glass transition temperature, T_g ; such a heat-treatment serves effectively to anneal the glass.
3. Phase separation can be avoided by annealing below T_g and heating the glass directly to temperatures ($> 750^\circ\text{C}$) whereby the formation of finely dispersed nuclei of a magnesium dititanate (or aluminotitanate) is accomplished by pseudo-spherulitic growth.
4. The metastable β -quartz solid solutions, magnesian-petalite and μ -cordierite are capable of co-existing over the approximate temperature range $800 - 1000^\circ\text{C}$.
5. The ratio of magnesian-petalite to μ -cordierite at a given crystallisation temperature is strongly influenced by prior phase separation as a result of compositional shifts of the crystallising glass phase.

6. There is a marked difference in the microstructural development of both magnesian petalite and μ -cordierite from glasses which exhibit phase separation and those which do not.
7. Deviations from stoichiometry are to a certain extent accommodated by long-range ordering, primarily in μ -cordierite. The resulting hexagonal unit cell has parameters of $a = 10.4\overset{\circ}{\text{\AA}}$ and $c = 10.7\overset{\circ}{\text{\AA}}$, i.e. a doubling of the original unit cell.
8. The effect of prior phase separation on microstructural development may be of practical interest in so much as it may strongly influence the physical properties of these technologically important materials, e.g. mechanical strength, microhardness and thermal expansion coefficient.

6.3 Future work

Many interesting topics have arisen from this work which would merit further investigation. Of singular importance is the question of glass-in-glass phase separation and its influence on subsequent microstructural development. The elucidation of local ordering prior to phase separation would require the employment of more powerful techniques, e.g. Extended X-ray Absorption Fine Structure (EXAFS) and "magic-angle" NMR spectroscopy, both of which give valuable information on the immediate local environment of selected atomic species and would therefore allow precrystallisation transformations and crystallisation itself to be studied on an atomic scale. EPR and high resolution TEM may serve as useful supplementary methods.

The fine scale of microstructure generally encountered has to some extent hampered studies on the kinetics of crystallisation and phase transformations. However, the materials investigated are of technological importance and require the inclusion of sizeable proportions of nucleating agent. A system with a lower nucleation density could offer an easier solution to some of the problems of analysing the compositional

distribution of atomic species during the development of such complex microstructures. An investigation of the long-range ordering ability of β -quartz solid solutions would be aided by the presence of large, faceted, single crystals with a clearly identifiable intergranular matrix. In essence, the enhancement of inherent phase separation in magnesium aluminosilicate glasses based on cordierite offers an additional and important factor in controlling the development of microstructure. A full understanding of this phenomenon and careful practical application could result in the production of glass-ceramic materials with improved physical properties.

REFERENCES

- (1) Zachariasen, W.H., J. Am. Ceram. Soc. 54, 3841 (1932)
- (2) Tamman, G. "The States of Aggregation", D. Van Nostrand + Co.
N.Y. (1925)
- (3) Gibbs, J.W., Collected Works, Vol 1 Longmans, Green + Co.
N.Y. (1928)
- (4) Becker, R. and Doering, W., Ann. Phys. 24, 719 (1935)
- (5) Frenkel, J., "Kinetic Theory of Liquids", Clarendon Press,
Oxford (1946)
- (6) Stanworth, J.E. "Physical Properties of Glass" p224, Clarendon Press,
Oxford (1950)
- (7) Turnbull, D. and Vonnegnt, B. Industr. Engng, Chem. 44, 1292 (1952)
- (8) Staveley, L.A.K., "The Vitreous State" p85, Glass Delegacy of
Univ. of Sheff. (1955)
- (9) Stookey, S.D., Glastech. Ber. V International Glass Congress, 32K,
Haft V (1959)
- (10) Turnbull, D. and Cohen, M.H., J. Chem. Phys. 29, 1049 (1958)
- (11) ibid - "Modern Aspects of the Vitreous State", Vol. 1, p38,
Butterworths, London (1960)
- (12) ibid - Nature 189, 131 (1961)
- (13) Turnbull, D., "Solid State Physics", Vol.3 p226, Academic Press,
N.Y. (1956)
- (14) Cahn, J.W., J. Chem. Phys., 42, 93 (1961)
- (15) Cahn, J.W. and Charles, R.J., Physics Chem. Glasses, 6, 181 (1965)
- (16) Kingery, W.D., "Introduction to Ceramics", p478, Wiley, N.Y. (1960)
- (17) Stookey, S.D., Brit. Patent No. 829,447 (1960)
- (18) Buzhinskii, I.M., Sabaeva, E.I., and Khonigakov, A.N., "The Structure
of Glass", Vol. III p133, Consultants Bureau, N.Y. (1964)

- (19) Blinov, V.A., J. Mat. Sci, 461 (1969)
- (20) Ohlberg, S.M., Golob, H.R. and Strickler, D.W. "Symposium on
Nucleation and Crystallisation in Glasses and Melts", p55,
American Ceramic Society, Columbus, Ohio (1962)
- (21) Vogel, W., Silikat Tech., 10 : 241 (1959)
- (22) ibid Silikat Tech., 16(5), 152 (1965)
- (23) Vogel, W. and Gerth, K., Glastech Ber., 31, 15 (1958)
- (24) Vogel, W. and Gerth, K., ibid (20) p11
- (25) Maurer, R.D. ibid (20) p5
- (26) Maurer, R.D., J. Appl. Phys. 33(6), 2132 (1962)
- (27) Weyl, W.A. "Coloured Glasses", Society of Glass Technology,
Sheffield (1967)
- (28) Bobovich, S.Y. ibid (18) p93
- (29) Zdaniewski, W. J. Mat. Sci. 8, 192 (1973)
- (30) Colbert, W., J. Am. Ceram. Soc. 29, 40 (1946)
- (31) Salah, A., J. Am. Ceram. Soc. 55, 137 (1972)
- (32) Hinz, W. and Kunth, P. Glastech. Ber. 34, 435 (1961)
- (33) Kondratiev, Y.N., Dokl. Akad. Nauk SSR, 153, 1370 (1963)
- (34) Hillig, W.B., "A Theoretical Experimental Investigation of
Nucleation Leading to Uniform Crystallisation of Glass",
Nuc. and Cryst. Symp. Ohio (1962)
- (35) Hanada, T. and Soga, N., Journ. Non. Cryst. Solids (38, 39), 105,
(1980)
- (36) Sandstrom, D.R. and co-workers, Journ. Non. Cryst. Solids 41, 201
(1980)
- (37) Winkler, H.G. - Acta Crystallogr. 1, 27-34 (1948)
- (38) Roy, R. and Osborn, E.F., Jour. Am. Chem. Soc. 71, 2086-2095 (1949)
- (39) Henglein, E., Fortschr. Min. 34, 40-43 (1956)
- (40) Skinner, B.I. and Evans H.T., Am. Journ. Sci. Bradley Vol 258A
312-324 (1960)

- (41) Buerger, M.J., Am. Min. 39, 600-614 (1954)
- (42) Rankin G.A. and Merwin H.E., Amer. J. Science (4) 45, 301-325 (1918)
- (43) Karkhawavala M.D. and Hummel F.A., J. Am. Ceram. Soc. 36, 393-397 (1953)
- (44) Schreyer W. and Schairer J.F., Carn. Inst. Wash. Year Book 197-199 (1958)
- (45) Roy, R., Kristallogr, Z. 111, 185-189 (1959)
- (46) Schreyer, W. and Schairer, J.F., Kristallogr Z., 116, 60-82 (1961)
- (47) Schulz, H. et al., Kristallogr Z., 133, 91-109 (1971)
- (48) Schreyer W. and Schairer, J.F., Am. Min. 47, 90-104 (1962)
- (49) Holmquist S.B., Kristallogr Z., 118, 477-478 (1963)
- (50) De Vekey R.C. and Majumadar A.J., Min. Mag., 37, 771-779 (1970)
- (51) Barry, T.I., Cox, J.M. and Morrell, R., J. Mat. Sci. 13, 594-610 (1978)
- (52) Norton, E.H., J. Am. Ceram. Soc. 22, 54 (1939)
- (53) Grimshaw, R.W. et al. Trans. Brit. Ceram. Soc., 44, 87 (1945)
- (54) Berg, P.W., Ber. Dent. Keram. Ges., 30, 231 (1953)
- (55) MacKenzie, R.C., "Differential Thermal Analysis of Clays" (Mineralogical Society, London, 1957)
- (56) Fleck, W.E.P., et al. Can. J. Chem., 38, 9 36 (1960)
- (57) Johnson, W.A. and Meyl, R.F., Trans. Am. Inst. Min. (Metall) Engs., 135, 416 (1939)
- (58) Avrami, M., J. Phys. Chem., 7, 1103 (1939); 8, 212 (1940); 9, 177 (1941)
- (59) Kissinger, H.E., J. Res. Nat. Bur. Stand., 57, 217 (1956); Anal. Chem., 29, 1702 (1957)
- (60) Henderson, D.W., J. Non. Cryst. Solids, 30, 301-315 (1979)
- (61) Briggs, J. and Carruthers, T.G., Phys. Chem. Glass, 17 (2) 30-34 (1976)

- (62) Matusita, K. et al., J. Mat. Sci. 10, 94-100 (1975)
- (63) Gregory, A.G. and Veasey, T.J., J. Mat. Sci. 8, 324-332 (1973)
- (64) Barry, T.I. et al. J. Mat. Sci. 4, 596-612 (1969)
- (65) Barry, T.I. et al. J. Mat. Sci. 13, 594-610 (1978)
- (66) Klug, H.P. and Alexander, L.E., "X-ray diffraction Procedures", Wiley (1954)
- (67) Scherrer, P., Gottinger Nachrichten, 2, 98, (1918)
- (68) Bragg, L., "The Crystalline State, Vol. 1, 189, London (1919)
- (69) Murdock, C.C., Phys. Rev., 49, 884 (1936)
- (70) Warren, B.E., Zeit. Krist., 99, 448 (1938)
- (71) Philips, "Horizontal Goniometer PW 1380"
- (72) Bowen, D.K. and Hall, C.R., "Microscopy of Materials", Macmillan (1975)
- (73) Glauret, "Practical methods in electron microscopy", North Holland (1972)
- (74) Houghton, J.T. and Smith, S.D., "Infra-red Physics", O.U.P. (1966)
- (75) Brugel, W., "Infra-red spectroscopy", Meuthen & Co., London (1962)
- (76) Meloon, C.E., "Elementary infra-red spectroscopy", Macmillan, N.Y. (1963)
- (77) Banwell, C.N., "Fundamentals of Molecular Spectroscopy", McGraw-Hill, (1972)
- (78) Wong, J. and Angell, C.A., "Glass structure by spectroscopy", Dekker (1976)
- (79) Simon, I., In "Modern Aspects of the Vitreous State", Butterworths (1960)
- (80) Simon, I. and McMahon, H.O., J. Am. Ceram. Soc. 36, 160 (1953)
- (81) Sigel, G.H. (Jr). In "Treatise on Materials Technology", Vol. 12, Academic Press (1977)

- (82) Jellyman, P.E. and Procter, J.P., J. Soc. Glass Tech. 39, 173T
- (83) Farmer, V.C., "The Infra-red spectra of Minerals (Mineralogical Soc) 1974.
- (84) Gregory, A.G. and Veasey, T.J., J. Mat. Sci. 8, 333-339 (1973)
- (85) Bamford, C.R., Phys. Chem. Glasses, 3, 189 (1962)
- (86) Tahn, H.A., Glasstech. Ber. 39, 118 (1966)
- (87) Stroud, J.S., J. Am. Ceram. Soc. 54, 401 (1971)
- (88) Paul, A., J. Mat. Sci. 10, 692 (1975)
- (89) Wong, J. et al., J. Non. Cryst. Solids - to be published
- (90) Kurkjian, C.R. and Sigety, E.A., Phys. Chem. Glasses 9, (3), 73 (1968)
- (91) Carson, D.S. and Manrer, R.D., J. Non. Cryst. Solids 11, 368 (1973)
- (92) Schultz, P. C. and Smyth, in "Proc. Conf. on Physics of non-crystalline solids III" p.455, Wiley (1972)
- (93) Peterson, G.E. et al., Bull. Am. Ceram. Soc. 51, 367 (1972)
- (94) Zdanor and Rusakor, Dokl. Akad. Nauk SSSR, 82, 901-4 (1952)
- (95) Kasper, Z., anorg. allgem. Chem., 354, 208-24 (1967)
- (96) Signrdson and Cole, AIME Trans., 185, 905 (1949)
- (97) Bell, G.A., Australian J. App. Sci., 2, 236 (1958)
- (98) Wong, J. et. al to be published
- (99) Langer, K and Schairer, W., Am. Min. 54, 1442-59 (1969)
- (100) Duchille, F. and Roy, R., Z. Krist 111, 462-70 (1959)
- (101) Hanna, R., J. Am. Ceram. Soc. 48, 595-99 (1965)
- (102) Bock, J., and Su, G-J., J. Am. Ceram. Soc. 53, 69-73 (1970)
- (103) Wyckoff, R.W.G., "Crystal Structures" Vol. 1, p.313-14, Interscience Publishers N.Y. (1963)
- (104) Konijnendijk, W.L., Philips Res. Repti. Suppl. No.1, p.76 (1975)
- (105) Garif'yanor, D., Sov. Phys - Sol. State, 6, 1137 (1964)
- (106) Castner, T. et. al., J. Chem. Phys. 32, 668 (1960)

- (107) Smith, H.L. and Cohen, A.J., Phys. Chem. Glasses, 4, 173 (1963)
- (108) Baiburt, L.G. et. al., Dokl. Phys. Chem. 162, 453 (1965)
- (109) Smith, G. and Streus, R.G.J., in "The Physics and Chemistry of Mineral Rocks", London - N.Y. (1976)
- (110) Varshal, B.G., Sov. J. Glass Phys. Chem. 7, 147-54 (1981)
- (111) Jones, G.O., "Glass", Northumberland Press Ltd. (1971)
- (112) Varshal, B.G., Fiz. Khim. Stekla, 1, No2, 127-33 (1975)
- (113) Leng-Ward, G., to be published.
- (114) Keith, H.D. and Padden, F.J., J. Appl. Phys. 34, 2409 (1963)
- (115) Goldschmidt, V.M., "Geochemische Verteilungsgesetze der Elementen", viii, Vid. Akad. (1926)

Appendix 1 - Spinodal decomposition

Spinodal decomposition refers to a continuous type of phase transformation in which initial change can be represented as compositional waves with a small amplitude and large in spatial extent. For a hypothetical mixture of two components, whose phase diagram contains a miscibility gap, plots of free energy (G) versus composition (C) exhibit two minima which move closer together with increasing temperature until they coincide at what is known as the upper consolute temperature, fig. A.1. The loci of the minima with temperature trace out an immiscibility dome, fig. A.2. A second inner dome is traced out by the points of inflection n and n' (fig. A.1). For compositions within the inner dome, i.e. between n and n' , $\partial^2 G / \partial C^2$ is negative and hence small fluctuations in composition will be stable and tend to grow without requiring nucleation. Phase separation within this region is known as spinodal decomposition. Compositions lying outside this dome, but within the outer dome, have $\partial^2 G / \partial C^2$ values which are positive and compositional fluctuations will be unstable and only continue to grow if they attain a critical size. Therefore, phase separation in this region requires a nucleation and growth process. Schematic concentration profiles for both spinodal decomposition and nucleation and growth as a function of time are shown in fig. A.3 (after Cahn, J.W. (14,15)). In spinodal decomposition the concentration of the phases varies until equilibrium is reached, interfaces are diffuse and the two phases are threaded through each other with a higher degree of connectivity. On the other hand, nucleation and growth promotes small, randomly spaced, spherical droplets with clearly defined interfaces and whose composition is constant at a given temperature.

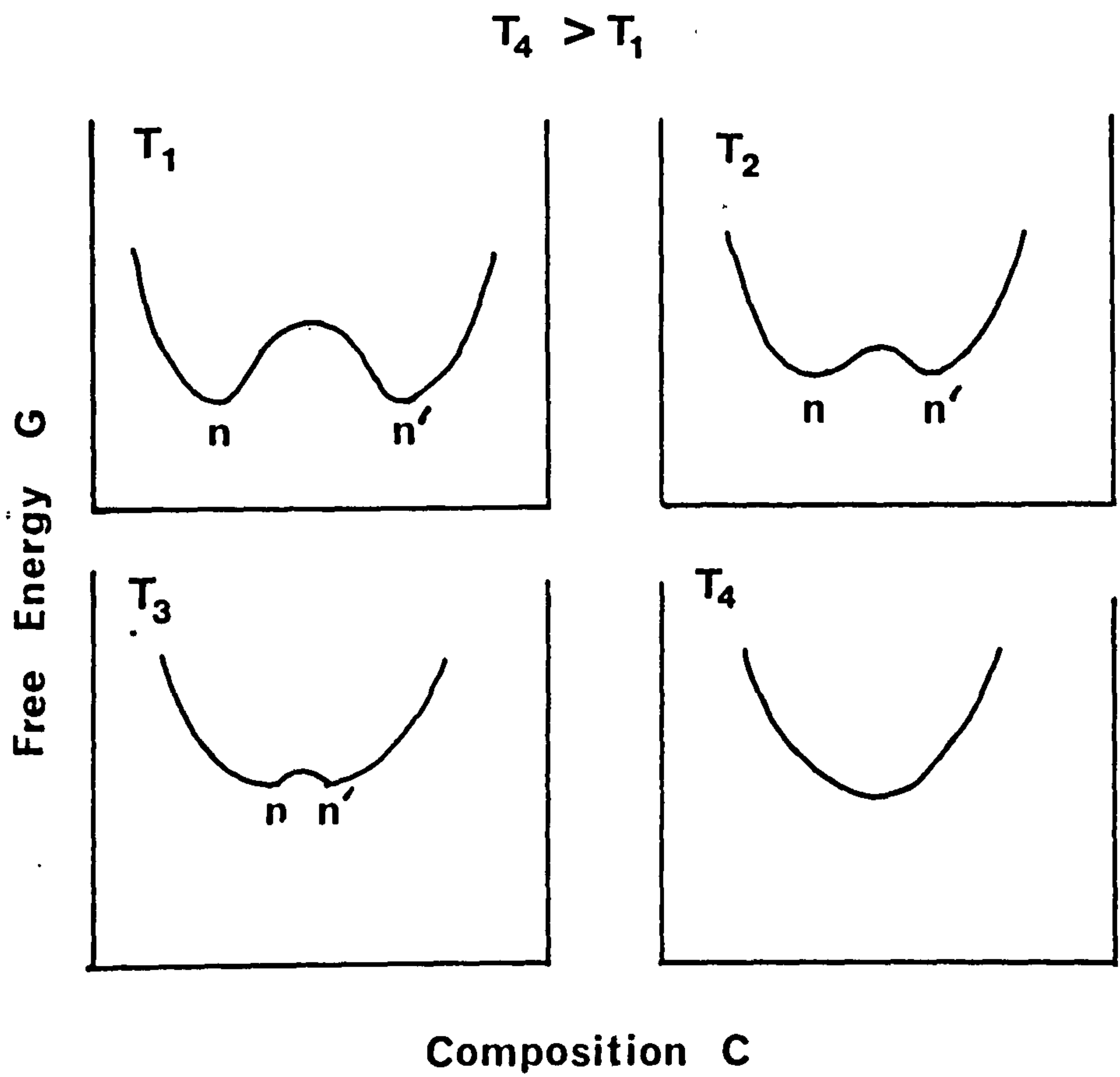


FIG. A.1

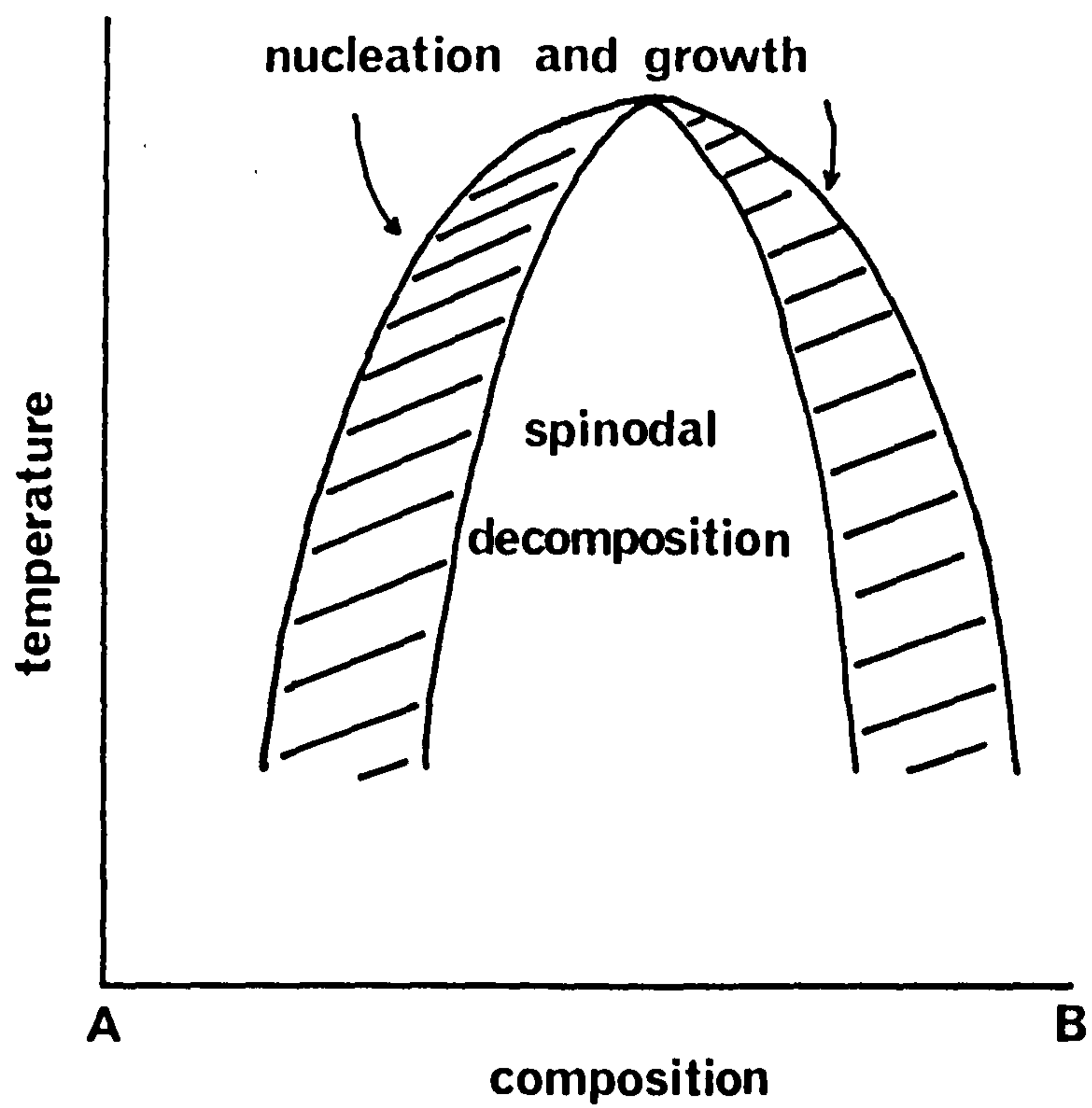


FIG. A.2

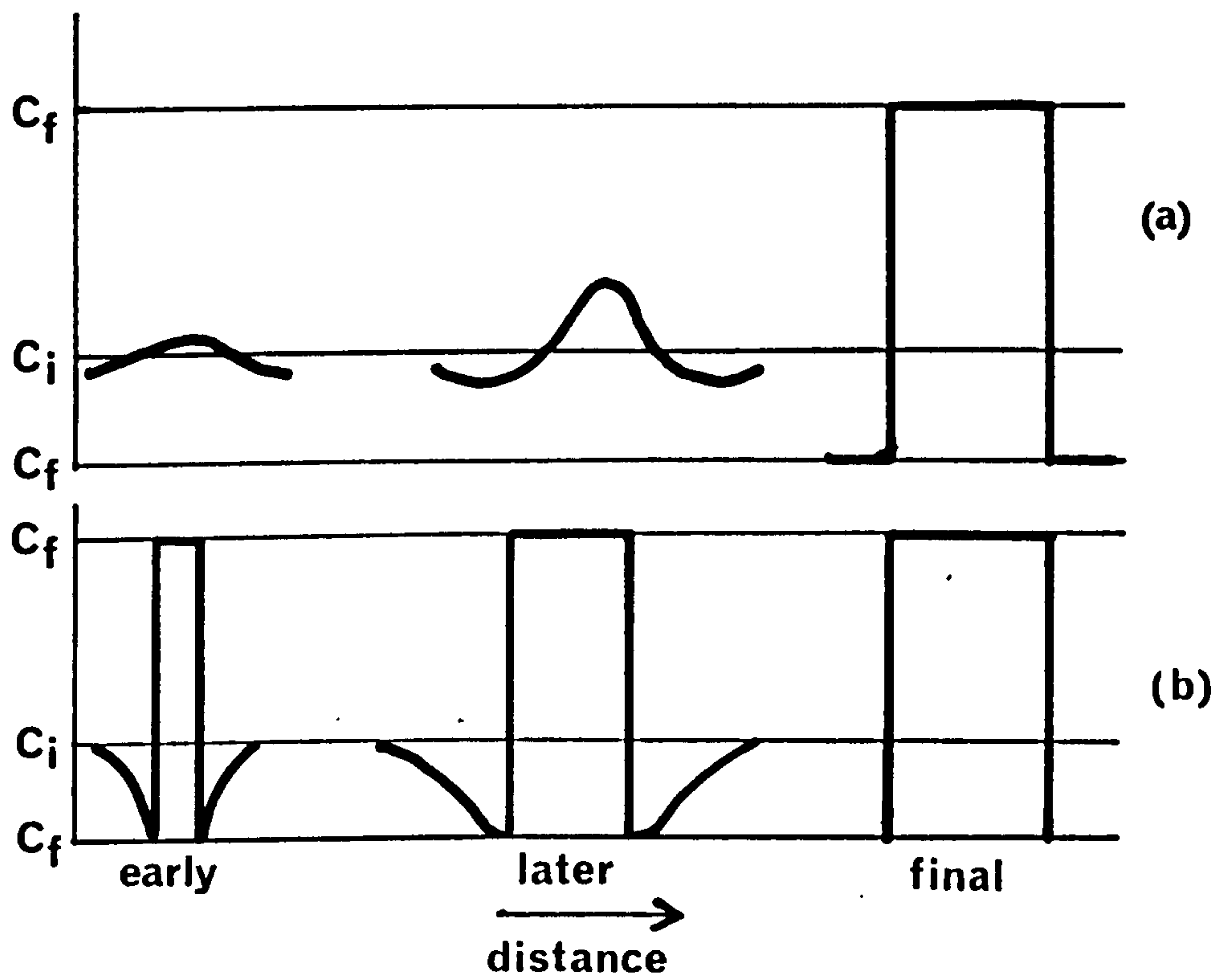


Fig. A.3 - Schematic concentration profiles for (a) spinodal decomposition and (b) nucleation and growth, after J.W. Cahn.

c_i = initial concentration

c_f and c'_f = respective final concentrations

Appendix II - X-ray diffraction data for magnesian petalite phases
after (a) Schreyer and Schairer (46) and (b) Holmquist
(49).

| | d Å | 2θ | I/I ₀ (estimated) |
|-----|--------|--------------------|------------------------------|
| (a) | 7.20 | 12.30 | 8 |
| | 4.65 | 19.10 | 1 |
| | 4.08 | 21.80 | 8 |
| | 3.79 | 23.50 [±] | 20 |
| | 3.69 | 24.10 | 100 |
| | 3.58 | 24.85 | 25 |
| | 2.99 | 29.90 | 8 |
| | 2.78 | 32.20 | 6 |
| | 2.55 | 35.20 | 11 |
| | 2.47 | 36.40 [±] | 8 |
| | 2.39 | 37.70 | 8 |
| | 2.06 | 44.00 [±] | 5 [±] |
| | 1.95 | 46.50 | 6 |
| | 1.93 | 47.00 | 8 |
| | 1.90 | 47.75 | 5 |
| (b) | 7.17 | 12.33 | 8 |
| | 3.74 | 23.77 | 100 |
| | 3.66 | 24.30 | 90 |
| | 3.56 | 25.00 | 15 |
| | 2.66 | 33.66 | 4 |
| | 2.62 | 34.19 | 6 |
| | 2.54 | 35.30 | 8 |
| | 2.45 | 36.64 | 3 |
| | 2.38 | 37.76 | 5 |
| | 2.10 | 43.03 | 2 |
| | 2.05 | 44.13 | 9 |
| | 1.93 | 47.04 | 4 |
| | 1.91 | 47.56 | 3 |
| | 1.72 | 53.20 | 3 |

Table XII